HYPERGRAPH BASED VISUAL CATEGORIZATION AND SEGMENTATION

BY YUCHI HUANG

A dissertation submitted to the

Graduate School—New Brunswick

Rutgers, The State University of New Jersey

in partial fulfillment of the requirements

for the degree of

Doctor of Philosophy

Graduate Program in Computer Science

Written under the direction of

Professor Dimitris N. Metaxas

and approved by

_____

_____

_____

_____

New Brunswick, New Jersey

October, 2010

ABSTRACT OF THE DISSERTATION

Hypergraph Based Visual Categorization and Segmentation

by Yuchi Huang

Dissertation Director: Professor Dimitris N. Metaxas

This dissertation explores original techniques for the construction of hypergraph models for computer vision applications. A hypergraph is a generalization of a pairwise simple graph, where an edge can connect any number of vertices. The expressive power of the hypergraph models places a special emphasis on the relationship among three or more objects, which has made hypergraphs better models of choice in a lot of problems. This is in sharp contrast with the more conventional graph representation of visual patterns where only pairwise connectivity between objects is described. The contribution of this thesis is fourfold:

(i) For the first time the advantage of the hypergraph neighborhood structure is analyzed. We argue that the summarized local grouping information contained in hypergraphs causes an 'averaging' effect which is beneficial to the clustering problems, just as local image smoothing may be beneficial to the image segmentation task.

(ii) We discuss how to build hypergraph incidence structures and how to solve the related unsupervised and semi-supervised problems for three different computer vision scenarios: video object segmentation, unsupervised image categorization and image retrieval. We compare our algorithms with state-of-the-art methods and the effectiveness of the proposed methods is demonstrated by extensive experimentation on various datasets.

(iii) For the application of image retrieval, we propose a novel hypergraph model — probabilistic hypergraph to exploit the structure of the data manifold by considering not only the local grouping information, but also the similarities between vertices in hyperedges.

(iv) In all three applications mentioned above, we conduct an in depth comparison between simple graph and hypergraph based algorithms, which is also beneficial to other computer vision applications.

Acknowledgements

I would like to express the deepest appreciation to my advisor, Professor Dimitris N. Metaxas, for his encouragement, guidance and support from the initial to the final level enabled me to develop an understanding of the subject. He has always directed me toward the interesting areas in our field, yet still given me great freedom to pursue independent work. He continually and convincingly conveyed a spirit of adventure and an excitement in regard to research. Without his guidance and persistent help this dissertation would not have been possible.

I want to thank Dr. Qingshan Liu, who has been working closely with me and contributed numerous ideas and insights to my research work.

I also thank my thesis committee members, Professor Ahmed Elgammal, Professor Vladimir Pavlovic, Professor Chandra Kambhamettu for their valuable suggestions regarding my research and writing of my dissertation. It is an honor for me to have each of them serve in my committees.

Last but not least, special thanks should be given to my colleagues, all the faculties and the staff members from CBIM (the Center for Computational Biomedicine Imaging and Modeling) and the Computer Science Department.

Dedication

This dissertation is dedicated to my parents: Zonggui Huang and Mingfang Yu.

Table of Contents

List of Tables

List of Figures

Chapter 1

Introduction

1.1 Motivation: Why Hypergraphs

In computer vision and other applied machine learning problems, a fundamental task is to cluster a set of data in a manner such that elements of the same cluster are more similar to each other than elements in different clusters. In these problems, we generally assume pairwise relationships among the objects of our interest. For example, a common distance measure for data points lying in a vector space is the Euclidean distance, which is used in a lot of unsupervised central clustering methods such as k-means [79], k-centers clustering [79] and affinity propagation [39]. Actually, a data set endowed with pairwise relationships can be naturally organized as a pairwise graph (for simplicity, we denote the pairwise graph as simple graph in the following), in which the vertices represent the objects, and any two vertices that have some kind of relationship are connected together by a graph edge. The simple graph partitioning problem in mathematics consists of dividing a graph G into k pieces, such that the pieces are of about the same size and there are few connections between the pieces. When $k = 2$, the problem is also referred to as the graph bisection problem or graph bi-partitioning problem. With a few notable exceptions, the similarities between objects in a simple graph are utilized to present the pairwise relationships. The simple graph can be undirected or directed, depending on whether the relationships among objects are symmetric or not. As to undirected graphs, a typical instance is the graph based image segmentation, in which pixel to pixel relations can be modelled as undirected edges because those relations are symmetric. As to directed graphs, a good instance is the World Wide Web, in which a hyperlink can be taken as a directed edge because the hyperlink based relationships are asymmetric. Usually a computed kernel matrix is associated to a directed or undirected graph, a lot of methods for unsupervised and semi-supervised learning can then be

formulated in terms of operations on this simple graph and achieve better clustering results compared to central clustering methods [92] [81] [107].

However, in many real world problems, it is not complete to represent the relations among a set of objects as simple graphs. This point of view is illustrated in a good example used in [113]. In this example, a collection of articles need to be grouped into different clusters by topics. The only information that we have is the authors of all the articles. One way to solve this problem is to construct an undirected graph in which two vertices are connected by an edge if they have at least one common author (Table 1.1 and Figure 1.1), and then spectral graph clustering can be applied [36] [18] [92]. Each edge weight of this undirected graph may be assigned as the number of authors in common between two articles. It is an easy, nevertheless, not natural way to represent the relations between the articles because this graph construction lose the information whether the same person is the author of three or more articles or not. Such information loss is unexpected because the articles by the same person likely belong to the same topic and hence the information is useful for our grouping task. A more natural way to remedy the information is to represent the data points as a hypergraph. An edge in a a hypergraph is called a hyperedge, which can connect more than two vertices; that is, a hyperedge is a subset of vertices. For this article clustering problem, it is quite straightforward to construct a hypergraph with the vertices representing the articles, and the hyperedges the authors (Figure 1). Each hyperedge contains all articles by its corresponding author. Furthermore, positive weights maybe be put on hyperedges to emphasize or weaken specific authors' work. For those authors working on a smaller range of fields, we may assign a larger weight to the corresponding hyperedge. Compared to simple pairwise graph, in this example hypergraph structure more completely illustrates the complex relationships among authors and articles.

Another reason to adopt hypergraphs is that, sometimes there does not exist a simple similarity measure for pairwise data points. Sometimes one may consider the relationship among three or more data points to determine if they belong to the same cluster. For example, in a k-lines clustering problem, we need to cluster data points in a d-dimensional vector space into k clusters where elements in each cluster are well approximated by a line [2]. In this problem, there does not exist a useful measure of similarity only using pairs of points, because we can

	e_1	e_2	e_3
v_1	1	0	0
v_2	1	0	1
v_3	0	0	1
v_4	0	0	1
v_5	0	1	0
v_6	0	1	1
v_7	0	1	0

Table 1.1: An author set $E = \{e_1, e_2, e_3\}$ and an article set $V = \{v_1, v_2, v_3, v_4, v_5, v_6, v_7\}$. The entry (v_i, e_j) is set to 1 if e_j is an author of article v_i and 0 otherwise.

not define a line only by a pair of data points. However, it is possible to define measures of similarity over three or more points that indicate how close they are to being collinear. This kind of similarity/dissimilarity measured over triples ore more of points can be referred as higher order relations, which is useful in a lot of model-based clustering task where the fitting error of a group of data points to a model can be considered a measure of the dissimilarity among them [1].

The study of measurement defined over triples or point sets of size greater than two is not new. In [1], a series of algorithms for hypergraph partitioning are analyzed and compared. These methods include clique expansion [116], star expansion [116], Rodriquez's Laplacian [86], Bolla's Laplacian [10] and Zhou's normalized Laplacian [113], etc. It is verified that that those methods are almost equivalent to each other and can be interconverted under specific conditions, especially for uniform hypergraphs whose hyperedge sizes are uniform within themselves. Another possible representation of higher order relations is a tensor, which is a generalization of matrices to higher dimensional arrays. The data tensor can be interpreted as a hypergraph and a co-clustering method can be proposed to solve partitioning problem based on spectral hypergraph clustering [19].

A powerful technique for partitioning simple graphs is spectral clustering. While the understanding of hypergraph spectral methods relative that of simple graphs is very limited, a number of authors have considered extensions of spectral graph theoretic methods to hypergraphs [86] [10] [113]. In our work, we adopt Zhou's normalized hypergraph Laplacian because of its efficiency and simplicity of implementation. In Zhou's work, spectral clustering techniques are generalized to hypergraphs; more specifically, the normalized cut approach of [92]. As in

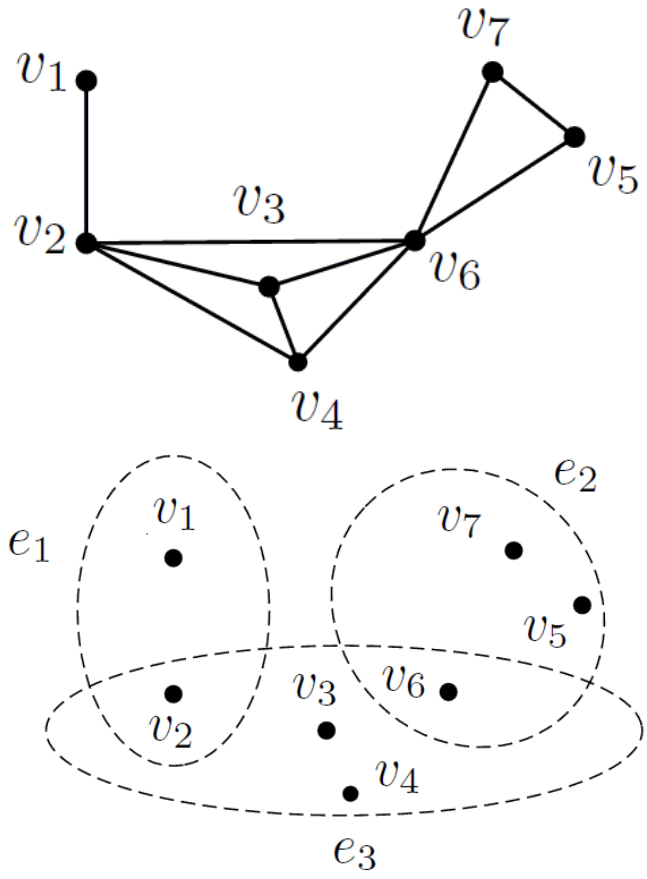

Figure 1.1: The hypergraph and corresponding simple graph, constructed from the incidence matrix in Table 1.1. Left: an undirected graph in which two articles are joined together by an edge if there is at least one author in common. Right: a corresponding hypergraph.

the case of simple graphs, a real-valued relaxation of the hypergraph normalized cut criterion leads to the eigen-decomposition of a positive semidefinite matrix called hypergraph laplacian, which can be regarded as an analogue of the Laplacian for simple graphs [24]. Based on the concept of hypergraph Laplacian, algorithms can be developed for unsupervised data partition, hypergraph embedding and transductive inference.

1.2 Contributions

This thesis describes original techniques for the construction of hypergraph models of three representative computer vision scenarios: video object segmentation, unsupervised image categorization and relevance feedback image retrieval. In the past decades, simple graph based methods have been applied in these applications and achieved considerable results. However, as illustrated above, the expressive power of the hypergraph models places a special emphasis on

the relationship among three or more objects, which may make them better models of choice in computer vision problems. This is in sharp contrast with the more conventional graph representation of visual patterns where only pairwise connectivity between objects is described. In this thesis, we choose to explore hypergraph incidence structures for above three applications. Through our theoretical discussion and experimental verification, we show that hypergraphs are better models to represent complex visual patterns on one hand and to keep important structural information on the other hand. In summary, the contribution of this thesis is fourfold:

(i) For the first time the advantage of the hypergraph neighborhood structure is analyzed. In our work, two hypergraph based algorithms, hypergraph cut and hypergraph ranking are adopted to solve optimization problems for computer vision under unsupervised and semi-supervised learning settings, respectively. We argue that the summarized local grouping information contained in hypergraphs causes an 'averaging' effect which is beneficial to the clustering problems in computer vision, just as local image smoothing may be beneficial to the image segmentation task.

(ii) We discuss how to build hypergraph incidence structures and how to solve the related unsupervised and semi-supervised problems for three different computer vision applications. We compare our algorithms with state-of-the-art methods and the effectiveness of the proposed methods is demonstrated by extensive experimentation on various datasets.

(iii) In the application domain of image retrieval, we propose a novel hypergraph model – probabilistic hypergraph to exploit the structure of the data manifold by considering not only the local grouping information, but also the similarities between vertices in hyperedges.

(iv) In all three applications mentioned above, we conduct an in depth comparison between simple graph and hypergraph based algorithms, which is also beneficial to other computer vision and machine learning applications.

1.3 Overview

The rest of this dissertation is organized as follows. In Chapter 2, we survey the related theoretic work on unsupervised and semi-supervised hypergraph learning. We lay heavy stress on the normalized hypergraph Laplacian and spectral hypergraph partitioning algorithms based on

it. Furthermore, for the first time the advantage of the hypergraph neighborhood structure is analyzed.

From Chapter 3 to Chapter 5, we will discuss how to build hypergraph incidence structures and how to solve the related unsupervised and semi-supervised problems for three different computer vision scenarios: video object segmentation, unsupervised image categorization and relevance feedback image retrieval. Two hypergraph based algorithms, hypergraph cut and hypergraph ranking are adopted to solve optimization problems under unsupervised and semi-supervised learning settings.

In Chapter 3, we present a framework of video object segmentation, in which we formulate the task of extracting prominent objects from a scene as the problem of hypergraph cut. We initially over-segment each frame in the sequence, and take the over-segmented image patches as the vertices in the graph. Then hypergraphs are used to represent the complex spatio-temporal neighborhood relationship among the patches. We assign each patch with several attributes that are computed from the optical flow and the appearance-based motion profile, and the vertices with the same attribute value is connected by a hyperedge. In this way the task of video object segmentation is equivalent to the hypergraph partition, which can be solved by a generalized spectral clustering technique – hypergraph cut algorithm.

In Chapter 4, we present a framework for unsupervised image categorization, in which images containing specific objects are taken as vertices in a hypergraph, and the task of image clustering is formulated as the problem of hypergraph partition. First, a novel method is proposed to select the region of interest (ROI) of each image, and then hyperedges are constructed based on shape and appearance features extracted from the ROIs. Each vertex (image) and its k-nearest neighbors (based on shape or appearance descriptors) form two kinds of hyperedges. The weight of a hyperedge is computed as the sum of the pairwise affinities within the hyperedge. Finally, hypergraph cut is used to solve the hypergraph partition problem of image categorization.

In Chapter 5, we propose a new transductive learning framework for image retrieval, in which the task of image search is formulated as the problem of hypergraph ranking. In this application, images are also taken as vertices in a hypergraph and a hyperedge is also formed by a centroid and its k-nearest neighbors. To further exploit the correlation information among

images, we propose a fuzzy hypergraph, which assigns each vertex to a hyperedge in a soft way. In the incidence structure of a fuzzy hypergraph, we describe both the higher order grouping information and the affinity relationship between vertices within each hyperedge. After feedback images are provided, our retrieval system ranks image labels by a transductive inference approach, which tends to assign the same label to vertices that share many incidental hyperedges, with the constraints that predicted labels of feedback images should be similar to their initial labels.

Finally, Chapter 6 summarizes the contributions of this work, along with a discussion of future work possibilities.

Chapter 2

Unsupervised and Semi-Supervised Learning with Hypergraphs

In this chapter at first we survey the related theoretic work on hypergraph learning. We survey a number of approaches from machine learning, VLSI CAD and graph theory that have been proposed for analyzing the structure of hypergraphs. We mention that there are two basic graph constructions that underlie all these studies; these constructions are essentially equivalent to the normalized Laplacian [1]. Then we focus on the derivation of spectral graph hypergraph theoretic methods for supervised and unsupervised learning, which is the theoretic basis of our work. At last we give a toy example on how to construct a hypergraph for practical problem.

2.1 Previous Work

The study of measurement defined over triples or point sets of size greater than two is not new. The primary focus of this literature is the study of topological and geometrical properties of these generalized measures [77]. While the work on n-metrics is theoretical, more practical works such as [48] try to measure triadic or higher order distance between its vertices. Multi-dimensional Scaling(DMS) [11] is a technique for embedding pairwise similarity or dissimilarity data in a low dimensional Euclidean space, which is used for the purposes of visualization and a preprocessing step for data analysis methods that require a coordinate representation of their input. Therefore, some researchers have developed generalizations of MDS to the case of triadic data or higher order data. representitive methods include Carroll & Chang's work which developed an algorithm for n-adic MDS using a generalization of the SVD to the case of n-dimensional matrices [17]; the work of Cox et al. which proposed an MDS algorithm based on a combination of a Gradient Descent and Isotonic Regression [27]; the works of Joly & LeCalv and Heiser & Bennani which developed axiomatic theories of triadic distances [52] [58].

The initial practical application of hypergraph partitioning algorithms occurs in the field of VLSI design and synthesis [2], which involves the partitioning of large circuits into k equally sized parts in a manner that minimizes the connectivity between the parts. In this application, the circuit elements are the vertices of the hypergraph and the nets that connect these circuit elements are the hyperedges [3]. The development of the tools for partitioning these hypergraphs is almost entirely heuristic and very little theoretical work exists that analyzes their performance beyond empirical benchmarks. The leading tools are based on two phase multi-level approaches [60]. In the first phase, a hierarchy of hypergraphs is constructed by incrementally collapsing the hyperedges of the original hypergraph according to some measure of homogeneity. In the second phase, starting from a partitioning of the hypergraph at the coarsest level, the algorithm works its way down the hierarchy and at each stage the partitioning at the level above serves as an initialization for the next level [35] [61].

The set of tools available for partitioning graphs are generalized and used on hypergraphs. An example is the generalization of Graph-Cut algorithms [14] for solving the max-flow min-cut problem on hypergraphs [83]. Some works consider to construct a graph that approximates the hypergraph and partition it; this partition in turn induces a vertex partitioning on the original hypergraph. Other works try to construct methods that operate directly on the hypergraph while implicitly working on its graph approximation. In this sense the previously proposed algorithms for partitioning a hypergraph can be divided into two categories. The first category aims at constructing a simple graph from the original hypergraph, and then partitioning the vertices by spectral clustering techniques. These methods include clique expansion [116], star expansion [55], Rodriquez's Laplacian [86] and clique averaging [2] etc. Clique Expansion and Star Expansion are two most commonly used graph approximations. Clique Expansion, as the name suggests, expands each hyperedge into a clique. Star expansion introduces a dummy vertex for each hyperedge and connects each vertex in the hyperedge to it [55]. As can be expected, the weights on the edges of the clique and the star determine the cut properties of the approximating graph [47] [57]. Another method to approximate the hypergraph using a weighted graph is clique averaging, which is closely related to clique expansion but is able to preserve more information contained in original hypergraphs. The second category of approaches define

a hypergraph 'Laplacian' using analogies from the simple graph Laplacian. Representative methods in this category include Bolla's Laplacian [10], Zhou's normalized Laplacian [113], etc. In [1], the above algorithms are analyzed and verified that they are equivalent to each other under specific conditions.

Another possible representation of higher order relations is a tensor, which is a generalization of matrices to higher dimensional arrays. In recent years, co-clustering of data with two or more than two types of entities has attracted increasing attention. The task of co-clustering is to simultaneously cluster the different types of entities. Bi-clustering is the name for co-clustering when there are two types of data need to be clustered. In this case not only the objects but also the features of the objects are clustered; i.e., the data is represented in a data matrix and the row and columns are clustered simultaneously. For example, in the text-mining scenario, we need to co-cluster documents and keywords, where a keyword is related to a document by the number of its occurrences in the document. The co-clustering of bi-type heterogeneous data has been widely investigated in a number of works such as [5] [31] [21]. If the data have more than two types, they can be represented as higher dimensional arrays. A real life example is audience-movies-casts in the film rating (collaborative filtering) scenario, where an audience gives a rating to a film that is cast by several actors or actresses. Although it is possible to cluster each type separately, but this approach would miss the potential leveraging that could be obtained from the interrelationships among different types. Representative work includes [7] [73] [74] which generalize bi-type methods for multi-type data, and [4] [20] which consider the interrelationships among all the entity types. In [19], the data tensor is interpreted as a hypergraph and propose a coclustering method based on spectral hypergraph partitioning.

2.2 Notation and Terminology

The key difference between the hypergraph and the simple graph lies in that the former uses a subset of the vertices as an edge, i.e., a *hyperedge* connecting more than two vertices. Let V represent a finite set of vertices and E a family of subsets of V such that $\bigcup_{e\in E} = V$, $G = (V, E, w)$ is called a hypergraph with the vertex set V and the hyperedge set E, and each hyperedge e is assigned a positive weight $w(e)$. For a vertex $v \in V$, its degree is defined to be

$d(v) = \sum_{\{e \in E | v \in e\}} w(e)$. For a hyperedge $e \in E$, its degree is defined by $\delta(e) = |e|$. Let us use D_v,D_e, and W to denote the diagonal matrices of the vetex degrees, the hyperedge degrees, and the hyperedge weights respectively. The hypergraph G can be represented by a $|V| \times |E|$ matrix H which $h(v, e) = 1$ if $v_H \in e_H$ and 0 otherwise. According to the definition of H, $d(v) = \sum_{e \in E} w(e)h(v, e)$ and $\delta(e) = \sum_{v \in V} h(v, e)$.

For a vertex subset $S \subset V$, let S^c denote the compliment of S. A cut of a hypergraph $G = (V, E, w)$ is a partition of V into two parts S and S^c. We say that a hyperedge e is cut if it is incident with the vertices in S and S^c simultaneously.

Given a vertex subset $S \subset V$, define the hyperedge boundary ∂S of S to be a hyperedge set which consists of hyperedges which are cut:

$$\partial S := \{e \in E | e \cap S \neq \emptyset, e \cap S^c \neq \emptyset\}. \tag{2.1}$$

Define the volume $volS$ of S to be the sum of the degrees of the vertices in S, that is, $volS := \sum v \in Sd(v)$. Moreover, define the volume of ∂S by

$$vol\partial S := \sum_{e \in \partial S} w(e) \frac{|e \cap S||e \cap S^c|}{|\delta(e)|}. \tag{2.2}$$

According to Equation 2.2, we have $vol\partial S = vol\partial S^c$. The definition given by above equations can be understood as follows: if we treat the defined volume of the hyperedge boundary across S and S^s as the connection between two clusters and the volume of S or S^c as the connection inside S or S^c, we try to obtain a partition in which the connection among the vertices in the same cluster is dense while the connection between two clusters is sparse. Then a natural partition can be formalized as follows:

$$\arg \min_{\emptyset \neq S \subset V} c(S) := vol(S, S^c) \left(\frac{1}{vol(S)} + \frac{1}{vol(S^c)} \right) \tag{2.3}$$

For a simple graph, $|e \bigcap S| = |e \bigcap S^c| = 1$, and $\delta(e) = 2$. According to the derivation in [19], the right-hand side of above equation reduces to the simple graph normalized cut [92] up to a factor $\frac{1}{2}$.

2.3 Hypergraph Learning Algorithms

In this section we introduce a number of existing methods for hypergraph learning which are surveyed in [1] and [2]. At first we present the methods which construct a graph representation using the initial structure of hypergraph. Then we introduce other methods define various hypergraph Laplacians. Particularly we focus on the derivation of normalized hypergraph Laplacian for supervised and unsupervised learning, which is the theoretic basis of our work.

2.3.1 Star Expansion

The star expansion algorithm constructs a graph $G^*(V^*, E^*)$ from original hypergraph $G(V, E)$ by introducing a new vertex for every hyperedge $e \in E$, thus $V^* = V \bigcup E$ [116]. It connects the new graph vertex e to each vertex in the hyperedge to it, i.e. $E^* = (u, e) : u \in e, e \in E$. Each hyperedge in E has a corresponding star in the graph G^* and that G^* is a bi-partite graph. Star expansion assigns the scaled hyperedge weight to each corresponding graph edge:

$$w^*(u, e) = \frac{w(e)}{\delta(e)} \tag{2.4}$$

Then the combinatorial or normalized Laplacian of the constructed simple graph is used to cluster vertices.

2.3.2 Clique Expansion

The clique expansion algorithm [116] constructs a graph $G^x(V, E^x V^2)$ from the original hypergraph $G(V, E)$ by replacing each hyperedge $e = (u_1, ..., u_{\delta(e)}) \in E$ with an edge for each pair of vertices in the hyperedge: $E^x = (u, v) : u, v \in e, e \in E$. The vertices in hyperedge e form a clique in the graph G^x. The edge weight $w^x(u, v)$ minimizes the difference between the weight of the graph edge and the weight of each hyperedge e that contains both u and v:

$$w^x(u, v) = \arg \min_{w^x(u,v)} \sum_{e \in E : u, v \in e} (w^x(u, v) - w(e))^2. \tag{2.5}$$

The solution of this criterion is

$$w^x(u,v) = \frac{1}{\mu(n,k)} \sum_{e \in E: u,v \in e} w(e). \tag{2.6}$$

where $\mu(n,k) = \begin{pmatrix} n-2 \\ k-2 \end{pmatrix}$ is the number of hyperedges that contain a particular pair of vertices; k is the size of the hyperedge and $|V| = n$. The relationship between a hyperedge and the edge weights in its clique in the above approach was the simplest possible, where one assumes that the hyperedge weight and the edge weights are equal to each other.

2.3.3 Clique Averaging

In [1], a new algorithm is proposed to transfer a hypergraph into a simple graph. In the method of clique averaging, the relationship between a hyperedge weight and its related simple graph weights are defined as follows:

$$w(e) = \begin{pmatrix} k \\ 2 \end{pmatrix}^{-1} \sum_{e_i, e_j \ in E, i<j} w(v_i, v_j). \tag{2.7}$$

the above equation states that the L_1 norm of the clique weights is proportional to the hyperedge weight. Without loss of generality we will assume that the set of hyperedges has been ordered in a lexicographic order based on the vertices incident on each hyperedge. A similar ordering is done on the set of graph edges too. We can now define the incidence matrix Υ. Υ is a zero-one matrix, that represents the incidence relationship between a hyperedge in a hypergraph and an edge in the related simple graph.

$$\Upsilon_{i,j} = \begin{cases} 1, & \text{if edge j is incident on hyperedge i} \\ 0, & \text{otherwise.} \end{cases} \tag{2.8}$$

Denote $\mathbf{d}_2$ as the vector of graph edge weights of length $\binom{n}{2}$ and, denote $\mathbf{d}_k$ the vector of hyperedge weights. Then Equation 2.7 can be written in matrix form as

$$\binom{k}{2} \Upsilon \mathbf{d}_2 = \mathbf{d}_k. \tag{2.9}$$

This equation assumes that $\mathbf{d}_2 \geq 0$, i.e., each element of the vector $\mathbf{d}_2$ is non-negative. If we enforce an upper bound $\mathbf{d}_2 \leq 1$ also, the graph approximation of hypergraph is given by the edge weight vector $\mathbf{d}_2$ that minimizes the following constrained minimization problem:

$$\min_{\mathbf{d}_2} \| \binom{k}{2} \Upsilon \mathbf{d}_2 - \mathbf{d}_k \|_F^2, 0 \leq \mathbf{d}_2 \leq 1. \tag{2.10}$$

Actually, this method is closely related to clique expansion. Denote $\mathbf{d}_2^e$ as the vector of approximation graph edge weights, we can derive the following equation from the solution equation of Clique Expansion 2.24:

$$\mu(n,k)\Upsilon \mathbf{d}_2^e = \Upsilon\Upsilon^\top \mathbf{d}_k. \tag{2.11}$$

Neglect the constants in Equations 2.9 and 2.11, they differ only in the right hand side by a pre-multiplication by the matrix $\Upsilon\Upsilon^\top$. This is a symmetric matrix, the effect of multiplying this matrix to d_k is equivalent to a convolution of the hyperedge weights by a quadratically decreasing kernel [1]. Thus $\Upsilon\Upsilon^\top d_k$ is a low passed version of d_k. This implies that Clique Expansion solves the same approximation problem as Clique Averaging, but instead of operating on the original hypergraph it operates on a low passed version of it. Although the approximation produced by Clique Averaging is of a higher quality theoretically, in practice there is virtually no difference between their performance, especially when values of σ are chosen carefully [2] (the parameter σ is used to convert a dissimilarity d into the affinity $\exp(-d/\sigma)$).

2.3.4 Bolla's Laplacian

Bolla defines a Laplacian for an unweighted hypergraph in terms of the diagonal vertex degree matrix D_v, the diagonal edge degree matrix D_e, and the incidence matrix H [10]:

$$L^o := D_v - HD_e^{-1}H^\top. \tag{2.12}$$

According to [10], the eigenvectors of Bolla's Laplacian L^o define the 'best' Euclidean embedding of the hypergraph. Bolla also shows a relationship between the spectral properties of L^o and the minimum cut of the hypergraph.

2.3.5 Rodriguez's Laplacian

In [86] a weighted graph $G^r(V, E^r = E^x)$ is constructed from an unweighted hypergraph $G(V, E)$. Like clique expansion, each hyperedge is replaced by a clique in the graph G^r. The weight $w^r(u, v)$ of an edge is set to the number of edges containing both u and v:

$$w^r(u, v) = |\{e \in E : u, v \in e\}|. \tag{2.13}$$

Then the graph Laplacian applied to G^r is expressed in terms of the hypergraph structure:

$$L^r(G^r) = D_v^r - HH^\top, \tag{2.14}$$

where D_v^r is the vertex degree matrix of the graph G^r. Like Bolla, Rodriguez also shows a relationship between the spectral properties of L^r and the cost of minimum partitions of the hypergraph.

2.3.6 Gibson's Dynamical System

In [42] the authors have proposed a dynamical system to cluster categorical data that can be represented using a hypergraph. They consider the following iterative process:

1. $s_{i,j}^{n+1} = \sum_{e:i\in e} \sum_{k\neq i\in e} w_e s_{k,j}^n$
2. Orthonormalize the vectors s_j^n.

And it is proven that the iterative procedure described above is the power method for calculating the eigenvectors of the adjacency matrix $S = D_v - HWH^{\ top}$.

2.3.7 Li's Adjacency Matrix

[71] formally define properties of a regular, unweighted hypergraph $G(V, E)$ in terms of the star expansion of the hypergraph. In particular, they define the $|V| \times |V|$ adjacency matrix of the hypergraph, $HH^\top$. They show a relationship between the spectral properties of the adjacency matrix of the hypergraph $HH^\top$ and the structure of the hypergraph.

2.3.8 Normalized Hypergraph Laplacian for Unsupervised and Semi-Supervised Learning

Recall the cost function in Equation 2.3:

$$c(S) = vol(S, S^c)\left(\frac{1}{vol(S)} + \frac{1}{vol(S^c)}\right).$$

The above objective function characterizes how an optimal partitioning of a given hypergraph should look like: the volume of the boundary $vol(\partial S)$ is minimized, while the 'size' of S and Sc are balanced; otherwise, a small $vol(S)$ or $vol(Sc)$ will make the objective value prohibitively large. According the derivation in [19], the objective value $c(S)$ coincides with a Rayleigh quotient. Let a column vector q have elements

$$q(v) := \begin{cases} +\sqrt{\eta_2/\eta_1}, & \text{if } v \in S \\ -\sqrt{\eta_1/\eta_2}, & \text{if } v \in S^c. \end{cases} \tag{2.15}$$

where $\eta_1 = vol(S)$ and $\eta_2 = vol(S^c)$, then

$$c(S) = \frac{q^T L q}{q^T \Lambda q}, \tag{2.16}$$

where $L = D_v - HWD_e^{-1}H^\top$ is called the Laplacian of the hypergraph and Λ is the diagonal matrix with diagonal elements equal to $vol(v)$. We call q the partition vector. The claim implies that the problem of finding an optimal hypergraph cut can be reduced to computing a vector q in the form 2.15 which minimizes the quotient 2.16. However, this is a combinatorial optimization problem that is NP-complete [41]. From standard results in linear algebra, minimizing the above quotient over real vectors q, is equivalent to finding the bottom eigenvector of the matrix pencil (L, Λ). According to [92], this problem can be further reduced to solve the second smallest eigenvector of the following matrix:

$$\Delta = I - D_v^{-1/2} H W D_e^{-1} H^\top D_v^{-1/2}, \tag{2.17}$$

where Δ is called the normalized hypergraph Laplacian. Actually, this result can be reached from another direction. For a hypergraph partition problem, the normalized cost function [113] $\Omega(f)$ could be defined as

$$\frac{1}{2}\sum_{e\in E}\sum_{u,v\in e}\frac{w(e)h(u,e)h(v,e)}{\delta(e)}\left(\frac{f(u)}{\sqrt{d(u)}}-\frac{f(v)}{\sqrt{d(v)}}\right)^2, \tag{2.18}$$

where the vector f is the image labels to be learned. By minimizing this cost function, vertices sharing many incidental hyperedges are guaranteed to obtain similar labels. Defining $\Theta = D_v^{-\frac{1}{2}} H W D_e^{-1} H^T D_v^{-\frac{1}{2}}$, we can derive Equation 5.4 as follows:

$$\begin{aligned}\Omega(f) =& \sum_{e\in E}\sum_{u,v\in e}\frac{w(e)h(u,e)h(v,e)}{\delta(e)}\left(\frac{f^2(u)}{d(u)}-\frac{f(u)f(v)}{\sqrt{d(u)d(v)}}\right)\\ =& \sum_{u\in V} f^2(u)\sum_{e\in E}\frac{w(e)h(u,e)}{d(u)}\sum_{v\in V}\frac{h(v,e)}{\delta(e)}\\ &-\sum_{e\in E}\sum_{u,v\in e}\frac{f(u)h(u,e)w(e)h(v,e)f(v)}{\sqrt{d(u)d(v)}\delta(e)}\\ =& f^T(I-\Theta)f,\end{aligned} \tag{2.19}$$

where I is the identity matrix. Above derivation shows that (i) $\Omega(f,w) = f^T(I-\Theta)f$ if and only if $\sum_{v\in V}\frac{h(v,e)}{\delta(e)} = 1$ and $\sum_{e\in E}\frac{w(e)h(u,e)}{d(u)} = 1$, which is true because of the definition of $\delta(e)$ and $d(u)$; (ii) $\Delta = I - \Theta$ is a positive semi-definite matrix introduced above – the normalized hypergraph Laplacian and $\Omega(f) = f^T\Delta f$. The above cost function has the similar formulation to the normalized cost function of a simple graph $G_s = (V_s, E_s)$:

$$\begin{aligned}\Omega_s(f) &= \frac{1}{2}\sum_{v_i,v_j\in V_s} A_s(i,j)\left(\frac{f(i)}{\sqrt{D_{ii}}}-\frac{f(j)}{\sqrt{D_{jj}}}\right)^2\\ &= f^T(I - D^{-\frac{1}{2}}A_sD^{-\frac{1}{2}})f = f^T\Delta_s f,\end{aligned} \tag{2.20}$$

where D is a diagonal matrix with its (i,i)-element equal to the sum of the i^{th} row of the affinity matrix A_s; $\Delta_s = I - \Theta_s = I - D^{-\frac{1}{2}}A_sD^{-\frac{1}{2}}$ is called the normalized simple graph Laplacian. In an unsupervised framework, Equation 5.4 and Equation 5.6 can be optimized by the eigenvector related to the smallest nonzero eigenvalue of Δ and Δ_s [113], respectively.

In the transductive learning setting [113], we define a vector y to introduce the labeling information and to assign their initial labels to the corresponding elements of y: $y(v) = 1$, if a vertex v is in the positive set Pos, $y(v) = -1$, if it is in the negative set Neg. If v is unlabeled,

$y(v) = 0$. To force the assigned labels to approach the initial labeling y, a regularization term is defined as follows:

$$\|f - y\|^2 = \sum_{u \in V} (f(u) - y(u))^2. \tag{2.21}$$

After the feedback information is introduced, the learning task is to minimize the sum of two cost terms with respect to f [112] [113], which is

$$\Phi(f) = f^T \Delta f + \mu \|f - y\|^2, \tag{2.22}$$

where $\mu > 0$ is the regularization parameter. Differentiating $\Phi(f)$ with respect to f, we have

$$f = (1 - \gamma)(I - \gamma\Theta)^{-1} y, \tag{2.23}$$

where $\gamma = \frac{1}{1+\mu}$. This is equivalent to solving the linear system $((1 + \mu)I - \Theta) f = \mu y$.

For the simple graph, we can simply replace Θ with Θ_s to fulfill the transductive learning.

2.3.9 The Connections between Hypergraph Learning Algorithms

In [1], different hypergraph learning algorithms are analyzed and proved to be equivalent to each other. At first, [1] verifies that for a k-uniform hypergraph (each hyperedge contains a fixed number of k vertices),the eigenvectors of the normalized Laplacian for the bipartite graph G_c^* (obtained from Star Expansion) are exactly the eigenvectors of the normalized Laplacian for the standard clique expansion graph G^x. This is a surprising result since the two graphs are completely different in the number of vertices and the connectivity between these vertices. Even for non-uniform hypergraphs, the difference between two formulations are not large and may obtain similar decomposed eigenvectors.

[1] also proved that all different hypergraph Laplacians correspond to either clique or star expansion of the original hypergraph under specific conditions. Bolla's Laplacian corresponds to the unnormalized Laplacian of the associated clique expansion with the appropriate weighting function. The Rodriguez Laplacian can similarly be shown to be the unnormalized Laplacian of the clique expansion of an unweighted graph with every hyperedge weight set to 1. Gibson's

algorithm calculates the eigenvectors of the adjacency matrix for the clique expansion graph. For Zhou's normalized Laplacian, it is equivalent to constructing a star expansion and using the normalized Laplacian defined on it.

2.4 Toy Examples

In this section, we quote two examples to explain how to construct hypergraphs for practical problems. The first example is also used in Zhou's work [113].

In the first example, the zoo data set from UCI Machine Learning Depository [38] is used. The zoo data set is usually referred to as the so-called categorical data. It contains totally 7 types and 101 animals:

1 – (41 kinds of animals) aardvark, antelope, bear, boar, buffalo, calf, cavy, cheetah, deer, dolphin, elephant, fruitbat, giraffe, girl, goat, gorilla, hamster, hare, leopard, lion, lynx, mink, mole, mongoose, opossum, oryx, platypus, polecat, pony, porpoise, puma, pussycat, raccoon, reindeer, seal, sealion, squirrel, vampire, vole, wallaby,wolf;

2 – (20 kinds of animals) chicken, crow, dove, duck, flamingo, gull, hawk, kiwi, lark, ostrich, parakeet, penguin, pheasant, rhea, skimmer, skua, sparrow, swan, vulture, wren;

3 – (5 kinds of animals) pitviper, seasnake, slowworm, tortoise, tuatara;

4 – (13 kinds of animals) bass, carp, catfish, chub, dogfish, haddock, herring, pike, piranha, seahorse, sole, stingray, tuna;

5 – (4 kinds of animals) frog, frog, newt, toad;

6 – (8 kinds of animals) flea, gnat, honeybee, housefly, ladybird, moth, termite, wasp;

7 – (10 kinds of animals) clam, crab, crayfish, lobster, octopus, scorpion, seawasp, slug, starfish, worm.

Specifically, each instance in this dataset is described by one or more attributes. Each attribute takes only a small number of values, each corresponding to a specific category. Attribute values cannot be naturally ordered linearly as numerical values. Totally there are 16 attributes as follows:

1. hair: Boolean
2. feathers: Boolean

3. eggs: Boolean
4. milk: Boolean
5. airborne: Boolean
6. aquatic: Boolean
7. predator: Boolean
8. toothed: Boolean
9. backbone: Boolean
10. breathes: Boolean
11. venomous: Boolean
12. fins: Boolean
13. legs: Numeric (set of values: 0,2,4,5,6,8)
14. tail: Boolean
15. domestic: Boolean
16. catsize: Boolean

In our experiments, we constructed a hypergraph for the zoo dataset, where attribute values were regarded as hyperedges. For Boolean attribute, we construct two hyperedges according to the value of each animal on each attribute ('true' or 'false'). For numeric value attribute (the attribute 13), we construct 6 hyperedges, according to the numerical value of each animal on this attribute. Then we totally get 36 hyperedges. The weights for all hyperedges were simply set to 1. How to choose suitable weights is definitely an important problem requiring additional exploration however.

The first task we addressed is to embed the animals in the zoo dataset into Euclidean space. We embedded those animals into Euclidean space by using the eigenvectors of the hypergraph Laplacian associated with the smallest eigenvalues. In Figure 2.1, the eigenvectors associated with the second and the third smallest eigenvalues are used as x and y coordinates. All the animals are illustrated in this figure and animals in a specific type use a specific text color. For example, all the mammals are shown red in Figure 2.1.

From this figure, It is apparent that most animals are well separated according their type in their Euclidean representations. For example, all the mammals distribute on the left hand

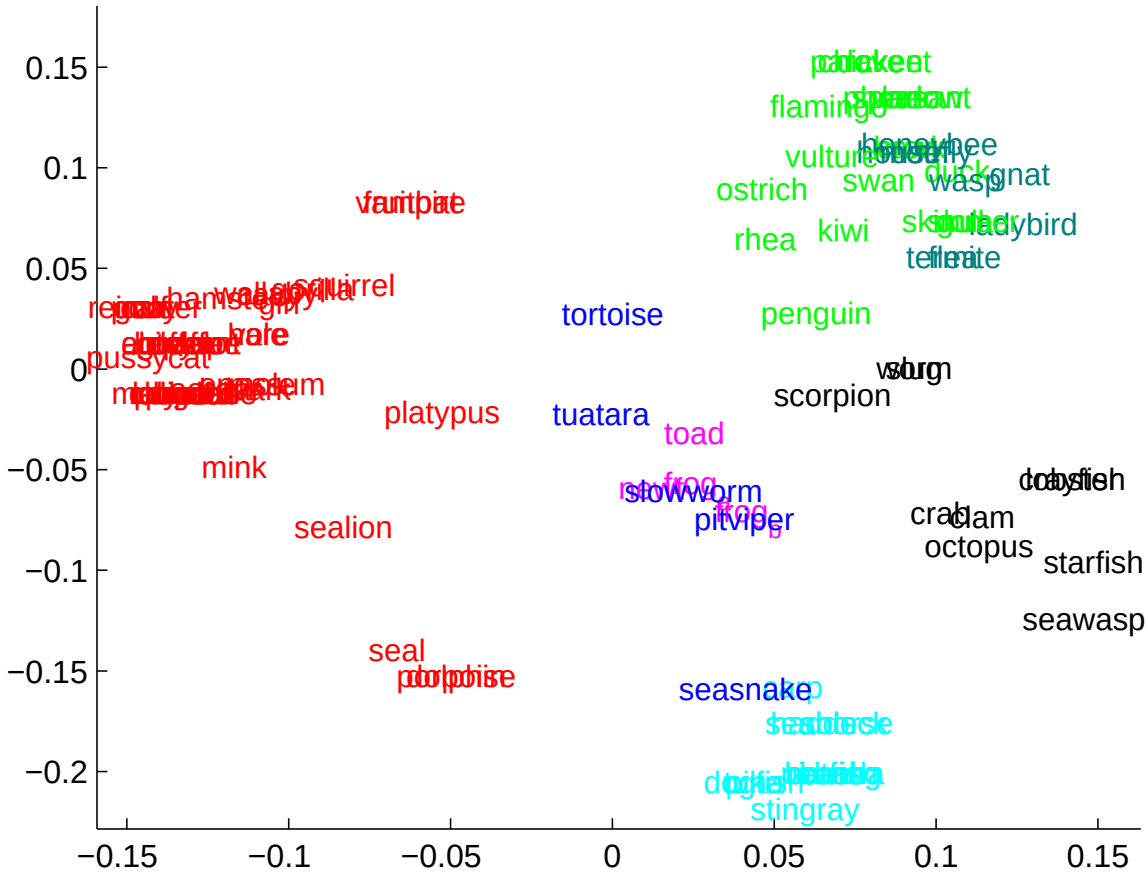

Figure 2.1: We embedded zoo data set animals into Euclidean space by using the eigenvectors associated with the second and the third smallest eigenvalues.

side of Figure 2.1; all the fishes distribute on the bottom of the graph. Moreover, it deserves a further look on the transition area of the graph. Platypus is significantly mapped to the positions between class 1 (mammals), and class 3 (reptiles). A similar observation also holds for sea-snake, which is very close to fish. Even in Figure 2.2 and Figure 2.3, we can still find that animals distribute intensively according to their category.

The second example is illustrated in Figure 2.4, which shows an example to explain how to construct a hypergraph. $v_1, v_2, ..., v_6$ are six points in a 2-D space and their interrelationships could be represented as a simple graph, in which pairwise distances between every vertex and its neighbors are marked on the corresponding edges. Assuming that each vertex and its two-nearest neighbors form a hyperedge, a vertex-hyperedge matrix H could be given as Figure 2.4(b). For example, the hyperedge e_4 is composed of vertex v_4 and its two nearest

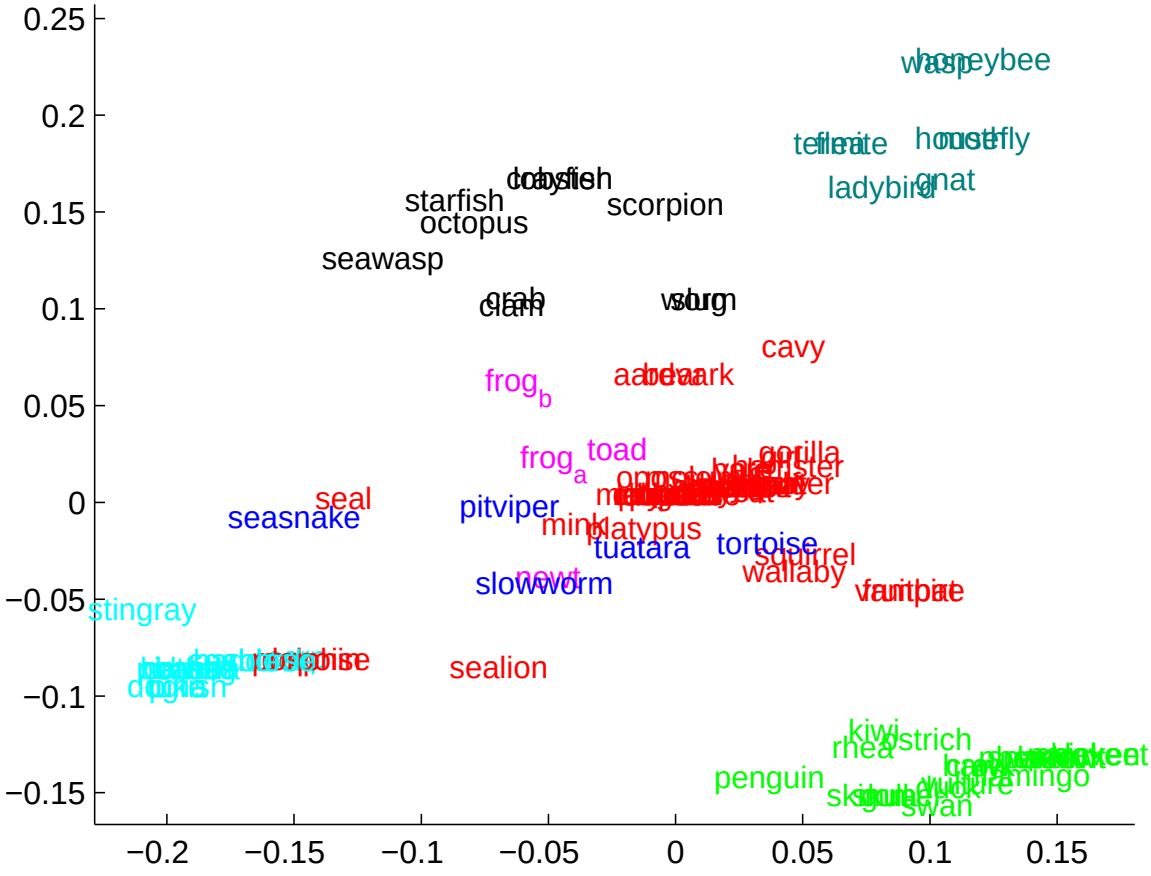

Figure 2.2: We embedded zoo data set animals into Euclidean space by using the eigenvectors associated with the third and the fourth smallest eigenvalues.

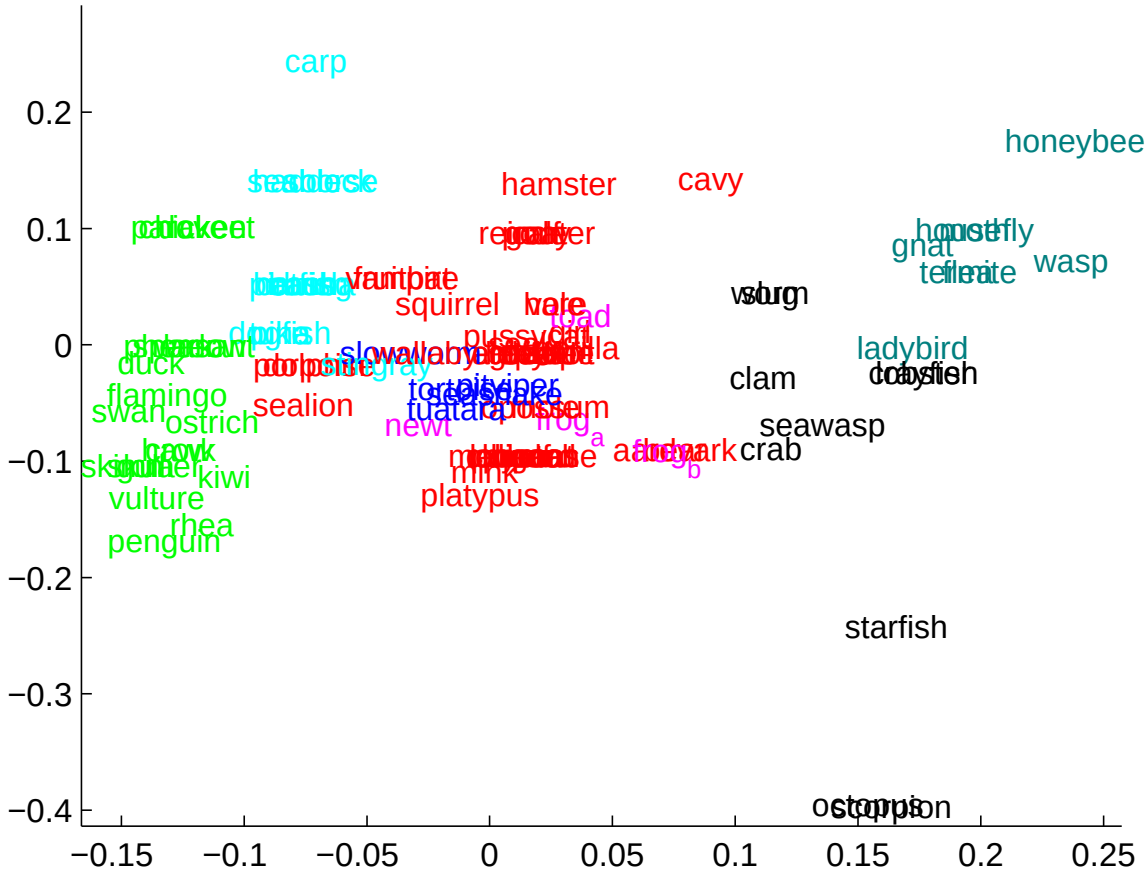

Figure 2.3: We embedded zoo data set animals into Euclidean space by using the eigenvectors associated with the fourth and the fifth smallest eigenvalues.

neighbors v_3 and v_5. Among all the hyperedges constructed in this example, e_1, e_2, e_3 correspond to the vertices subset $\{v_1, v_2, v_3\}$ and e_5, e_6 correspond to the vertices subset $\{v_4, v_5, v_6\}$ (Figure 2.4(c)). To measure the affinity among the vertices in each hyperedge, we can define the hyperedge weight as the sum of reciprocals of all the pairwise distances in a hyperedge.

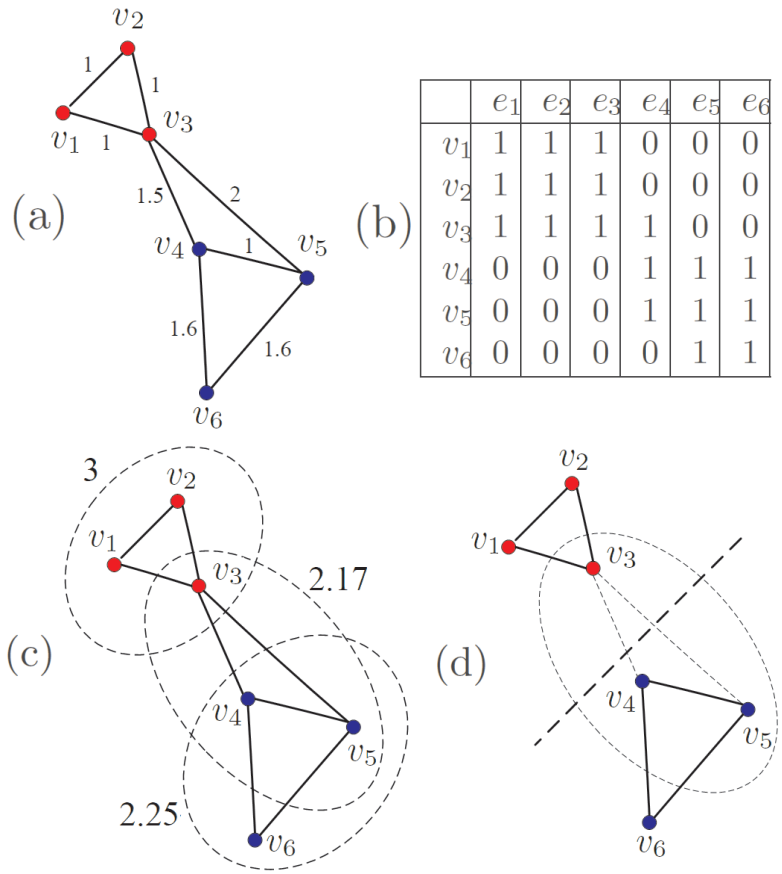

	e_1	e_2	e_3	e_4	e_5	e_6
v_1	1	1	1	0	0	0
v_2	1	1	1	0	0	0
v_3	1	1	1	1	0	0
v_4	0	0	0	1	1	1
v_5	0	0	0	1	1	1
v_6	0	0	0	0	1	1

Figure 2.4: (a): A simple graph of six points in 2-D space. Pairwise distances between v_i and its neighbors are marked on the corresponding edges. (b) The H matrix. The entry (v_i, e_j) is set to 1 if a hyperedge e_j contains v_i, or 0 otherwise. (c): The corresponding hypergraph w.r.t. the H matrix. The hyperedge weight is defined as the sum of reciprocals of all the pairwise distances in a hyperedge. (d) A hypergraph partition which is made on e_4.

In order to bipartition the hypergraph in Figure 2.4(c)), intuitively the hyperedges with the smallest weights should be removed, and at the same time as many hyperedges with larger weights as possible should be kept. Since e_4 has the smallest hyperedge weight, a hypergraph partition could be made on it (Figure 2.4(d)) to classify $v_1, v_2, ..., v_6$ into two groups. This is exactly the result obtained by normalized hypergraph cut.

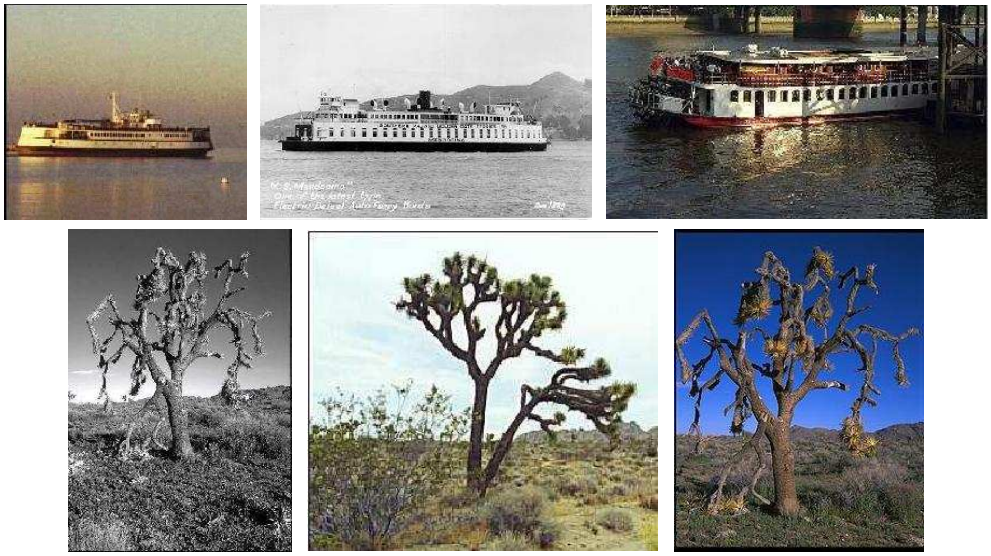

Figure 2.5: Six images from *Caltech-101* [69]. The first three images in the first row are from the 'ferry' class; the last three images in the second row are from the 'joshua tree' class.

	v_1	v_2	v_3	v_4	v_5	v_6
v_1	1.0000	0.5342	0.4795	0.2566	0.4558	0.2667
v_2	0.5342	1.0000	0.4603	0.2935	0.4311	0.2758
v_3	0.4795	0.4603	1.0000	0.5976	0.6547	0.6083
v_4	0.2566	0.2935	0.5976	1.0000	0.7062	0.8245
v_5	0.4558	0.4311	0.6547	0.7062	1.0000	0.7804
v_6	0.2667	0.2758	0.6083	0.8245	0.7804	1.0000

Table 2.1: The similarity matrix for the six data points corresponding to six images in Fig 2.5.

2.5 Analysis of the Advantage of the Hypergraph Structure

In order to better explain the neighborhood structure of hypergraphs, we can revisit the Clique Expansion [116] algorithm and inversely transfer a hypergraph into a simple graph. Clique Expansion builds a new simple graph from a hypergraph by replacing each hyperedge with edges for each pair of vertices in the hyperedge. In this new simple graph, the pairwise edge weight between two vertices is proportional to the sum of their incident hyperedge weights:

$$w^x(u,v) = \frac{1}{\mu(n,k)} \sum_{e \ inE:u,v\in e} w(e). \tag{2.24}$$

According to the analysis in Agarwal's work [1], for a uniform hypergraph, it is verified that the eigenvectors of the hypergraph normalized Laplacian are equivalent to the eigenvectors of the simple graph obtained by Clique Expansion. For a nonuniform hypergraph, the eigenvectors

	e_1	e_2	e_3	e_4	e_5	e_6
v_1	1	1	0	0	0	0
v_2	1	1	0	0	0	0
v_3	1	1	1	0	0	0
v_4	0	0	0	1	1	1
v_5	0	0	1	1	1	1
v_6	0	0	1	1	1	1

Table 2.2: The H matrix for the six data points corresponding to six images in Fig 2.5. Here each point and its two nearest neighbors are taken as one hyperedge.

of the simple graph obtained by Clique Expansion is very close to those of the hypergraph normalized Laplacian. Consider that we take the sum of the pairwise similarities inside a hyperedge as the hyperedge weight (similar configurations are used in the following chapters). We transfer this hypergraph into a simple graph by Clique Expansion. In the obtained simple graph, the edge weight between two vertices v_i and v_j is not decided by the pairwise affinity $A_{i,j}$ between two vertices, but the averaged neighboring affinities close to them; furthermore, this edge weight is influenced more by those pairwise affinities whose two incident vertices share more hyperedges with v_i and v_j. Through the hyergraph, the 'higher order' or 'local grouping' information is used for the construction of graph neighborhood. We argue that such an 'averaging' effect may be beneficial to the image clustering task, just as local image smoothing may be beneficial to the image segmentation task.

To clearly show the advantage of the hypergraph model over simple graph based model, here we present an example including six images from two classes, shown in Figure 2.5. In Figure 2.6, these six images are denoted as six vertices $v_1, v_2, ..., v_6$ and pairwise affinities between each pair of vertices are presented in the matrix A^t(Table 2.1). A simple graph is built in Figure 2.6(above), in which each vertex is connected to its two nearest neighbors. The edge weight between two vertices equals their pairwise affinity if there is an edge between them; otherwise it is set to be 0. Intuitively this simple graph can be partitioned by removing two weakest edges v_1v_3 and v_2v_3. This is the result of the normalized cut to minimize the follow formula:

$$NScut(S, S^c) := Scut(S, S^c) \left(\frac{1}{assoc(S, V)} + \frac{1}{assoc(S^c, V)} \right), \tag{2.25}$$

where $Scut(S, S^c) = \sum_{u \in S, v \in S^c} w^s(u, v)$ and $w^s(u, v)$ is a simple graph edge weight between u and u; $assoc(S, V) = \sum_{u \in S, v \in V} w^s(u, v)$ and $assoc(S^c, V)$ is similarly defined. According to

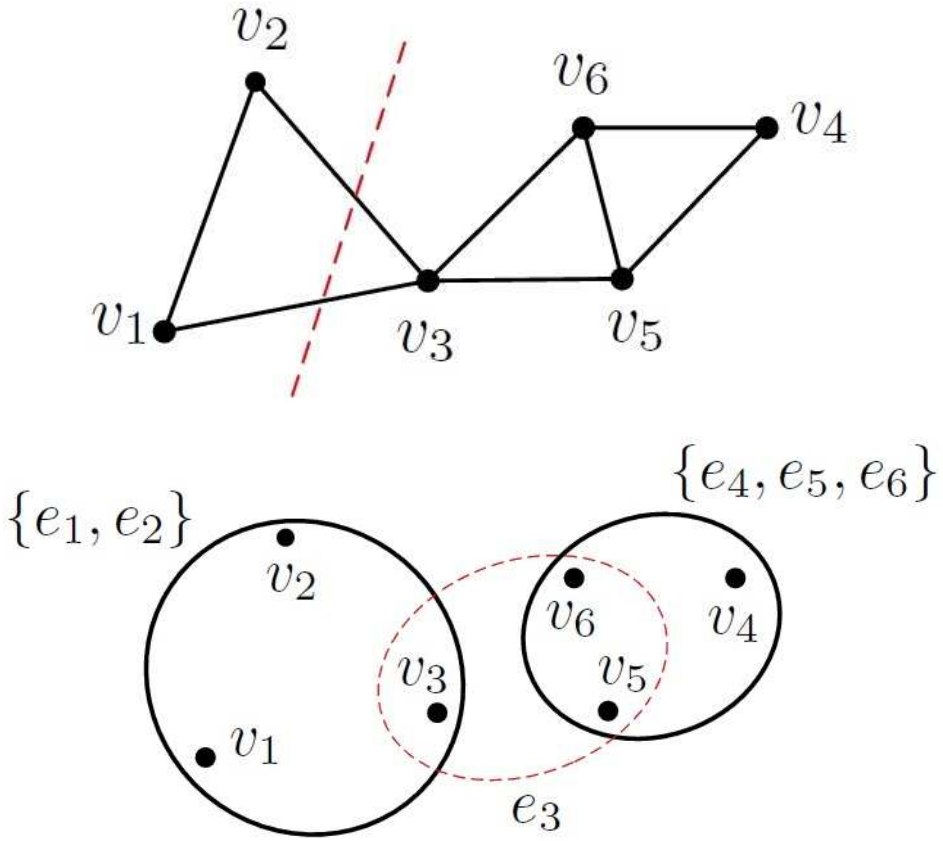

Figure 2.6: The simple graph and corresponding hypergraph, constructed from the similarity matrix in Table 2.1. Note that in the hypergraph, e_3 is cut and the hypergraph is divided to two groups: $\{v_1, v_2, v_3\}$ and $\{v_4, v_5, v_6\}$. In the simple graph each data point is corrected to its two nearest neighbors; the edges are cut to form two groups $\{v_1, v_2\}$ and $\{v_3, v_4, v_5, v_6\}$. The point v_3 is not correctly classified in the simple graph.

this criterion, v_3 (a ferry) is falsely classified into the 'joshua tree' class.

For comparison, we construct a hypergraph in Figure 2.6(Bottom). Let each vertex and its two-nearest neighbors form a hyperedge, a vertex-hyperedge matrix H could be formed (Table 2.1). Among all the hyperedges constructed in this example, e_1 and e_2 correspond to $\{v_1, v_2, v_3\}$; e_3 corresponds to $\{v_3, v_5, v_6\}$; e_4, e_5 and e_6 correspond to $\{v_4, v_5, v_6\}$ (Figure 2.6(Bottom)). We take the sum of the pairwise similarities inside a hyperedge as the hyperedge weight. The hyperedge weights for e_1 to e_6 are $\{1.4740, 1.4740, 2.0434, 2.3111, 2.3111, 2.3111\}$. In order to bipartition the hypergraph in Figure 2.6(Bottom), intuitively the 'weakest' vertex group or the hyperedge set with the smallest total weights should be removed, and at the same time hyperedge sets with larger total weights should be kept as many as possible. For the three vertex group ($\{v_1, v_2, v_3\}$, $\{v_3, v_5, v_6\}$ and $\{v_4, v_5, v_6\}$) mentioned above, the total hyperedge

weights are 2.9480, 2.0434 and 6.9333, respectively. Therefore a hypergraph partition could be made by removing e_3 and the six vertices could be correctly classified into two groups. From another perspective, if we transfer the hypergraph on the left to a new simple graph (**NOT** the simple graph shown in Figure 2.6(Above)) by Clique Average, in this simple graph the pairwise edge weights within $\{v_1, v_2, v_3\}$ or $\{v_4, v_5, v_6\}$ will be strengthened, while edge weights within $\{v_3, v_5, v_6\}$ will be weakened; thus this simple graph can produce the correct classification result. This is exactly the classification result achieved by above normalized hypergraph partition algorithm.

In the following, we use hypergraph incidence structures in three computer vision applications and verified the advantage of hypergraph models statistically by extensive experiments.

Chapter 3

Hypergraph based Video Object Segmentation

In this chapter, we present a new framework of video object segmentation, in which we formulate the task of extracting prominent objects from a scene as the problem of hypergraph cut. We initially over-segment each frame in the sequence, and take the over-segmented image patches as the vertices in the graph. Then we use *hypergraph* to represent the complex spatio-temporal neighborhood relationship among the patches. We assign each patch with several attributes that are computed from the optical flow and the appearance-based motion profile, and the vertices with the same attribute value is connected by a hyperedge. Through all the hyperedges, not only the complex non-pairwise relationships between the patches are described, but also their merits are integrated together organically. The task of video object segmentation is equivalent to the hypergraph partition, which can be solved by the hypergraph cut algorithm. The effectiveness of the proposed method is demonstrated by extensive experiments on nature scenes.

3.1 Introduction

Video object segmentation is a hot topic in the communities of computer vision and pattern recognition, due to its potential applications in background substitution, video tracking, general object recognition, and content-based video retrieval. Compared to the object segmentation in static images, temporal correlation between consecutive frames, i.e., motion cues, will alleviate the difficulties in video object segmentation. Prior works can be divided into two categories. The first category aims at detecting objects in videos mainly from input motion itself. Representative work is layered motion segmentation [82] [96] [111]. They assume fixed number of layers and near-planar parametric motion models for each layer, and then employ some reasoning scheme to obtain the motion parameters for each layer. The segmentation results are obtained by assigning each pixel to one layer. When a non-textured region is presented in the scene, layered

segmentation methods may not provide satisfactory results due to only using motion cues. The methods in [66] [90] [104] also belong to this category. They predefine explicit geometric models of the motion, and use them to infer the occluded boundaries of objects. When the motion of the data deviates from the predefined models, the performances of these methods will be degenerated.

The second category of approaches attempts to segment video objects with spatio-temporal information. In [30], the mean shift strategy is employed to hierarchically cluster pixels of 3D space-time video stack, which are mapped to 7-dimensional feature points, i.e., three color components and 4 motion components. [110] first uses the appearance cue as a guide to detect and match interest points in two images, and then based on these points, the motion parameters of layers are estimated by the RANSAC algorithm [37]. The method in [23] begins with a layered parametric flow model, and the objects are extracted and tracked by both the region information (provided by appearance and motion coherence) and the boundary information (provided by the result of the active contour). Recently, a complicated method is introduced to detect and group object boundaries by integrating appearance and motion cues [97]. This approach starts from over-segmented images, and then motion cues estimated from segments and fragments are fed to learned local classifiers. Finally the boundaries of objects are obtained by a global inference model. Different from the above methods, Shi and Malik [91] have proposed a pairwise graph based model to describe the spatio-temporal relations in the 3D video data and have employed the spectral clustering analysis to solve the video segmentation problem, which is beautiful and has achieved promising results.

As introduced in Chapter 1 and Chapter 2, in many real world problems, maybe it is more complete to represent the relations among a set of objects as hypergraphs. For example, based on affinity functions computed from different features, we may build different pairwise graphs. To combine these representations, one may consider a weighted similarity measure using all the features, but simply taking their weighted sum as the new affinity function may lead to the loss of some information which is crucial to the clustering task. On the other hand, sometimes one may consider the relationship among three or more data points to determine if they belong to the same cluster. In this chapter, we propose a novel framework of video object segmentation

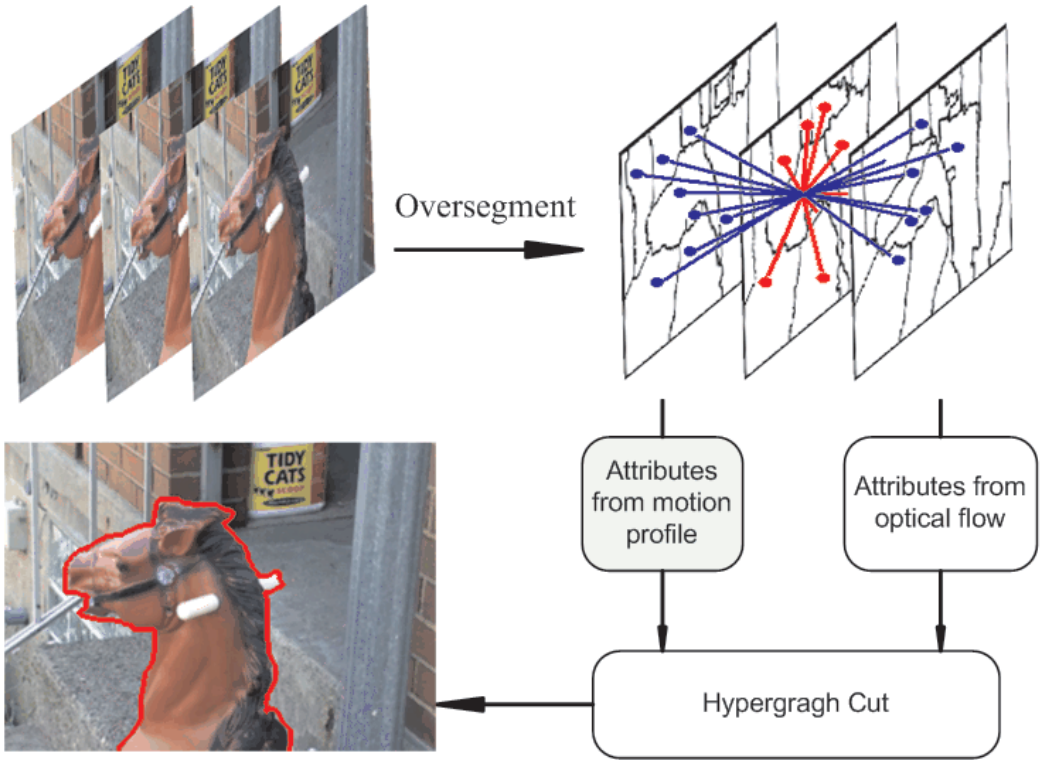

Figure 3.1: Illustration of our framework.

based on *hypergraph*. Inspired by [97], we first over-segment the images by the appearance information, and we take the over-segmented image patches as the vertices of the graph for further clustering. The relationship between the image patches becomes complex due to the coupling of spatio-temporal information, while forcibly squeezing the complex relationship into pairwise will lead to the loss of information. To deal with this issue, we present to use the hypergraph [113] to model the relationship between the over-segmented image patches. We describe the over-segmented patches in spatio-temporal domain with the optical flow and the appearance based motion profile. The hypergraph is presented to integrated them together closely. Graph vertices which have the same attribute value can be connected by a hyperedge. Through all the hyperedges, the complex non-pairwise relationship between image patches is described. We take the task of attribute assignment as a problem of binary classification. We perform the spectral analysis on two different motion cues respectively, and produce several attributes for each patch by some representative spectral eigenvectors. Finally, we use the hypergraph cut algorithm to obtain global optimal segmentation of video objects under a variety of conditions, as evidenced by extensive experiments.

The rest chapter is organized as follows: the proposed framework is introduced in Section 3.2; we address the hyperedge computation in Section 3.3; experiments are reported in Section 3.4, and followed by the conclusions finally.

3.2 Overview of the proposed Framework

Video object segmentation can be regarded as clustering the image pixels or patches in the spatio-temporal domain. Graph model is demonstrated to be a good tool for data clustering, including image and video segmentation [91] [93]. In a simple graph, the data points are generally taken as the vertices, and the similarity between two data point is connected as an edge. However, for video object segmentation, the relationship among the pixels or patches may be far more complicated than the pairwise relationship due to the coupling of spatio-temporal information. Within a simple graph, these non-pairwise relationships should be squeezed to pairwise ones enforcedly, so that some useful information may be lost. In this section, we present to use the hypergraph to describe the complex spatio-temporal structure of video sequences. Before we overview the hypergraph based framework, we first introduce the concept of the hypergraph.

3.2.1 HyperGraph based Framework of Video Object Segmentation

In this chapter, we develop a video object segmentation framework based on the hypergraph, shown in Figure 4.1. There contains three main components: the selection of the vertices, the hyperedge computation, and the hypergraph partition.

Inspired by [97], we initially over-segment the sequential images into small patches with consistent local appearance and motion information, as shown in Figure 3.2. Using the pixel values in the LUV color space, we get a 3-D features (l, u, v) for each pixel in the image sequence. With this feature, we adopt a multi-scale graph decomposition method [25] to do over-segmentation, for its ability to capture both the local and middle range relationship of image intensities, and its linear time complexity. This over-segmentation provides a good preparation for high-level reasoning of spatial-temporal relationship among the patches. We take these over-segmented patches as the vertices of the graph.

The computation of the hyperedges is actually equivalent to generating some attributes of the image patches. We treat the task of attribute assignment as a problem of binary classification according to different criteria. We first perform the spectral analysis in the spatio-temporal domain on two different motion cues, i.e., the optical flow and the appearance based motion profile, respectively. Then we cluster the data into two classes (2-way cut) on each spectral eigenvector respectively. Some representative 2-way cut results are finally selected to indicate the attributes of the patches. By analyzing the 2-way cut results, we assign different weights to different hyperedges. The details are described in Section 3.3.

After we obtain the vertices and the hyperedges, the hypergraph is built. We will use the hypergraph cut to partition the video into different objects.

Figure 3.2: A frame of oversegmentation results extracted from the rocking-horse sequence used in [97].

3.3 Hyperedge Computation

As mentioned above, the hyperedge is used to connect the vertices with same attribute value, so the task of hyperedges computation is actually to assign attributes for each image patch in spatio-temporal domain. In this section, we present to use spectral analysis for the attribute assignment. Before this, we will introduce how to represent the over-segmented patches in the

spatio-temporal domain, and finally we discuss how to assign weights to the hyperedges.

3.3.1 Computing Motion Cues

We use the optical flow and the appearance based motion profile to describe the over-segmented patches in the spatio-temporal domain. The Lucas-Kanade optical flow method [76] is adopted to obtain the translations (x, y) of each pixel, and we indicate each pixel with the motion intensity $z = \sqrt{x^2 + y^2}$ and the motion direction $o = arctan(\frac{x}{y})$. We assume that pixels in the same patch have a similar motion, and then the motion of a patch can be estimated, $f^o = (u, d)$, by computing the weighted average of all the pixel motions in a patch:

$$u = \frac{1}{N}\sum_i \omega_i z_i, d = \frac{1}{N}\sum_i \omega_i o_i, \tag{3.1}$$

where N is the total number of pixels in a region, and w_i is the weight generated from a low-pass 2-D Gaussian centered on the centroid of the patch. u, d are the motion intensity and the motion angle of the patch, respectively. Since the motion of the pixels near the patch boundaries may be disturbed by other neighborhood patches, we discard the pixels near the boundaries (3 pixels to the boundaries).

Besides the optical flow, we also apply the appearance based motion profile to describe the over-segmented patches, inspired by the idea in [91]. Based on a reasonable assumption that the pixels in one patch have the same movement and color components and remain stable between consecutive frames too, the motion profile is defined as a measure of the probability distribution of image velocity to every patch based on appearance information. Let $I^t(X_i)$ denote the vector containing all the (l, u, v) pixel values of patch i centered at X, and denote $P_i(dx)$ as the probability of the image patch i at time t corresponding to another image patch $I^{t+1}(X_i + dx)$ at $t + 1$:

$$P_i(dx) = \frac{S_i(dx)}{\sum_{dx} S_i(dx)} \tag{3.2}$$

where $S_i(dx)$ denotes the similarity between $I^t(X_i)$ and $I^{t+1}(X_i + dx)$, which is based on on the SSD difference between $I^t(X_i)$ and $I^{t+1}(X_i + dx)$:

$$S_i(dx) = exp(-SSD(I^t(X_i), I^{t+1}(X_i + dx))). \tag{3.3}$$

3.3.2 Spectral Analysis for Hyperedge Computation

The idea of spectral analysis is based on an affinity matrix A, where $A(i,j)$ is the similarity between sample i and j [93] [81] [109]. Based on the affinity matrix, the Laplacian matrix can be defined as $L = D^{-\frac{1}{2}}(D-A)D^{-\frac{1}{2}}$, where D is the diagonal matrix $D(i,i) = \sum_j A(i,j)$. Then unsupervised data clustering can be achieved by doing eigenvalue decomposition of the Laplacian matrix. The popular way is to use the k-means method on the first several eigenvectors associated with the smallest non-zero eigenvalues [81] to get the final clustering result.

To set up the hyperedges, we perform the spectral analysis on the optical flow and the appearance based motion profile respectively. As in [93] [81] [109], only local neighbors are taken into account for the similarity computation. We defined two patches to be *spatial-temporal* neighbors if 1) in the same frame they are 8-connected or both their centroids fall into a ball of radius R, or 2) in the adjacent frames (± 1 frame in the work) their regions are overlapped or 8-connected, as illustrated in Figure 4.1.

Denote the affinity matrices of the optical flow as A^o and the motion profile as A^p respectively. For the motion profile, we define the similarity between two neighbor patches i and j is defined as:

$$A^p(i,j) = e^{-\frac{dis(i,j)}{\sigma^p}},\ dis(i,j) = 1 - \sum_{dx} P_i(dx)P_j(dx), \tag{3.4}$$

where $dis(i,j)$ is defined as the distance between two patches i and j, and σ^p is constant computed as the standard deviation of $dis(i,j)$.

Based on the optical flow, the similarity metric between two neighbor patches i and j is defined as:

$$A^o(i,j) = e^{-\frac{\|f_i^m - f_j^m\|_2}{\sigma^o}}, \tag{3.5}$$

where σ^o is a constant computed as the standard deviation of $\|f_i^o - f_j^o\|_2$.

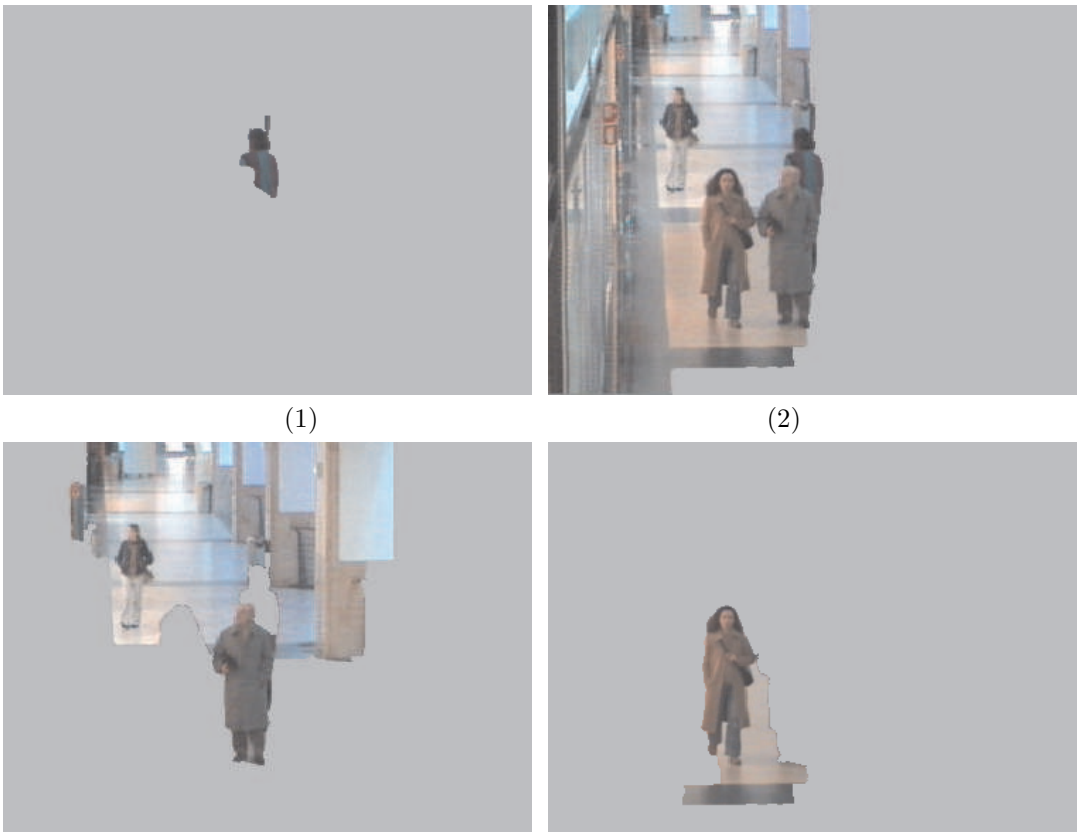

(1) (2)

(3) (4)

Figure 3.3: Four binary partition results got by the first 4 eigenvectors computed from motion profile (for one frame of the sequence *WalkByShop1cor.mpg*, CAVIAR database.).

Based on A^o and A^p, we can compute the corresponding Laplacian matrix of L^o and L^p and their eigenvectors associated with the first k smallest non-zero eigenvalues respectively. Each of these eigenvectors may lead to a meaningful but not optimal 2-way cut result. Figure 3.3 shows some examples, where the patches without the gray mask are regarded as the vertices having the *attribute* value 1 and the patches with the gray mask having the *attribute* 0. A hyperedge can be formed by those vertices with same attribute values. With all the hyperedges, the complex relationship between the image patches can be represented by the hypergraph completely.

3.3.3 Hyperedge Weights

According to [93], the eigenvectors of the smallest k non-zero eigenvalues can be used for clustering. Then a nature idea is to choose the first k eigenvectors to compute the hyperedges, and weight those heyperedges with their corresponding reciprocals of the eigenvalues. In our experiments, we find that the eigenvalues of the first k eigenvectors are very close and may

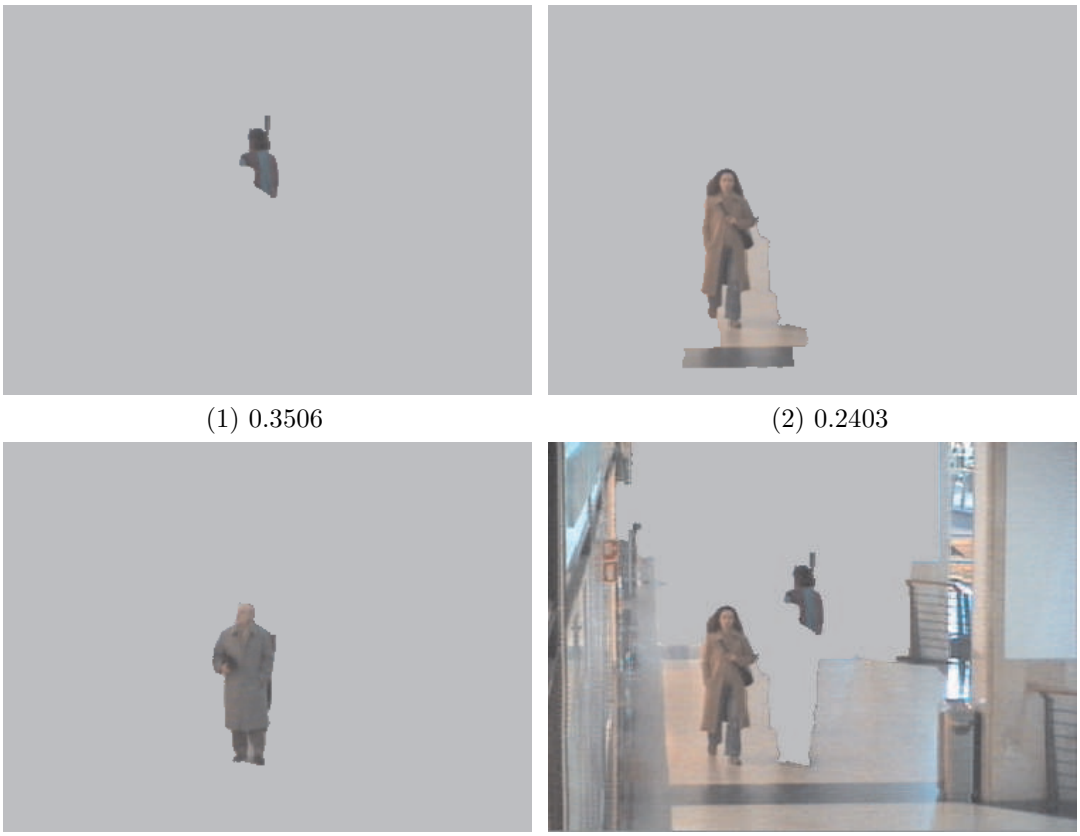

(1) 0.3506 (2) 0.2403

(3) 0.2378 (4) 0.0986

Figure 3.4: 4 binary partition results with largest hyperedge weights (for one frame of *WalkByShop1cor.mpg*). Obviously that the heperedge got from the 1st and 4th frames have a good description of objects we want to segment according to their importance. The computed hyperedge weights are shown below those binary images.

not absolutely reflect the importance of the corresponding eigenvectors. In order to emphasize more important hyperedges which contain moving objects, larger weights should be assigned to them.

We impose the weights to the hyperedges from two different cues, w_H^o and w_H^p, by the following equations:

$$w_H^o = c^o \| f_1^o - f_0^o \|_2 \tag{3.6}$$

$$w_H^p = c^p dis(1,0) \tag{3.7}$$

where c^o and c^p are constant, and $dis(1,0)$ means the dissimilarity between two regions in the binary image with value 1 and 0, based on the first motion feature; f_1^o and f_0^o means the weighted motion intensity and direction of two regions in the binary image with value 1 and 0.

Based on above definition, a larger weight is assigned to the binary frame whose two segmented regions have distinct appearance (motion) distributions.

In practice, we select the first 5 hyperedges with larger weights computed from appearance and motion respectively; and then proper c^p and c^o are chosen to let $\sum_{i=1}^{5} w_H^p(i) = 1$ and $\sum_{i=1}^{5} w_H^o(i) = 1$. In 3.4, we show the corresponding weight values under the binary attribute images. It is obvious that more meaningful attributes are assigned larger weights in our algorithm.

After the construction of hypergraphs for video object segmentation, the theoretical solution of this real value problem is the eigenvector associated with the smallest non-zeros eigenvector of the *hypergraph Laplacian matrix* $\Delta = I - D_v^{-\frac{1}{2}} H W D_e^{-1} H^T D_v^{-\frac{1}{2}}$. As in [81], to make a multi-way classification of vertices in a hypergraph, we take the first several eigenvectors with non-zeros eigenvalues of Δ as the indicators (we take 3 in this work), and then use a k-means clustering algorithms on the formed eigenspace to get final clustering results.

3.4 Experiments

3.4.1 Experimental Protocol

To evaluate the performance of our segmentation method based on the hypergraph cut, we compare it with three clustering approaches based on the simple graph, i.e., the conventional simple graph with pairwise relationship. In these three approaches, we measure the similarity between two over-segmented patches using (1) the optical flow, (2) the motion profile, and (3) both the motion cues. The similarity matrix for (1) and (2) just follow Equation 3.5 and Equation 3.4. For (3), the similarity is defined as follows:

$$A(i,j) = e^{-\frac{\|f_i^m - f_j^m\|_2}{\sigma^o} - \frac{dis(i,j)}{\sigma^p}}, \tag{3.8}$$

where σ^o and σ^p are constants. Notice that σ values in Equation 3.8, Equation 3.4 and Equation 3.5 are all tuned to get the best segmentation results for both the hypergraph based and the simple graph based methods for comparison. Then corresponding Laplacian matrix of these three approaches can be computed accordingly and the k-means algorithm can be performed

on the first n eigenvectors with nonzero eigenvalues. In our experiment, we choose $n = 10$ for all these three simple graph based methods.

3.4.2 Results on Videos under Different Conditions

We first report the experiments on the rocking-horse sequence and the squirrel sequence used in [97]. We choose them because the movement of objects in these two sequences are very subtle and their backgrounds are cluttered and similar to the objects. Figure 3.5 and 3.6 show the ground truth frames, the results of three simple graph based methods, and the results of hypergraph cut for these two sequences. To illustrate a distinctive comparison with the ground truth, we plot the red edge of the segmented patches in our results. Compared with the results in [97] and the simple graph based methods, in both sequences our method gives more meaningful segmentation results for the foreground objects, although a few local details are lost in the squirrel sequence. In all these figures, the number of cluster classes is set to 2 (K=2).

We also compare four algorithms on the image sequences in which the video object has complicated movements. The sequence shown in Figure 3.7 (*Walk1.mpg*, from CAVIAR database) contains a person browsing back and forth and rotating during the course of his movement. In this example, we cluster the scene to two classes (K=2) too. From Figure 3.7, we can observe that our method can give very accurate segmentation result for the moving objects, in spite of the small perturbation in the left corners of this sequence. However, the simple graph based methods can not completely extract the moving person from background and some unexpected small patches are classified into the moving objects.

In the real world, the video objects may be occluded or interacted with each other during their movements. We also test the proposed method on such examples with occlusion. In Figure 3.8, four algorithm are compared on a running-car sequence with an artificial occlusion, in which the hypergraph cut extracts the car and the pedestrian from the background accurately, while the simple graph based methods can extract the car or the pedestrian. In the sequence shown in Figure 3.9 (*WalkByShop1front.mpg*, from CAVIAR database), a couple walk along the corridor, and another person moves to the door of the shop hastily and is occluded by the couple during his moving. When we set K=2, the person with largest velocity of movement

Sequence Name	MP	OP	MP+OP	Hypergraph Cut
Rocking-horse	0.87/0.02	0.96/0.76	0.96/0.92	0.91/0.02
Squirrel	0.91/0.86	0.89/1.32	0.72/0.02	0.89/0.01
Walk1	0.92/15.3	0.92/6.4	0.92/12.7761	0.94/0.03
car running	0.14/0.03	0.82/0.02	0.82/3.22	0.89/0.03
WalkByShop1front	0.32/0.47	0.56/0.81	0.79/0.66	0.84/0.37

Table 3.1: Average accuracy/error for all the experimental frames of every sequence, where MP means simple graph method by the motion profile, OP means simple graph method by the optical flow and MP+OP means the simple graph method using both cues. Mention that for *WalkByShop1front.mpg* we only consider the case when K=4.

is segmented. When we set K=3, K=4 and K=5, three primary moving objects are extracted one by one only with a small patch between the couple, which is caused by the noise of motion estimation. For the simple graph based methods, we give the best case (the best result under different K). For $K > 3$, simple graph based methods usually give very cluttered and not meaningful results. For the simple graph based methods using the motion profile or the optical flow, K =2 can give the most meaningful results, and K =3 can give a good extraction of the couple for the simple graph method using both motion cues.

In Table 3.1, the average segmentation accuracy and segmentation error are estimated and compared on the experimental frames of all the image sequences. The segmentation accuracy for one frame is defined as the number of 'true positive' pixels (the true positive area) divided by the number of the ground truth pixels(the ground truth area). The segmentation error for one frame is defined as the number of 'false positive' pixels (the false positive area) divided by the number of the ground truth pixels(the ground truth area).

3.5 Conclusions

In this chapter, we proposed a framework of video object segmentation , in which hypergraph is used to represent the complex relationship among frames in videos. We first used the multi-scale graph decomposition method to over-segment the images and took the oversegmented image patches as the vertices of the hypergraph. The spectral analysis was performed on two motion cues respectively to set up the hyperedges, and the spatio-temporal information is integrated by the hyperedges. Furthermore, a weighting procedure is discussed to put larger weights on more important hyperedges. In this way, the task of video object segmentation is

transferred into a hypergraph partition problem which can be solved by the hypergraph cut algorithm. The effectiveness of the proposed method is demonstrated by extensive experiments on nature scenes. Since our algorithm is a open system, in the future work, we may add more motion or appearance cues (such as texture information, the occlusions between frames) into our framework to construct more hyperedges and further improve the accuracy of these results.

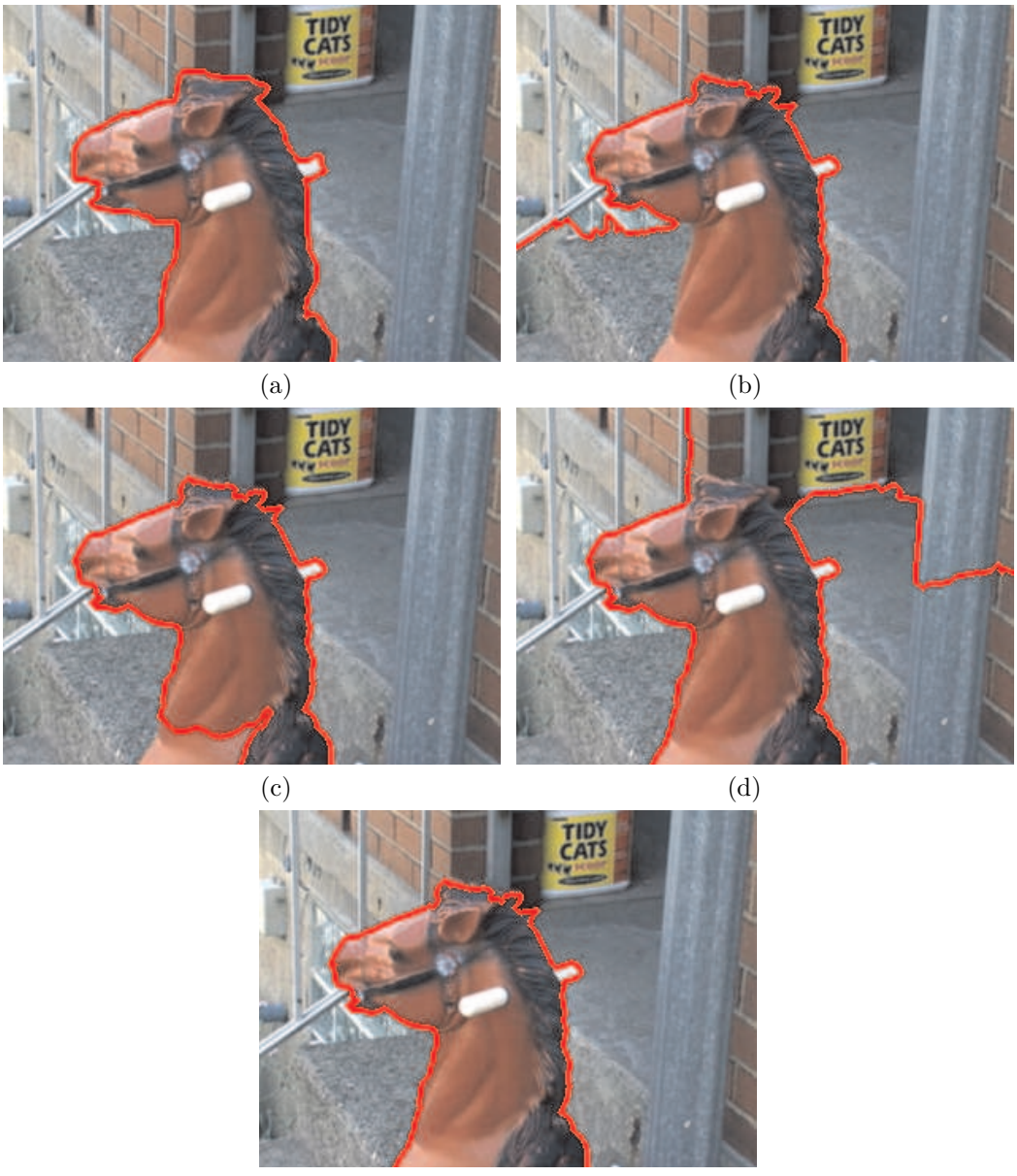

Figure 3.5: Segmentation results for the 8th frame of the rocking-horse sequence. (a) The ground truth, (b) the result by the simple graph based segmentation using optical flow, (c) the result by the simple graph based segmentation using motion profile, (d) the result by the simple graph based segmentation using both motion cues, and (e) the result by the hypergraph cut.

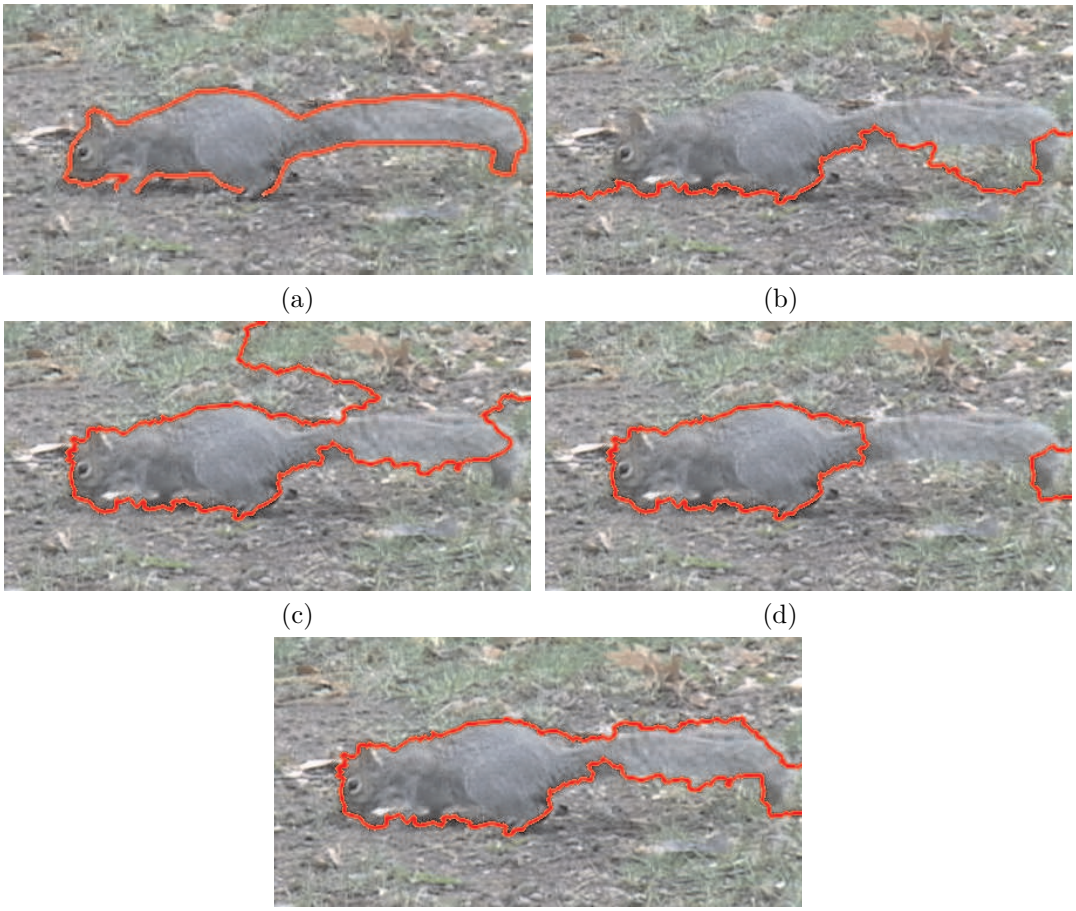

(a) (b) (c) (d) (e)

Figure 3.6: Segmentation results for the 4th frame of the squirrel sequence. (a) The ground truth, (b) the result by the simple graph based segmentation using optical flow, (c) the result by the simple graph based segmentation using motion profile, (d) the result by the simple graph based segmentation using both motion cues, and (e) the result by the hypergraph cut.

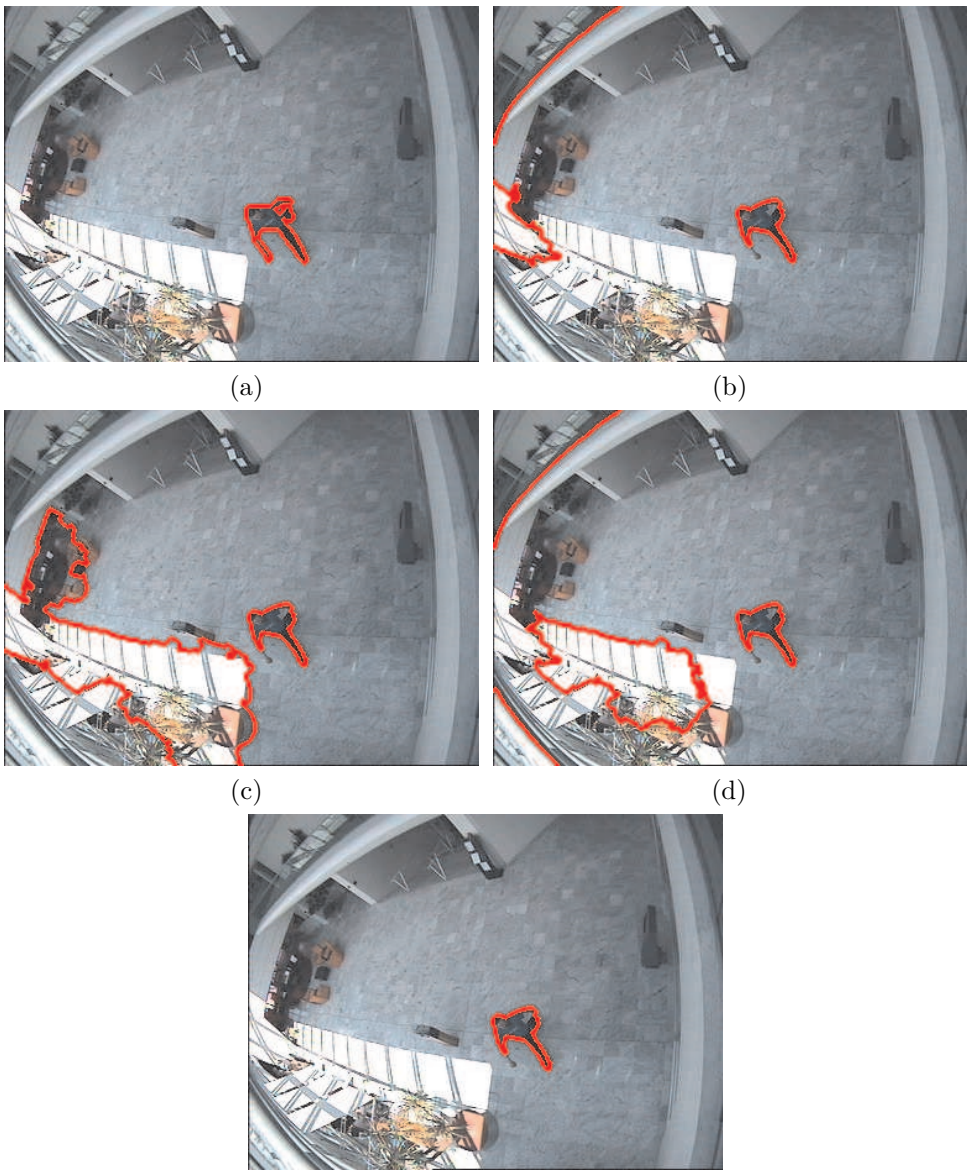

(a) (b) (c) (d) (e)

Figure 3.7: Segmentation results for one frame of *Walk1.mpg*, CAVIAR database. (a) The ground truth, (b) the result by the simple graph based segmentation using optical flow, (c) the result by the simple graph based segmentation using motion profile, (d) the result by the simple graph based segmentation using both motion cues, and (e) the result by the hypergraph cut.

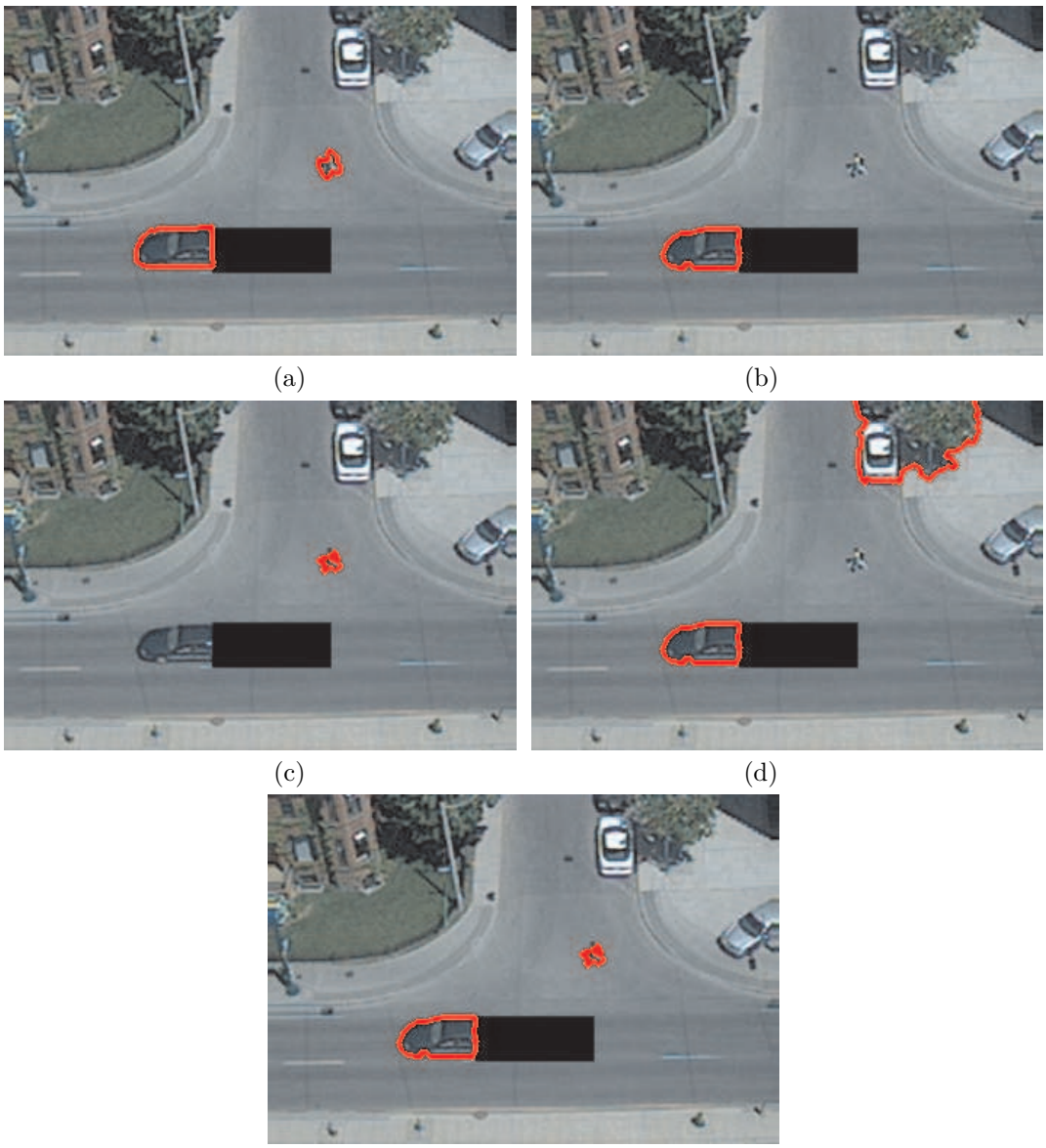

(a) (b) (c) (d) (e)

Figure 3.8: Segmentation results for the 16th frame of the car running sequence with occlusion. (a) The ground truth, (b) the result by the simple graph based segmentation using optical flow, (c) the result by the simple graph based segmentation using motion profile, (d) the result by the simple graph based segmentation using both motion cues, and (e) the result by the hypergraph cut.

(a) (b) (c) (d) (e) (f) (g) (h)

Figure 3.9: Segmentation results for one frame of the *WalkByShop1front.mpg*, different colors denote different clusters in each sub-figure. (a) The ground truth, (b) the result by the simple graph based segmentation using optical flow (K=2), (c) the result by the simple graph based segmentation using motion profile (K=2), (d) the result by the simple graph based segmentation using both motion cues (K=3), (e) the result by the hypergraph cut (K=2), (f) the result by the hypergraph cut (K=3), (g) the result by the hypergraph cut (K=4), and (h) the result by the hypergraph cut (K=5).

Chapter 4

Unsupervised Image Categorization by Hypergraph Partition

In this chapter, we present a framework for unsupervised image categorization, in which images containing specific objects are taken as vertices in a hypergraph, and the task of image clustering is formulated as the problem of hypergraph partition. First, a novel method is proposed to select the region of interest (ROI) of each image, and then hyperedges are constructed based on shape and appearance features extracted from the ROIs. Each vertex (image) and its k-nearest neighbors (based on shape or appearance descriptors) form two kinds of hyperedges. The weight of a hyperedge is computed as the sum of the pairwise affinities within the hyperedge. Through all the hyperedges, not only the local grouping relationships among the images are described, but also the merits of the shape and appearance characteristics are integrated together to enhance the clustering performance. We use the generalized spectral clustering technique to solve the hypergraph partition problem. We compare the proposed method to several methods and its effectiveness is demonstrated by extensive experiments on three image databases.

4.1 Introduction

Unsupervised image categorization based on some similarity measurements is a critical preprocessing step in many computer vision problems. Supervised approaches (such as SVM, boosting, etc.) of object detection and recognition typically require a lot of training images whose classes are labelled and/or bounding boxes of the objects of interest are annotated. Generally this training data is manually selected and annotated, which is expensive to obtain and may introduce bias information into the training stage. An unsupervised technique (such as k-centers clustering [79] and affinity propagation based clustering [39] etc) bases its categorization decision directly on the data. It not only recovers image categories naturally, but also provides

a powerful tool to collect exemplar images for learning based applications. For unsupervised image categorization, topic model based clustering has been demonstrated to outperform classical methods such as k-means by extensive experiments [94] [70] [85]. [34] and [72] extend the topic models with spatial information to boost categorization results. Topic models can also be combined with image segmentation information [88] or with a hierarchical class structure [95]. In [101], a complicated model based on tree matching is proposed for unsupervised discover of topic hierarchies. Other works, such as [40] and [84], try to discover object classes and locations by detecting reoccurring structure or frequent features sets. [59] presents an iterative method to amplify 'consistency' existing in objects of the same class, by using a novel star-like geometric model and an appearance learning tool. This unsupervised algorithm leads to precise part localization and classification performance comparable to supervised approaches, but mainly for class vs. non-class mixes (i.e. sets formed by some images of one specific class and some other non-class images). Recent related works include organizing images into a tree shaped hierarchy by a Bayesian model [46] and discovering object shapes from unlabeled images [68], etc.

Different from the above methods, recently Grauman et al. [44] and Kim et al. [62] [63] adopt the pairwise graph (for simplicity, we denote the pairwise graph as simple graph in the following) to model relationship between unlabeled images. These works differ in how to measure the similarities between images: in [44], image-to-image affinities are computed by pyramid matching kernel (PMK) [43]; while in [62] and [63], the distance metric between images is based on link analysis techniques, which largely improves the object detection/categorization performance on some classes of *Caltech-101* [69]. [80] encodes object similarity and spatial context between object exemplars into simple graphs with two kinds of pairwise edges. Spectral clustering [81] is usually utilized to solve the simple graph based partitioning problem [43] [62] and its superiority over previous methods is verified in [103].

To overcome the limitations of simple graph based methods mentioned above, we propose a hypergraph based framework to exploit the correlation information among unlabeled images containing distinct objects, and adopt a hypergraph partition algorithm to improve unsupervised image categorization performance. Different from simple graph, hypergraph contains summarized local grouping information, which may be beneficial to the global clustering. Moreover,

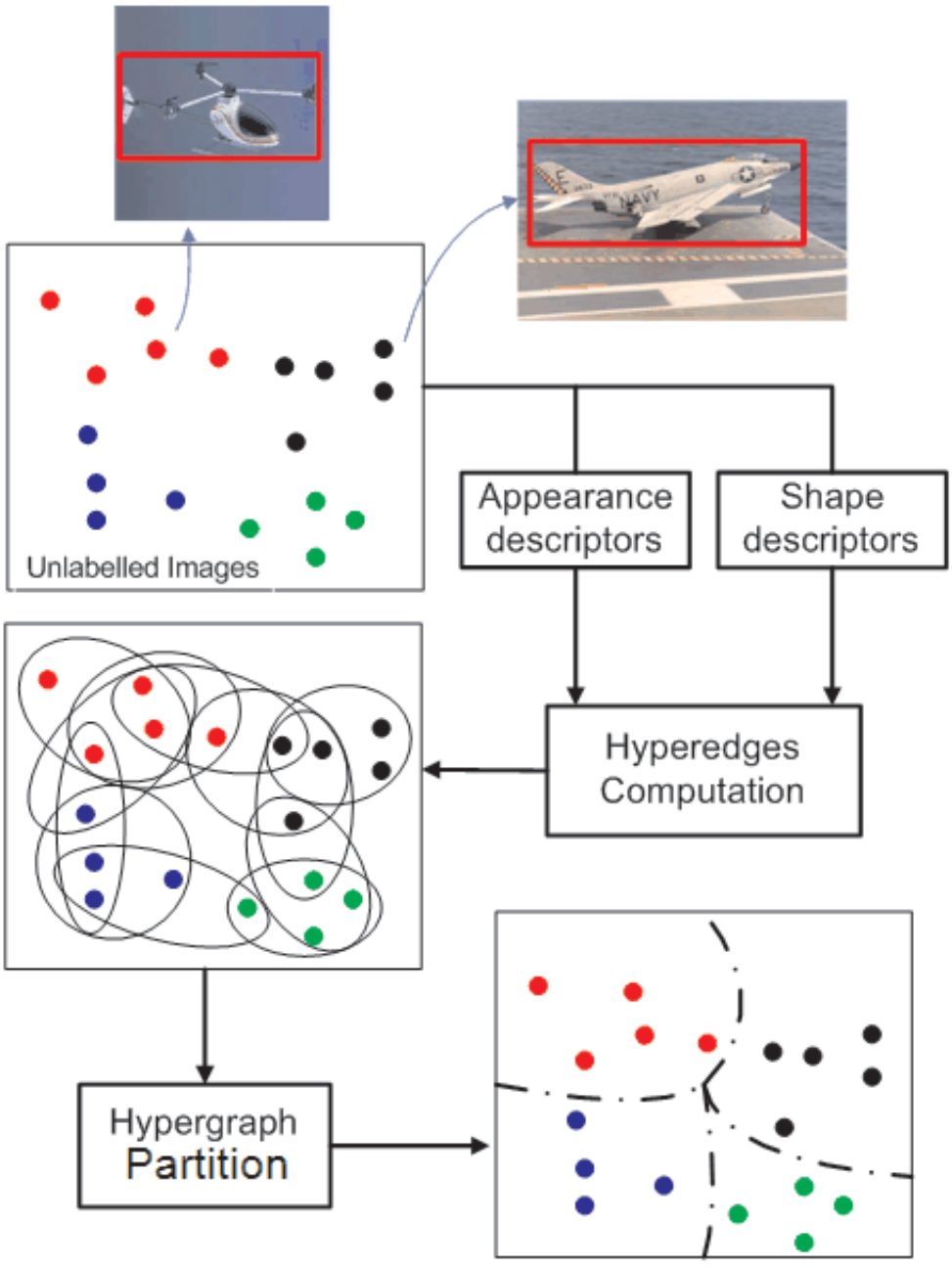

Figure 4.1: Illustration of our framework.

in a hypergraph we can construct several kinds of hyperedges based on different attributes, as shown in the previous chapter. These hyperedges co-exist in a hypergraph and provide useful and diversified grouping information for final partition. In this work, our purpose is to use hypergraph to model the complex relationship among the unlabeled images for image categorization. The proposed framework is shown in Figure 4.1. First, we develop an unsupervised method to select the ROIs of the unlabeled images. Based on the appearance and shape descriptors extracted from the ROIs, we use spatial pyramid matching [67] to measure two kinds of similarities between two images. Then we can form two kinds of hyperedges and compute their corresponding weights based on these two kinds of similarities respectively. In this way, not only are the higher order relationships among the images described, but also the merits of shape and appearance characteristics are integrated naturally to enhance the clustering performance. Finally, we use the hypergraph partition algorithm [113] to solve the image categorization problems. The proposed method is tested in three benchmarks including the data sets of *Caltech-101* [69], *Caltech-256* [45], and Pascal VOC2008 [33], compared to the-state-of-the-art by extensive experiments.

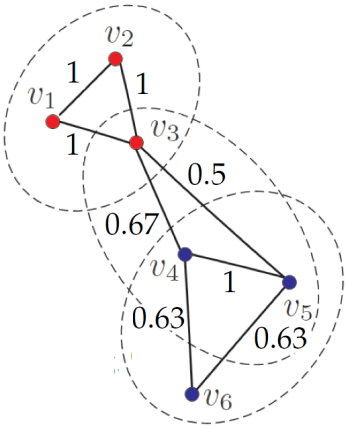

	e_1	e_2	e_3	e_4	e_5	e_6
v_1	1	1	1	0	0	0
v_2	1	1	1	0	0	0
v_3	1	1	1	1	0	0
v_4	0	0	0	1	1	1
v_5	0	0	0	1	1	1
v_6	0	0	0	0	1	1

Figure 4.2: A hypergraph example and its H matrix.

According to the above definition, different hyperedges may contain different number of vertices. For simplicity, in this work we only consider the case where all the hyperedges have the same degree; this kind of hypergraph is called *uniform* hypergraph. We define a hyperedge as a group of vertices which contain a 'centroid' vertex and this centroid's k-nearest neighbors. In Figure 4.2 an example is shown to explain how to construct such a hypergraph. According to the

similarities on the pairwise edges, each vertex and its two-nearest neighbors form a hyperedge. In Figure 4.2, hyperedges are marked by ellipses. For example, the hyperedge e_4 is composed of vertex v_4 and its two nearest neighbors v_3 and v_5. The corresponding vertex-hyperedge matrix H could be formed as in the right side of Fig. 4.2.

In order to bipartition this hypergraph, intuitively the hyperedges with the smallest weights should be removed, and at the same time as many hyperedges with larger weights as possible should be kept. Since e_4 has the smallest hyperedge weight, a hypergraph partition could be made on it to classify $v_1, v_2, ..., v_6$ into two groups. This is exactly the result obtained by the normalized hypergraph partition.

4.2 Our Two-Step Method for Unsupervised ROI Detection

Besides cluttered background, various positions and scales of interesting objects in images also make it unreliable to measure the similarities based on whole images. To overcome this problem, previous works [12] [22] proposed to extract rectangle ROIs of object instances based on iterative conditional model [8]. However, they are based on the assumption that the categorization information of images is known, so they can not work when no prior information (such as the class labels of objects) is provided. In this work, we propose a novel two-step method to detect the ROIs from the unlabeled images.

Consider an image set **S** that contains not only images from one or several object classes, but also other non-class images. At first we go over the entire set **S** to compute every image's k–nearest neighbors (KNN). We use a KNN algorithm based on vantage point trees, which is able to provide the best performance for computer vision applications and speed up the search effectively [64]. To measure the degree of closeness between each image with its neighbors, we get scores by summing up the distances between each image with its five nearest neighbors. We sort all the images in **S** by these scores. Then bottom 5% images with lowest scores are selected from **S** and taken as the initial exemplars for the given query. Our object annotation approach alternates between **Rough Localization Phase** and **accurate ROI localization**, with a continuous expansion of the exemplar set. In this manner the process not only exploits

ROI localization results at a given stage to guide the next stage, but also identifies more high-likelihood images as exemplars related to the input query.

4.2.1 Rough Localization Phase

Initialization is a crucial step in many optimization tasks. A bad initialization may lead to a local maximum or minimum which is far from the satisfactory solution. In this subsection we propose efficient initialization procedures to predict the *ROI*s of the exemplar images. For the initial exemplars, we create a novel feature weighting framework to divide the foreground and background; for the new incoming exemplars in the subsequential loops, rough *ROI*s are found by a query-by-example technique.

Rough Localization for initial exemplars. The dense SURF features are extracted every 12 pixels from three pyramid scales of all the images and a *2000*–bins codebook is organized by k–means algorithm. For each image, we assume that some codewords (bins) in the codebook are more relevant to the foreground objects while some other codewords are more relevant to the background. Taking each initial exemplar as the centroid, we collect its $n_{pos} = 3\% \times N$ nearest neighbors as the *positive* set (where N is the total number of the unlabelled images); we randomly sample $n_{neg} = 10\% \times N$ images from the top 30% farthest neighbors as the *negative* set. Intuitively, foreground features should have more contribution to the similarity between the centroid image and the images in the *positive* set; the similarity between the centroid image and the images in the *negative* set is caused by false matches in some bins. For each codeword, we accumulate the pairwise intersection between the histogram (on the level $l = 0$) of the centroid image and the histograms of the images from the *positive*/ *negative* set respectively. After normalization, we can obtain two density functions $DES_i^{pos}(w)$ and $DES_i^{neg}(w)$ for the exemplar image i, which describe the overall distributions of matches on two image sets:

$$DES_i^{pos}(w) = \frac{\sum\limits_{j \in P_i} min(His_0^i(w), His_0^j(w))}{\sum_{k=1}^{|V|} DES_i^{pos}(v_k)}, \tag{4.1}$$

$$DES_i^{neg}(w) = \frac{\sum\limits_{j \in N_i} min(His_0^i(w), His_0^j(w))}{\sum_{k=1}^{|V|} DES_i^{neg}(v_k)}. \tag{4.2}$$

where P_i and N_i are the *positive* set and the *negative* set for the exemplar i, respectively.

For simplicity, we denote these two density functions as the *positive* and *negative* distributions respectively. The value of $DES_i^{pos}(w) - DES_i^{neg}(w)$ reveals to what extend a codeword w is related to the foreground objects or the background. Since every SURF feature is quantized into a histogram by soft assignment according to Eq. 5.10, we can assign weights to all SURF features based on these two distributions:

$$weight^i(f) = \frac{\sum_{j=1}^{|V|}[DES_i^{pos}(v_j) - DES_i^{neg}(v_j)]K_\sigma(D(v_j, f))}{\sum_{j=1}^{|V|} K_\sigma(D(v_j, f))} \tag{4.3}$$

where $weight^i(f)$ is the weight of the SURF feature f in the exemplar image i. According to the above analysis, localizing the ROIs roughly is equivalent to finding a rectangular region R in the centroid image to maximize the sum of all the feature weights:

$$\arg\max_{R\in\mathcal{R}} \sum_{\forall f\in R} weight(f) = \arg\max_{R\in\mathcal{R}}\{F^+(R) + F^-(R)\} \tag{4.4}$$

where $\mathcal{R}$ is the set of all possible rectangles in the image, $F^+(R)$ and $F^-(R)$ are the sum of all the positive weights and the sum of all the negative weights in R, respectively. To solve Eq. 4.6, traditional methods need to exhaustively search all the possible windows in the image. In this work, we adopt a 'beyond sliding windows' scheme [65] to obtain the optimal solution of Eq. 4.6 in typically sublinear time. The details are shown in Algorithm 1.

Algorithm 1 *Learning the rough ROIs of initial exemplars*

1: **for** each image i: **do**
2: collect its positive set P_i and its negative set N_i based on the spatial pyramid matching algorithm [67];
3: accumulate and normalize the intersection scores between the exemplar image i and the images in the positive set P_i, from codeword to codeword, according to Eq. 4.1;
4: accumulate and normalize the intersection scores between the exemplar image i and the images in the negative set N_i, from codeword to codeword, according to Eq. 4.2;
5: compute the weight for each feature according to Eq. 4.3;
6: obtain the rough ROI of the exemplar image i by maximizing Eq. 4.6 by the 'beyond sliding windows' [65] method.
7: **end for**

Rough Localization for subsequent exemplars. The rough *ROI* localization results in initial exemplars can be refined with the method introduced in Section 4.2. Then those refined *ROI*s in the current exemplar set are used as query examples to search for their most similar subregions in all the non-exemplar images. In [65], the 'beyond sliding windows' method is also employed to search for similar subregions efficiently in multiple images. For simplicity,

we only search each *ROI*'s most similar subregion from non-exemplar images, add that image to the exemplar set and take the subregion as its rough *ROI*. The new exemplar is taken as the 'child' of the query exemplar. If a new incoming exemplar has two ore more ancestors, the rough *ROI* it contained is the most similar subregion to all its ancestors. Similar to those initial exemplars, the positive and negative set of every new exemplar will be prepared for the accurate ROI localization phase.

4.2.2 Accurate ROI Localization

After obtaining the rough *ROI* locations in all images of the current exemplar set, we need to refine them and obtain the final ROIs by maximizing the following cost function:

$$\sum_{i=1}^{|E|}\{-\sum_{j\in P_i} DIS(i,j)+\sum_{k\in N_i} DIS(i,k)\} \tag{4.5}$$

where $|E|$ is the number of images in the current exemplar set; P_i and N_i are the *positive* set and the *negative* set for the exemplar i, respectively. DIS is the distance function based on the shape descriptors and the appearance descriptors, which are computed according to Eq. **??**. In Eq. 4.5, we try to optimize the *ROI* of each exemplar by minimizing the distance between each exemplar and its positive set, while simultaneously maximizing the distance between each exemplar and its negative set. It is very expensive to optimize Eq. 4.5 exhaustively. To overcome this problem, We adopt a sub-optimal scheme based on the iterative conditional model(ICM) [8], which is used in previous works [12] [22]. We first enlarge the rough ROIs by 15% and search refined ROIs in this enlarged range using several window sizes(we obtain search window sizes by extending and shrinking the width or(and) the length of a rough ROI by 5% and 10%). To reach this goal, we define the following function and maximize it:

$$L(R_1,...,R_{|V|})=\sum_{i=1}^{|V|}\{\sum_{j\in P_i}(A^s_{i,j}+A^a_{i,j})-\sum_{k\in N_i}(A^s_{i,k}+A^a_{i,k})\}, \tag{4.6}$$

where $|V|$ is the number of all the images; $A^s_{i,j}$ is the abbreviation of $A^s(R_i,R_j)$, R_i is the ROI candidate of the ith image; P_i and N_i are the *positive* set and *negative* set of the ith image, respectively; A^s and A^a are two different affinity functions based on the appearance descriptor and the shape descriptor respectively to measure the similarities between two ROI candidates.

We will address how to define the similarities between two ROIs in Section 4.1. The idea of Equation 4.6 is to optimize the ROI in each image by maximizing the similarity between it and its positive set, and simultaneously minimizing the similarity between it and its negative set. However, it is too expensive to optimize Equation 4.6 exhaustively, so we use a sub-optimal scheme based on iterative conditional model to solve this problem, which is demonstrated to be efficient in our experiments. For each image i, we search the best R_i by fixing ROIs in other images, and maximizing the following function:

$$\sum_{j \in P_i} (A^s_{i,j} + A^a_{i,j}) - \sum_{k \in N_i} (A^s_{i,k} + A^a_{i,k}). \tag{4.7}$$

This procedure circulates through all the images until the search of 90% ROIs converges.

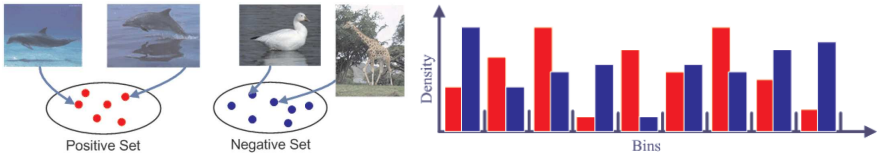

Figure 4.3: Positive/Negative set (for a dolphin image) and accumulated intersection scores. Based on these scores we can decide the features in which bin are 'positive' or 'negative'.

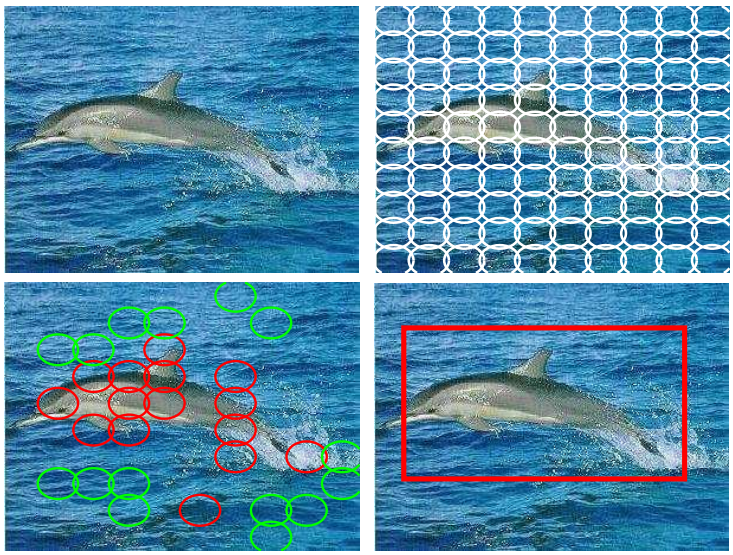

Figure 4.4: An illustration on how to get the rough ROI of an unlabeled image. On the second image 10×10 dense features are extracted. On the third image the 15 most significant positive/negative features are shown as red/green ellipses. On the last image the rough ROI is obtained.

4.3 Hypergraph Partition for Image Categorization

4.3.1 Similarity Measurements Between the ROIs

As mentioned above, we represent each image by the features extracted from its ROI, and the hyperedge defined in the proposed hypergraph is formed by an image and its k-nearest neighbor. Therefore, how to define the similarity measurement between the ROIs is a key issue to build the hypergraph, besides the issue of ROI refinement addressed in the last Section. In this work, we utilize two kinds of feature descriptors on the ROIs, i.e., the SURF based appearance feature descriptor and the PHOG (the pyramid histograms of edge oriented gradients) based shape feature descriptor [28] [13]. Based on these two features we obtain two different similarities, i.e., A^s and A^a in Equation 4.7 respectively. We use the speed up robust feature (SURF) as the appearance descriptor [6] because it approximates or even outperforms previously proposed local appearance features such as the SIFT [75], and it can be computed much faster. PHOG is known as a good descriptor to capture shape information.

As shown in Figure 4.5, the SURF features are densely sampled at three scales. Given a ROI, we densely extract SURF features from 15×15 rectangular grids of the ROIs. For those very small ROIs, we double their sizes to extract the features. We create a 128-bin codebook of SURF features by k–means, and totally 225 features are quantized into a histogram by soft assignment as in [106], because such soft assignment technique was proven to make remarkable improvement in object recognition [106]. For the PHOG descriptor, in each image grid we discretize it into 20 bins (that is, the length of each 'bin' is $360/20 = 18$ degree). Since 3 pyramid levels (the grid configurations are 1X1, 2X2, 4X4) are used, so there are actually 420 bins in a PHOG based histogram.

We adopt the spatial pyramid matching(SPM) [67] (illustrated in Figure 4.5) to calculate the similarities because of its better performance when image ROIs are obtained. Given the local histograms His_i^l and His_j^l at each level of two images i and j based on the appearance or shape features, the similarity is computed using a kernel function as follows:

$$A(R_i, R_j) = \exp\{-\frac{1}{\beta}\sum_{l=0}^{L}\frac{1}{2^{L-l}}dis(His_i^l, His_j^l)\}, \tag{4.8}$$

where β is the standard deviation of $\sum_{l \in L} \frac{1}{2^{L-l}} dis(His_i^l, His_j^l)$ over all the data; dis is the distance function computed with an improved pyramid matching kernel (PMK) algorithm [43] [44]. In this work, we set $L = 2$, as shown in Figure 4.5.

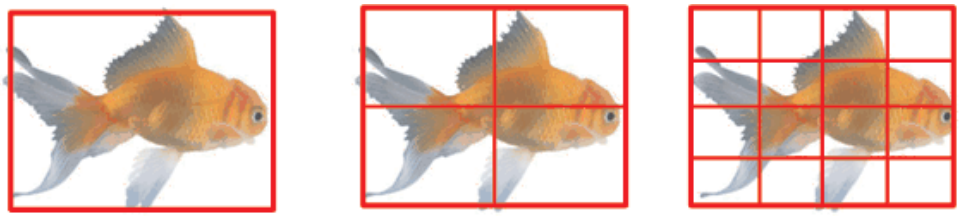

Figure 4.5: From left to right: levels $l = 0$ to $l = 2$ of the spatial pyramid grids for the appearance and shape descriptors.

4.3.2 Computation of the Hyperedges

In this work, we take each image as a centroid and collect its k-nearest neighbors by the shape and appearance descriptors respectively. Then two kinds of hyperedges (based on the shape/apperance descriptors) can be constructed over these $K+1$ images with different hyperedge weights. The hyperedge weight $w(e)$ is computed as follows:

$$w(e) = \sum_{\substack{v_i, v_j \in e \\ i<j}} A_{i,j}, \tag{4.9}$$

where the affinity function $A_{i,j}$ is computed according to Equation4.8. If a hyperedge is constructed by the appearance descriptor, the $w(e)$ is computed by A^a. The w(e) is computed by A^s when the shape descriptor is used.

For practical hypergraph partition problems, the choice of hyperedge size is crucial to the final clustering results. Except for the hyperedge size, all the parameters in our framework are computed from the experimental data directly. Intuitively, very small-size hyperedges only contain 'micro-local' grouping information which will not help the global clustering over all the images, and very large-size hyperedges may contain images from different classes and suppress the diversity information. To optimize the clustering results, it is necessary to perform a sweep over all the possible values of the hyperedge size. In Section 5.2, a sensitivity analysis is made to investigate the robustness of our algorithm by illustrating how the clustering accuracy varies

along with the hyperedge size.

4.3.3 Hypergraph Partition Algorithm

In this work, we adopt the algorithm proposed in [113] to partition the hypergraph because of its efficiency and simplicity of implementation. As in [81], to make a multi-way classification of vertices in a hypergraph, we take the first several eigenvectors with non-zero eigenvalues of the hypergraph Laplacian matrix Δ as the indicators (we take 3 in this work), and then use a k-means clustering algorithm on the formed eigenspace to get final clustering results.

4.4 Experiments

4.4.1 Experimental Protocol

In the following, we first make a sensitivity analysis to show the robustness of our algorithm when the hyperedge size varies. Then we compare our results to the-state-of-the-art [62] on the same data sets using the same testing protocol. We also compare our method with three different unsupervised methods: 1. the k-centers clustering [79], 2. the affinity propagation [39], 3. the simple graph based normalized cut. We test these methods and our proposed method on three different data sets, which are *Caltech-101* [69], *Caltech-256* [45], and Pascal VOC2008 [33] respectively. For above three clustering methods, the affinity between two images is defined as $A^v = A^s + A^a$ based on the features in the selected ROIs. For the simple graph based method, we build the simple graph by connecting each vertex (image) with its k-nearest neighbors by pairwise edges. The affinity matrix is constructed as $W(i,j) = A^v_{i,j}$ if two vertices are connected and $W(i,j) = 0$ otherwise. The spectral analysis is employed to solve an eigen-decomposition problem, and the first several (we use 3 in this work) eigenvectors are fed to k-means algorithm to get the final classification results. In our experiments the number of obtained clusters are set the same as the number of true classes. To evaluate how well the unlabeled images are clustered according to their ground truth labels, we follow the measurement used in [44] and [62] by computing the average accuracies over all classes. The image ROI prediction error is defined as

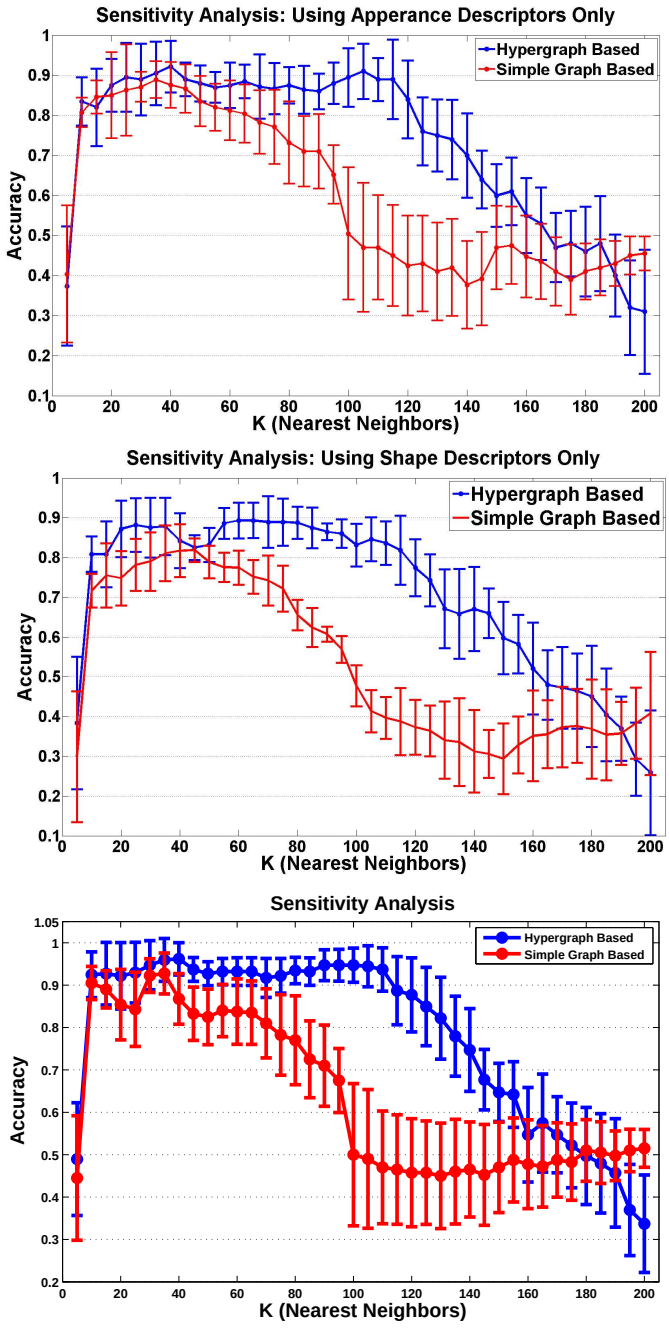

Figure 4.6: The sensitivity analysis on the hyperedge size. the clustering accuracy and its standard deviation are plotted. Notice that for most of K values, the hypergraph based method illustrates a much more stable trend of variation on the accuracy.

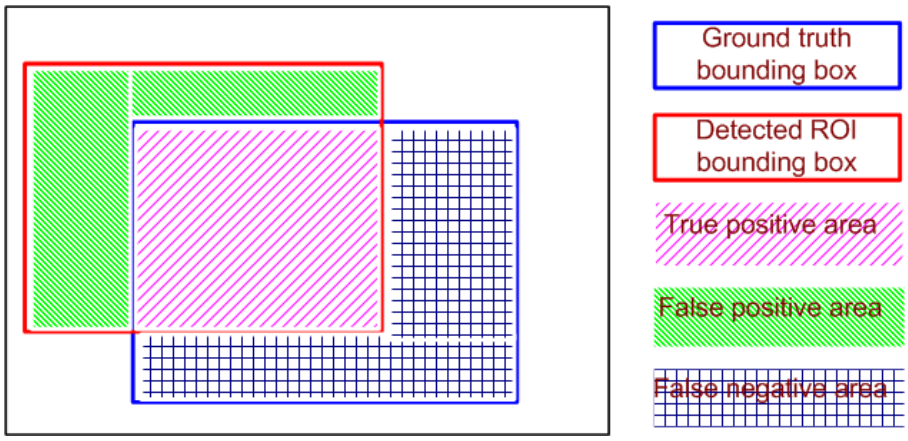

Figure 4.7: An illustration for several definitions used in Eq. 4.10.

$$err_{loc} = \frac{0.5 \times (FPA + FNA)}{FPA + FNA + TPA}, \tag{4.10}$$

where TPA denotes true positive area; FPA denotes false positive area and FNA denotes false negative area, as shown in Fig. 4.7. Eq. 4.10 can be used as a good single-value measurement for object localization since a small localization error guarantees small false positive and small false negative areas at the same time.

4.4.2 Sensitivity Analysis of the Hyperedge Size

Since both the hyperedges in the hypergraph and the edges in the simple graph are formed by each vertex and its K-nearest neighbors, we report the classification accuracy as a function of K. To obtain an indication of significance, the bootstrap method [9] is used to estimate the confidence intervals for classification accuracy. In this analysis, we provide a pool of 200 unlabeled images from Caltech-101 (at first 4 classes are randomly selected from Caltech-101, and then 50 images are randomly chosen from each of the 4 classes). For each K value plotted, we run both the hypergraph method and the simple graph method 50 times, each time with a different random subset of 4 classes. We performe the sensitivity analysis under three circumstances: using appearance descriptors, using shape descriptors and using both descriptors(if one descriptor is used, we only use A^s or A^a as the similarity measure in a simple/hypergraph). In Figure 4.6 the average accuracy and the standard deviation over 50 runs are reported for each K value. As illustrated in Figure 4.6, the hypergraph based clustering not only obtains better clustering

accuracies on most of K values, but also illustrates a much more stable trend of variation on the accuracy as K increases, especially when $20 < K < 100$. By contrast, the simple graph based clustering shows a lower robustness of the performance on the selection of the parameter K. In the comparison of the following experiments, we will show the best accuracy of both two methods by tuning K value.

Here we give an intuitive explanation for why performance of hypergraph models in Figure 4.6 is still high when $K = 100$ are used in the hypergraphs. Consider that we transfer a hypergraph into an equivalent simple graph by Clique Expansion. The pairwise similarity between two vertices is proportional to the sum of their corresponding hyperedge weights. That is, in the obtained simple graph, the edge weight between two vertices v_i and v_j is not decided by the pairwise affinity $A_{i,j}$ between two vertices, but the averaged neighboring affinities close to them; furthermore, this edge weight is influenced more by those pairwise affinities whose two incident vertices share more hyperedges with v_i and v_j. In this way the adverse impact caused by some 'noise' similarities may be weakened by this weighted averaging or smoothing effect of the hypergraph construction, even when K is relatively large.

4.4.3 Results on Caltech Data Sets

Compared to [62]. [62] is the latest work on unsupervised image categorization, and it is based on simple graph partition. So we first compare to this work under the same experiment setting to show the effectiveness of our framework. Following the approach in [62], we select six object classes (airplane, motorbikes, rear cars, faces, watches, ketches) from *Caltech-101* to the proposed hypergraph method. For ROI localization results, we report the average err_{loc} and its standard deviation (std) in Table 4.1 according to Eq. 4.10. The ROI detection results shown in Table 4.1 is desirable, since objects in images of *Caltech-101* are roughly aligned and backgrounds in those images are relatively simple. For categorization results, Table 4.2 shows the confusion matrices with increasing number of classes (from four to six). Each experiment is iterated ten times as in [62], in which 100 images per object are randomly picked from each object class. As illustrated in Table 4.2, our clustering result for four object classes(98.53%) is comparable to [62] (98.55%). In the cases of five and six object classes, our results achieve

	A	M	C	F	W	K
Error	8.1	5.2	6.8	4.7	9.6	5.5
STD	7.6	4.3	5.7	8.2	6.9	7.5

Table 4.1: Average localization errors and standard deviations, computed using Eq. 4.10. A:Airplanes, C: Cars, F: Faces, M: Motorbikes, W: Watches, K: Ketches)

97.38% and 96.05%, which are slightly better than [62] (97.30% and 95.42%). Average clustering accuracies/std errors are computed using the diagonal entries in corresponding confusion matrices.

More results on Caltech Data Sets. To further evaluate the performance of our model, we design a more universal and difficult experiment setting for comparison, which is rarely used in previous work. We use all image classes from *Caltech-101* and *Caltech-256* respectively, and then randomly choose 4, 8, or 12 classes to run 4-category clustering, 8-category clustering or 12-category clustering tasks. In each task, we run the experiment for 100 times to obtain the average accuracy and the standard deviation. Before each run 4, 8 or 12 image classes are randomly selected, and then 50 images are randomly chosen from each class to form a pool of images (for the class in which total number of images is less than 50, all the images in this class will be used). For the clustering results, as shown in Table 4.3, the hypergraph based method excels the other three methods on both *Caltech-101* and *Caltech-256* data sets.

4.4.4 Results on the PASCAL VOC2008

We also test the proposed method on PASCAL VOC2008 database [33]. Unlike *Caltech* databases, PASCAL VOC2008 is much more challenging for its class variations and cluttered backgrounds. To decrease the difficulty, we choose around 800 images from six easier classes (person, aeroplane, train, boat, moto-bike, and horse) of the VOC2008 for our experimental comparison. Since in the VOC2008 one image may contain multiple objects, we classify each image to one specific class according to the most significant object it contains. Same as above, we increase object classes from 4 to 6 for the clustering tasks. Each experiment is iterated for 50 times, in which 100 images per object are randomly picked from each object class. In Fig. 4.9, the first three images are examples with accurate ROI detection results. We also show some difficult cases in Fig. 4.9: the detection bounding boxes of the 4th and 5th images are not well located,

	A	M	C	F
A	**99.5**/0.9	0.0	0.5/0.9	0.0
M	0.0	**97.9**/0.4	2.0/0.5	0.1/0.3
C	1.2/0.8	0.1/0.2	**98.3**/1.1	0.4/0.4
F	1.1/1.2	0.3/0.5	0.2/0.3	**98.4**/1.3

	A	M	C	F	W
A	**98.9**/1.7	0.1/0.2	0.6/0.6	0.1/0.3	0.3/0.4
M	0.5/0.7	**97.8**/0.9	1.6/1.0	0.0	0.1/0.2
C	1.6/1.5	0.2/0.4	**97.5**/1.6	0.6/1.1	0.1/0.3
F	0.8/1.3	0.4/0.4	0.6/0.5	**96.9**/1.4	1.3/1.6
W	2.1/1.7	0.7/0.9	0.1/0.1	1.4/1.2	**95.7**/1.3

	A	M	C	F	W	K
A	**97.3**/3.0	0.2/0.3	0.3/0.5	0.1/0.3	0.1/0.2	2.0/1.8
M	0.4/0.7	**94.5**/2.9	1.4/1.1	0.2/0.2	0.4/0.3	3.1/3.4
C	0.9/0.6	0.2/0.4	**97.6**/2.1	0.1/0.3	0	1.2/1.5
F	1.0/0.8	0.4/0.8	0.1/0.4	**96.1**/2.5	0.9/1.3	1.5/1.8
W	1.9/1.7	0.2/0.3	0.1/0.2	0.1/0.1	**94.6**/3.9	3.1/3.5
K	2.2/1.6	0.2/0.4	0.3/0.5	0.4/0.2	0.7/0.9	**96.2**/2.4

Number of Classes	4	5	6
Our method	98.53/0.93	97.38/1.38	96.05/2.80
[62]	98.55/0.98	97.30/1.44	95.42/2.87

Table 4.2: The first three tables are confusion matrix for increasing number of Caltech-101 objects from four to six. The average accuracies (%) and the standard deviations (%) are shown in the tables. Comparison to [62] is reported in the last table. The numbers in this table are computed from the diagonals of first three tables.

because of cluttered background or similar objects shown in the same image. In the 6th image, the detected ROI is misplaced because of the misleading texture in the background. As shown in Table 4.4(Above), we obtain higher average ROI localization errors on *Pascal* database, compared to the results on *Caltech* (Table 4.1). This affects the image categorization results shown in Table 4.4(Bottom), which are not as good as the categorization results on *Caltech* (Table 4.2 and Table 4.3). However, based on the same ROI results, we can still see that the proposed hypergraph partition method outperforms the other three methods for the image categorization task.

4.5 Conclusion

In this section, we have presented a hypergraph based framework for unsupervised image categorization. We first use a new method to extract the ROIs from the unlabeled images, and then construct hyperedges among images based on shape and appearance features in their ROIs. The hyperedges are defined as a group formed by each vertex and its k-nearest neighbors, and their weights are calculated by the sums of the pairwise affinities. Different from the simple

Dataset	Caltech 101			Caltech 256		
Image Classes	4	8	12	4	8	12
Hypergraph Based	**95.8** 3.3	**86.2** 4.4	**71.5** 6.8	**87.7** 4.6	**77.1** 6.7	**64.3** 7.0
Simple Graph Based	92.8 4.0	82.1 6.2	66.2 7.1	77.9 5.7	72.5 7.6	59.0 8.5
Affinity Propagation	76.1 5.7	62.5 6.8	54.1 7.6	69.7 7.7	57.2 6.6	51.4 9.1
k-center	72.6 5.1	56.9 6.5	47.9 9.6	67.8 8.0	53.7 7.5	50.2 9.9

Table 4.3: Results of unsupervised image categorization on both *Caltech-101* and *Caltech-256*.

	P	A	T	B	M	H
Error	17.2	9.8	16.3	21.6	7.9	13.8
STD	10.8	6.7	5.4	15.4	8.1	6.7

Dataset	PASCAL VOC2008		
Image Classes	4	5	6
Hypergraph Based	**81.3** 3.4	**77.2** 4.6	**69.3** 6.5
Simple Graph Based	74.9 4.1	71.3 5.2	63.7 6.1
Affinity Propagation	62.7 4.7	57.3 6.4	47.9 7.0
k-center	58.9 5.3	53.6 5.1	41.2 5.9

Table 4.4: The first table: average localization errors and standard deviations of the VOC2008, computed using Eq. 4.10. (P:person, A: Aeroplane, T: Train, B:Boat, M: moto-bike, H: Horse). The second table: results of unsupervised image categorization on PASCAL VOC2008. 4-class case: {P,A,T,B}. 5-class case: {P,A,T,B,M}.

graph, the hypergraph not only represents the higher order relationships between the images, but also efficiently integrates different visual feature descriptors together. We formulate the image clustering as the problem of hypergraph partition and solve it with a generalized spectral clustering technique. The effectiveness of the proposed method has been demonstrated by extensive experiments on various database.

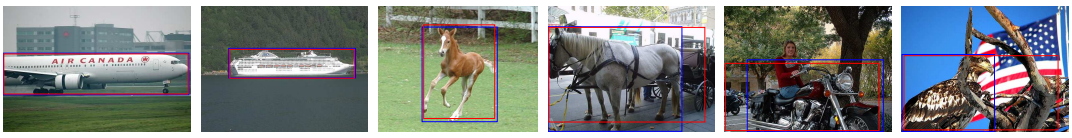

Figure 4.8: ROI detection results. The red bounding boxes are the ROI detection results and the blue boxes are the ground truths. In the first three images very good detection results are obtained. We also give three examples in which ROIs are not well detected.

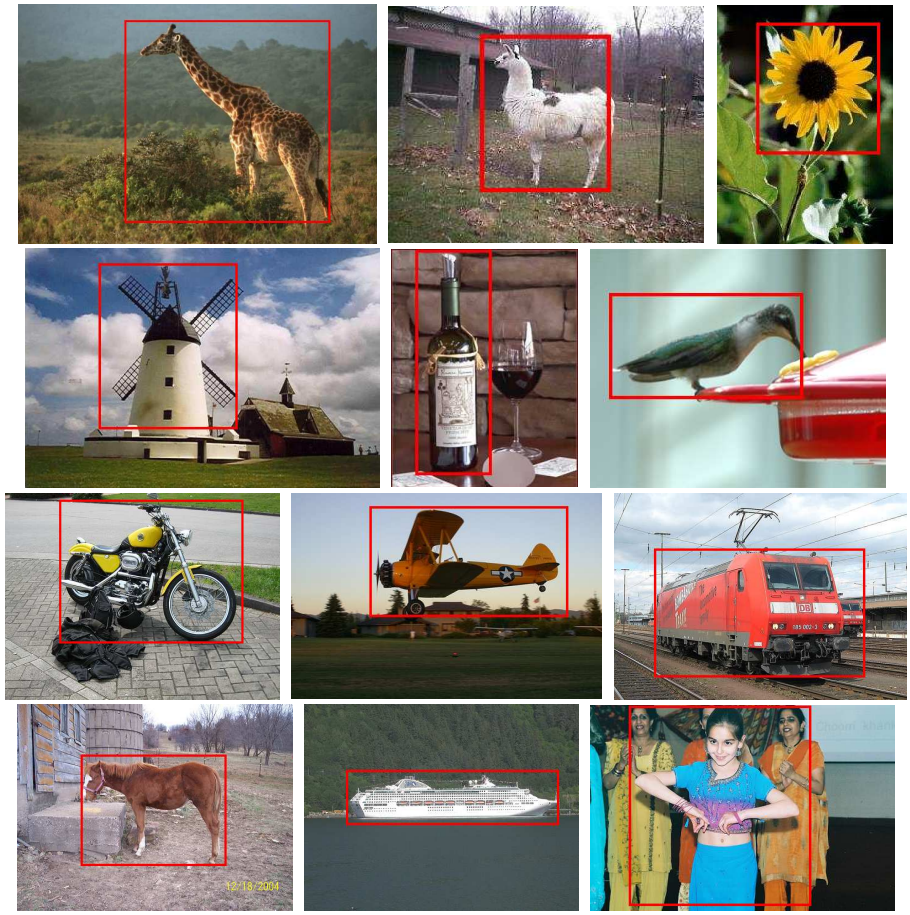

Figure 4.9: ROI detection results. The first two rows are images from *Caltech* 256; the last two rows are images from PASCAL VOC2008.

Chapter 5

Image Retrieval via Fuzzy Hypergraph Ranking

In this chapter, we propose a new transductive learning framework for image retrieval, in which images are taken as vertices in a weighted hypergraph and the task of image search is formulated as the problem of hypergraph ranking. Based on the similarity matrix computed from various feature descriptors, we take each image as a 'centroid' vertex and form a hyperedge by a centroid and its k-nearest neighbors. To further exploit the correlation information among images, we propose a probabilistic hypergraph, which assigns each vertex v_i to a hyperedge e_j in a probabilistic way. In the incidence structure of a probabilistic hypergraph, we describe both the local grouping information and the affinity relationship between vertices within each hyperedge. After feedback images are provided, our retrieval system ranks image labels by a transductive inference approach, which tends to assign the same label to vertices that share many incidental hyperedges, with the constraints that predicted labels of feedback images should be similar to their initial labels. We compare the proposed method to several other methods and its effectiveness is demonstrated by extensive experiments on Corel5K, the Scene dataset and Caltech 101.

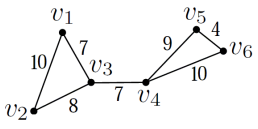

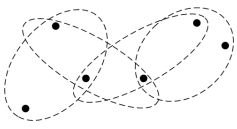

	e_1	e_2	e_3	e_4	e_5	e_6
v_1	1.0	0.28	0.41	0	0	0
v_2	0.28	1.0	0	0	0	0
v_3	0.41	0.36	1.0	0.41	0	0
v_4	0	0	0.41	1.0	0.32	0.28
v_5	0	0	0	0.32	1.0	0.60
v_6	0	0	0	0	0.60	1.0

Figure 5.1: Left: A simple graph of six points in 2-D space. Pairwise distances ($Dis(i,j)$) between v_i and its 2 nearest neighbors are marked on the corresponding edges. Middle: A hypergraph is built, in which each vertex and its 2 nearest neighbors form a hyperedge. Right: The H matrix of the probability hypergraph shown above. The entry (v_i, e_j) is set to the affinity $A(j,i)$ if a hyperedge e_j contains v_i, or 0 otherwise. Here $A(i,j) = \exp(-\frac{Dis(i,j)}{\bar{D}})$, where $\bar{D}$ is the average distance.

5.1 Introduction

In content-based image retrieval (CBIR) visual information instead of keywords is used to search images in large image databases. Typically in a CBIR system a query image is provided by the user and the closest images are returned according to a decision rule. In order to learn a better representation of the query concept, a lot of CBIR frameworks make use of an online learning technique called relevance feedback (RF) [87] [51]: users are asked to label images in the returned results as 'relevant' and/or 'not relevant', and then the search procedure is repeated with the new information. Previous work on relevance feedback often aims at learning discriminative models to classify the relevant and irrelevant images, such as, RF methods based on support vector machines (SVM) [102], decision trees [78], boosting [100], Bayesian classifiers [26], and graph-cut [89]. Because the user-labeled images are far from sufficient for supervised learning methods in a CBIR system, recent work in this category attempts to apply transductive or semi-supervised learning to image retrieval. For example, [54] presents an active learning framework, in which a fusion of semi-supervised techniques (based on Gaussian fields and harmonic functions [115]) and SVM are comprised. In [50] and [49], a pairwise graph based manifold ranking algorithm [112] is adopted to build an image retrieval system. Cai et al. put forward semi-supervised discriminant analysis [16] and active subspace learning [15] to relevance feedback based image retrieval. The common ground of [89], [54], [50] and [16] is that they all use a pairwise graph to model relationship between images. In a simple graph both labeled and unlabeled images are taken as vertices; two similar images are connected by an edge and the edge weight is computed as image-to-image affinities. Depending on the affinity relationship of a simple graph, semi-supervised learning techniques could be utilized to boost the image retrieval performance.

In this chapter, we propose a hypergraph based transductive algorithm to the field of image retrieval. As in the previous chapter, we take each image as a 'centroid' vertex and form a hyperedge by a centroid and its k-nearest neighbors, based on the similarity matrix computed from various feature descriptors. To further exploit the correlation information among images, we propose a novel hypergraph model called the *probabilistic hypergraph*, which presents not only whether a vertex v_i belongs to a hyperedge e_j, but also the probability that $v_i \in e_j$. In

this way, both the local grouping information and the local relationship between vertices within each hyperedge are described in our model. To improve the performance of content-based image retrieval, we adopt the hypergraph-based transductive learning algorithm to learn beneficial information from both labeled and unlabeled data for image ranking. After feedback images are provided by users or active learning techniques, the hypergraph ranking approach tends to assign the same label to vertices that share many incidental hyperedges, with the constraints that predicted labels of feedback images should be similar to their initial labels. We further design a random strategy to reduce the computational cost of the proposed method and make it possible for larger scale image retrieval. The effectiveness and superiority of the proposed method is demonstrated by extensive experiments on *Corel5K* [32], the Scene dataset [70] and *Caltech-101* [69].

In summary, the contribution of this work is fourfold: (i) we propose a new image retrieval framework based on transductive learning with hypergraph structure, which considerably improves image search performance; (ii) we propose a probabilistic hypergraph model to exploit the structure of the data manifold by considering not only the local grouping information, but also the similarities between vertices in hyperedges; (iii) in this work we conduct an in-depth comparison between simple graph and hypergraph based transductive learning algorithms in the application domain of image retrieval, which is also beneficial to other computer vision and machine learning applications. (IV) we introduce a random strategy to reduce the computational cost rapidly.

5.2 Probabilistic Hypergraph Model

Let V represent a finite set of vertices and E a family of subsets of V such that $\bigcup_{e\in E} = V$. $G = (V, E, w)$ is called a hypergraph with the vertex set V and the hyperedge set E, and each hyperedge e is assigned a positive weight $w(e)$. A hypergraph can be represented by a $|V| \times |E|$ incidence matrix H_t:

$$h_t(v_i, e_j) = \begin{cases} 1, & \text{if } v_i \in e_j \\ 0, & \text{otherwise.} \end{cases} \tag{5.1}$$

The hypergraph model has proven to be beneficial to various clustering and classification tasks [2] [98] [56] [99]. However, the traditional hypergraph structure defined in Equation 5.1 assigns a vertex v_i to a hyperedge e_j with a binary decision, i.e., $h_t(v_i, e_j)$ equals 1 or 0. In this model, all the vertices in a hyperedge are treated equally; relative affinity between vertices is discarded. This 'truncation' processing leads to the loss of some information, which may be harmful to the hypergraph based applications.

In this work, we propose a probabilistic hypergraph model to overcome this limitation. Assume that a $|V| \times |V|$ affinity matrix A over V is computed based on some measurement and $A(i, j) \in [0, 1]$. We take each vertex as a 'centroid' vertex and form a hyperedge by a centroid and its k-nearest neighbors. That is, the size of a hyperedge in our framework is $k + 1$. The incidence matrix H of a probabilistic hypergraph is defined as follows:

$$h(v_i, e_j) = \begin{cases} A(j, i), & \text{if } v_i \in e_j \\ 0, & \text{otherwise.} \end{cases} \tag{5.2}$$

According to this formulation, a vertex v_i is 'softly' assigned to e_j based on the similarity $A(i, j)$ between v_i and v_j, where v_j is the centroid of e_j. A probabilistic hypergraph presents not only the local grouping information, but also the probability that a vertex belongs to a hyperedge. In this way, the correlation information among vertices is more accurately described. Actually, the representation in Equation 5.1 can be taken as the discretized version of Equation 5.2. The hyperedge weight $w(e_i)$ is computed as follows:

$$w(e_i) = \sum_{v_j \in e_i} A(i, j). \tag{5.3}$$

Based on this definition, the 'compact' hyperedge (local group) with higher inner group similarities is assigned a higher weight. For a vertex $v \in V$, its degree is defined to be $d(v) = \sum_{e \in E} w(e)h(v, e)$. For a hyperedge $e \in E$, its degree is defined as $\delta(e) = \sum_{v \in e} h(v, e)$. Notice that these definitions are relaxed from those definition in ordinary hypergraphs. Let us use D_v,D_e and W to denote the diagonal matrices of the vertex degrees, the hyperedge degrees and the hyperedge weights respectively. Figure 5.1 shows an example to explain how to construct a probabilistic hypergraph.

5.3 Hypergraph Ranking Algorithm

Algorithm 2 *Probabilistic Hypergraph Ranking*

1: Compute similarity matrix A based on various features using Equation 5.13, where $A(i,j)$ denotes the similarity between the i^{th} and the j^{th} vertices.
2: Construct the probabilistic hypergraph G. For each vertex, based on the similarity matrix A, collect its k-nearest neighbors to form a hyperedge.
3: Compute the hypergraph incidence matrix H where $h(v_i, e_j) = A(j,i)$ if $v_i \in e_j$ and $h(v_i, e_j) = 0$ otherwise. The hyperedge weight matrix is computed using Equation 5.3.
4: Compute the hypergraph Laplacian $\Delta = I - \Theta = I - D_v^{-\frac{1}{2}} H W D_e^{-1} H^T D_v^{-\frac{1}{2}}$.
5: Given a query vertex and the initial labeling vector y, solve the linear system $((1+\mu)I - \Theta) f = \mu y$. Rank all the vertices according to their ranking scores in descending order.

Algorithm 3 *Manifold Ranking*

1: Same to Algorithm 1.
2: Construct the simple graph G_s. For each vertex, based on the similarity matrix A, connect it to its k-nearest neighbors.
3: Compute the simple graph affinity matrix A_s where $A_s(i,j) = A(i,j)$ if the i^{th} and the j^{th} vertices are connected. Let $A_s(i,i) = 0$. Compute the vertex degree matrix $D = \sum_j A_s(i,j)$.
4: Compute the simple graph Laplacian $\Delta_s = I - \Theta_s = I - D^{-\frac{1}{2}} A_s D^{-\frac{1}{2}}$.
5: Same to Algorithm 1, expect that Θ is replaced with Θ_s.

Let's revisit the hypergraph based transductive learning algorithm. For a hypergraph partition problem, the normalized cost function [113] $\Omega(f)$ could be defined as

$$\frac{1}{2} \sum_{e \in E} \sum_{u,v \in e} \frac{w(e) h(u,e) h(v,e)}{\delta(e)} \left(\frac{f(u)}{\sqrt{d(u)}} - \frac{f(v)}{\sqrt{d(v)}} \right)^2, \tag{5.4}$$

where the vector f is the image labels to be learned in our retrieval problem. By minimizing this cost function, vertices sharing many incidental hyperedges are guaranteed to obtain similar labels. Defining $\Theta = D_v^{-\frac{1}{2}} H W D_e^{-1} H^T D_v^{-\frac{1}{2}}$, we can derive Equation 5.4 as follows:

$$\begin{aligned}
\Omega(f) &= \sum_{e \in E} \sum_{u,v \in e} \frac{w(e) h(u,e) h(v,e)}{\delta(e)} \left(\frac{f^2(u)}{d(u)} - \frac{f(u) f(v)}{\sqrt{d(u) d(v)}} \right) \\
&= \sum_{u \in V} f^2(u) \sum_{e \in E} \frac{w(e) h(u,e)}{d(u)} \sum_{v \in V} \frac{h(v,e)}{\delta(e)} \\
&\quad - \sum_{e \in E} \sum_{u,v \in e} \frac{f(u) h(u,e) w(e) h(v,e) f(v)}{\sqrt{d(u) d(v)} \delta(e)} \\
&= f^T (I - \Theta) f,
\end{aligned} \tag{5.5}$$

where I is the identity matrix. Above derivation for probabilistic hypergraphs shows that (i)

$\Omega(f,w) = f^T(I-\Theta)f$ if and only if $\sum_{v\in V}\frac{h(v,e)}{\delta(e)} = 1$ and $\sum_{e\in E}\frac{w(e)h(u,e)}{d(u)} = 1$, which is true because of the definition of $\delta(e)$ and $d(u)$ in Section 2; (ii) $\Delta = I - \Theta$ is a positive semi-definite matrix called the hypergraph Laplacian and $\Omega(f) = f^T\Delta f$. The above cost function has the similar formulation to the normalized cost function of a simple graph $G_s = (V_s, E_s)$:

$$\begin{aligned}\Omega_s(f) &= \frac{1}{2}\sum_{v_i,v_j\in V_s} A_s(i,j)\left(\frac{f(i)}{\sqrt{D_{ii}}} - \frac{f(j)}{\sqrt{D_{jj}}}\right)^2 \\ &= f^T(I - D^{-\frac{1}{2}}A_sD^{-\frac{1}{2}})f = f^T\Delta_s f, \end{aligned} \tag{5.6}$$

where D is a diagonal matrix with its (i,i)-element equal to the sum of the i^{th} row of the affinity matrix A_s; $\Delta_s = I - \Theta_s = I - D^{-\frac{1}{2}}A_sD^{-\frac{1}{2}}$ is called the simple graph Laplacian. As shown in previous chapters, in an unsupervised framework Equation 5.4 and Equation 5.6 can be optimized by the eigenvector related to the smallest nonzero eigenvalue of Δ and Δ_s [113], respectively.

In the transductive learning setting [113], we define a vector y to introduce the labeling information of feedback images and to assign their initial labels to the corresponding elements of y: $y(v) = \frac{1}{|Pos|}$, if a vertex v is in the positive set Pos, $y(v) = -\frac{1}{|Neg|}$, if it is in the negative set Neg. If v is unlabeled, $y(v) = 0$. To force the assigned labels to approach the initial labeling y, a regularization term is defined as follows:

$$\|f - y\|^2 = \sum_{u\in V}(f(u) - y(u))^2. \tag{5.7}$$

After the feedback information is introduced, the learning task is to minimize the sum of two cost terms with respect to f [112] [113], which is

$$\Phi(f) = f^T\Delta f + \mu\|f - y\|^2, \tag{5.8}$$

where $\mu > 0$ is the regularization parameter. Differentiating $\Phi(f)$ with respect to f, we have

$$f = (1-\gamma)(I - \gamma\Theta)^{-1}y, \tag{5.9}$$

where $\gamma = \frac{1}{1+\mu}$. This is equivalent to solving the linear system $((1+\mu)I - \Theta)\, f = \mu y$.

For the simple graph, we can simply replace Θ with Θ_s to fulfill the transductive learning. In [50] and [49], this simple graph based transductive reasoning technique is used for image retrieval with relevance feedback. The procedures of the probabilistic hypergraph ranking algorithm and simple graph based manifold ranking algorithm are listed in Algorithm 2 and Algorithm 3.

5.4 Random Hypergraph Ranking

As above description, the hypergraph Laplacian matrix Δ plays an important role in the ranking algorithm. The dimensionality of the matrix Δ is $N \times N$, where N is the data size, and it directly dominates the computational complex of the ranking algorithm. According to Equation 5.9, we can see the computational complexity increases with the data size at least by N^2. Thus, its efficiency will be degraded in the case of large-scale data. To handle this issue, we adopt a random strategy to speed up the proposed method, especially for the large-scale data. The technique of random sampling has widely used in the community of machine learning [53] [108]. The basic idea is to generate multiple subsets of feature or data from the original one by randomly sampling and to learn multiple classifiers. Finally combining all these classifiers to make the final decision. Motivated by this idea, we present a scheme of random hypergraph ranking for image retrieval.

Assuming in the image data $X = \{x_1, x_2, ...x_l\}$ is the label images and $X' = \{x'_1, x'_2, ..., x'_p\}$ is the unlabeled images, $l + p = N$. The goal of hypergraph ranking is to predict the labels of X' according to the labeled images X by (9). Usually the size of X is small, so we generate m subset of X' by sampling, $\{X'_1, X'_2..., X'_m\}$. We denote the vector $S = \{s_1, s_2, ..., s_p\}$ to index the selected number of each unlabeled image. In our sampling trick, we keep each sample $x'_i \in X'$ be selected at least one time, i.e., $s_i \geq 1$. We combine X with each X'_i to generate a new image set, $X^*_i = X \cup X'_i$, and perform the hypergraph ranking algorithm on each X^*_i respectively. Thus, for each unlabeled image x'_i, we can obtain s_i predictions, $y^1_i, y^2_i, ..., y^{s_i}_i$, and we finally decide its label by the value of $\hat{y}_i = \frac{1}{s_i} \sum_{j=1}^{s_i} y^j_i$. With the help of sampling, we only need to perform the hypergraph ranking learning on the image set X^*_i, which is smaller than the original set $X \cup X'$, so the computational cost can be reduced rapidly. The detailed

performance will be evaluated in the Section of Experiments.

5.5 Feature Descriptors and Similarity Measurements

Figure 5.2: The spatial pyramids for the distance measure based on the appearance descriptors. Three levels of spatial pyramids for the appearance features are: 1×1(whole image, $l = 0$), 1×3(horizontal bars, $l = 1$),2×2(image quarters, $l = 2$).

To define the similarity measurement between two images, we utilize the following descriptors: SIFT [75], OpponentSIFT, rgSIFT, C-SIFT, RGB-SIFT [105] and PHOG [28] [13]. The first five are appearance-based color descriptors that are studied and evaluated in [105]. It is verified that their combination has the best performance on various image datasets. HOG (histogram of oriented gradients) is the shape descriptor widely used in object recognition and image categorization. Similar to [105], we extract both the sparse and the dense features for five appearance descriptors to boost image search performance. The sparse features are based on scale-invariant points obtained with the Harris-Laplace point detectors. The dense features are sampled every 6 pixels on multiple scales. For sparse features of each appearance descriptor, we create 1024-bin by k–means; for dense features of each appearance descriptor, we create 4096-bin codebooks because each image contains much more dense features than the sparse features. For each sparse (or dense) appearance descriptor, we follow the method in [106] to obtain histograms by soft feature quantization, which was proven to provide remarkable improvement in object recognition [106]:

$$His(w_f) = \frac{1}{n}\sum_{i=1}^{n}\frac{K_\sigma(D(w_f, f_i))}{\sum_{j=1}^{|V|}K_\sigma(D(v_j, f_i))}, \tag{5.10}$$

$$where\ K_\sigma(x) = \frac{1}{\sqrt{2\pi}\sigma}\exp\left(-\frac{1}{2}\frac{x^2}{\sigma^2}\right). \tag{5.11}$$

In Equation 5.10 n is the number of features (of a descriptor) in an image; f_i is the ith feature;

$D(w_f, f_i)$ is the distance between a codeword w_f and the feature f_i; $His(w_f)$ is the histogram value on the codeword (bin) w. In practice σ in the Gaussian kernel is tuned to make the distance measure more discriminative by cross-validation. Equation 5.10 distributes different probability mass to all relevant codewords(bins), where relevancy is determined by the ratio of the kernel values for all codewords v in the vocabulary V.

For the PHOG descriptor, we discretize gradient orientations into 8 bins to build histograms. For each of above 11 features (5 sparse features + 5 dense features + 1 HOG feature), we use a spatial pyramid matching(SPM) approach [67] to calculate the distances between two images $\{i, j\}$ because of its good performance:

$$Dis(i,j) = \sum_{l=0}^{L} \frac{1}{\alpha^l} \sum_{p=1}^{m(l)} \beta_p^l \chi^2(His_p^l(i), His_p^l(j)). \tag{5.12}$$

In the above equation, $His_p^l(i)$ and $His_p^l(j)$ are two image's local histograms at the p^{th} position of level l; α and β are two weighting parameters; $\chi^2(\cdot,\cdot)$ are the chi-square distance function used to measure the distance between two histograms. For the sparse and dense appearance features, we follow the setting of [105]: three levels of spatial pyramids (as shown in Figure 5.2) are 1×1(whole image, $l = 0$, $m(0) = 1$, $\beta_1^0 = 1$), 1×3(three horizontal bars, $l = 1$, $m(1) = 3$, $\beta_1^1 \sim \beta_3^1 = \frac{1}{3}$), 2×2(image quarters, $l = 2$, $m(2) = 4$, $\beta_1^2 \sim \beta_4^2 = \frac{1}{4}$); $\alpha^0 \sim \alpha^2 = 3$. For the HOG feature, we employ $L = 4$ levels ($l = 0 \sim 3$) of the spatial pyramids as in [13]: 1×1, 2×2, 4×4 and 8×8; $\alpha^0 = 2^L$ and $\alpha^l = 2^{L-l+1}$ for $l = 1, 2, 3$. After all the distance matrices for 11 features are obtained, the similarity matrix A between two images can be computed as follows:

$$A(i,j) = \exp(-\frac{1}{11} \sum_{k=1}^{11} \frac{Dis_k(i,j)}{\overline{D}_k}), \tag{5.13}$$

where $\overline{D}_k$ is the mean value of elements in the k^{th} distance matrix.

5.6 Experiments

5.6.1 Experimental Protocol

In this section, we used SVM and similarity based ranking as the baselines. The similarity based ranking method sorts retrieved image i according to the formula $\frac{1}{|Pos|} \sum_{j \in Pos} A(i,j) -$

$\frac{1}{|Neg|}\sum_{k\in Neg} A(i,k)$, where Pos and Neg denote positive/negative sets of feedback images respectively. We compare the proposed hypergraph ranking frameworks to the simple graph based manifold ranking algorithm [50] [49], and we also evaluate the performances of the probabilistic hypergraph ranking against the hypergraph based ranking. The hypergraph ranking algorithm is the same as Algorithm 1 except for using the binary incidence matrix (where $h_t(v_i, e_j) = 1$ or 0). For the parameter γ in Equation 5.9, we follow the original work [112] [114] and fix it as 0.1 for the best performance of both the hypergraph and the simple graph based algorithms. We use the respective optimal hyperedge size or the vertex degree (in the simple graph) in all experiments. Other parameters are directly computed from experimental data. Three general purpose image databases are used in this chapter: *Corel5K* [32], the *Scene dataset* [70] and *Caltech-101* [69]. Two measures are employed to evaluate the performance of above five ranking methods: (1) the precision vs. scope curve, (2) the precision vs. recall curve. We use each image in a database as a query example and both measures are averaged over all the queries in this database.

To provide a systematic evaluation, in the first round of relevance feedback 4 positive images and 5 negative images are randomly selected for each query image to form a training set containing 5 positive/ 5 negative examples. In the second and third round, another 5 positive/ 5 negative examples are randomly labeled for training, respectively. In this way a total of 10,20 and 30 images are marked after each of the three relevance feedback cycles. The rest of the images are used as testing data.

Besides the above passive learning setting, we also explore the active learning technique on *Corel5K*. Same setting as in [50], [49], [16] and [15], the ground truth labels of the 10 top ranked examples are used as feedback images after each round of retrieval cycle.

5.6.2 In-depth Analysis on Corel5K

We choose to conduct an in-depth analysis on *Corel5K* [32] because it is used as the benchmark in [50] and [49] for the manifold ranking method and a lot of other work [29]. Since all 50 categories of *Corel5K* contain the same number of 100 images, the precision-scope curve is used by [50] and [49] as the measurement. Therefore, we choose the precision-scope curve here in

order to make a direct comparison with [50] and [49].

r (scope)	Manifold Ranking **P(r)**	Hypergraph Ranking **P(r)**	Probabilistic Hypergraph Ranking **P(r)**
20	0.695 (at $K = 40$)	0.728 (at $K = 40$)	**0.748** (at $K = 40$)
40	0.606 (at $K = 40$)	0.644 (at $K = 30$)	**0.659** (at $K = 40$)
60	0.537 (at $K = 40$)	0.571 (at $K = 40$)	**0.583** (at $K = 40$)
80	0.475 (at $K = 40$)	0.508 (at $K = 40$)	**0.519** (at $K = 40$)
100	0.424 (at $K = 40$)	0.450 (at $K = 40$)	**0.459** (at $K = 50$)

Table 5.1: Selection of the hyperedge size and the vertex degree in the simple graph. We list the optimal precisions and corresponding K values at different retrieved image scopes. K denotes the hyperedge size and the vertex degree in the simple graph.

Combination of multiple complementary features for image retrieval. As presented in Section 4, we utilize totally 11 features to compute the similarity matrix A. To demonstrate the advantage of combining multiple complementary features, we employ the similarity based ranking method on *Corel5K* using the combined feature and all 11 single features. In this group experiment, only query image is provided and no relevance feedback is performed. As shown in Figure 5.3, the combined feature outperforms the best single feature (sparse C-SIFT) by $5 \sim 12\%$ for the different retrieval scopes r. All our comparisons are made on the similarity matrix computed with the **same** combined feature.

Computation cost and Selection of the sampling size. The most time consuming parts in both Algorithm 1 and Algorithm 2 are to solve the linear system in the 5th steps, which have the same time complexity. Thus, the computational cost of the hypergraph ranking is similar to that of the simple graph-based manifold ranking. In Fig. 5.4(Left), it is shown that the average cost of computation time (ms) to solve the linear system increases rapidly along with the size of H matrix. For example, on a desktop with Intel 2.4GHz Core2-Quad CPU and 8GB RAM, our Matlab code, without code optimization, takes 12.3 and 3930.3 milliseconds (ms) to solve a 500×500 linear system and a $5000X5000$ linear system, respectively. However, on the other hand, too small subset sampling size of unlabelled images will lead to deteriorated ranking accuracies. In Fig. 5.4(Right), the precision values (at r = 20) of different sampling configurations (on Corel5K dataset, under the passive learning setting, after the 1st round of relevance feedback) are shown and compared to the algorithm without random sampling. In this work, we adopt the configuration (500,100) in which we randomly sample subsets of 500

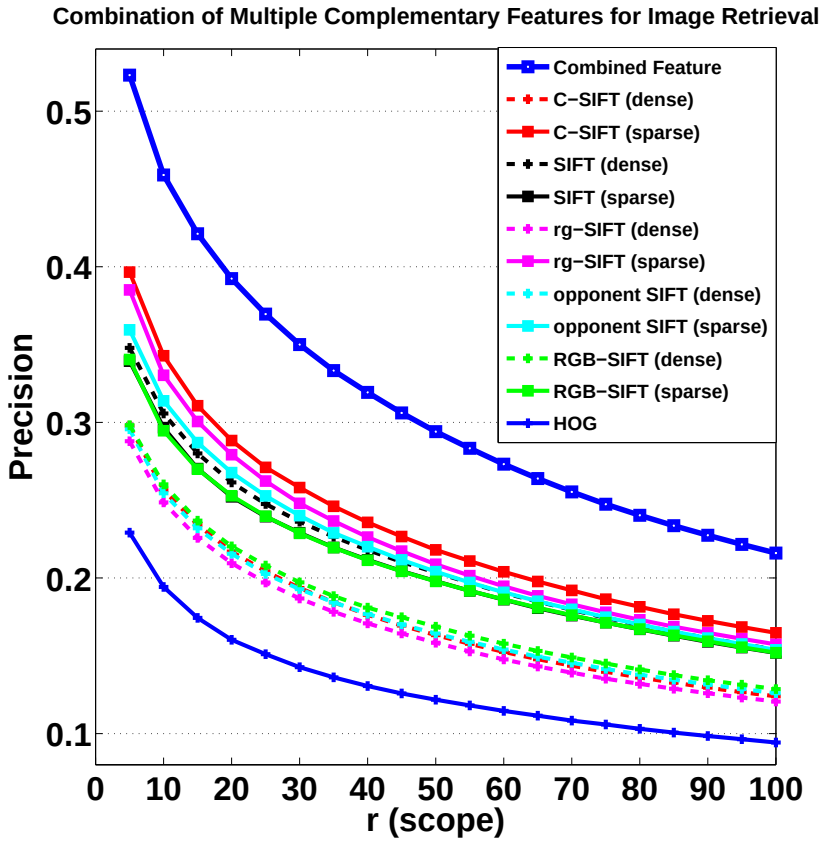

Figure 5.3: Combination of multiple complementary features for image retrieval. Best viewed in color.

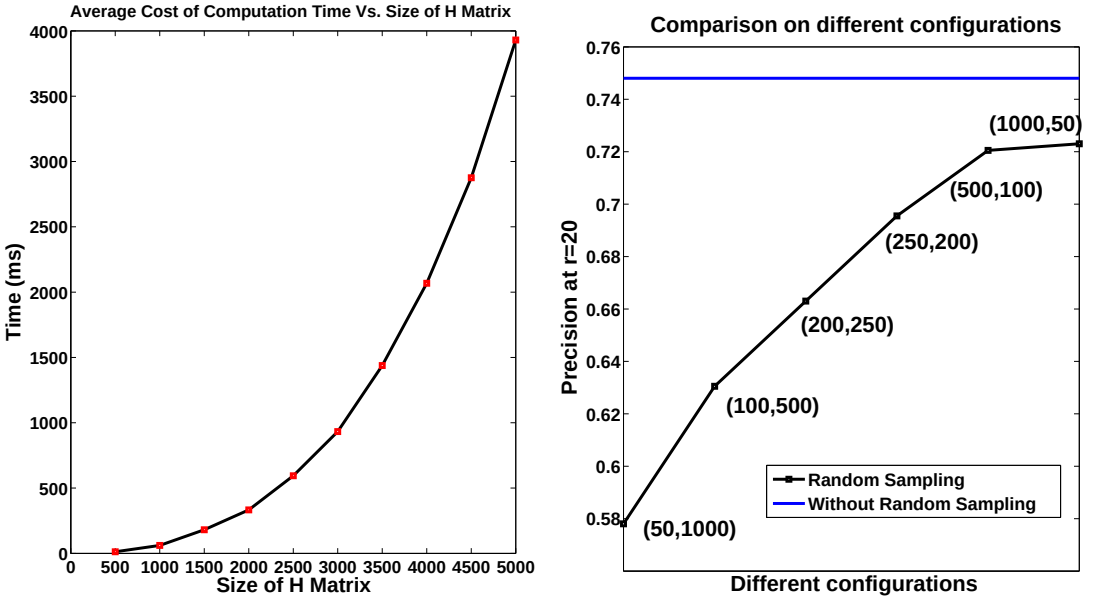

Figure 5.4: Left: the average cost of computation time (ms) to solve the linear system increases rapidly along with the size of H matrix. Right: the precision values (at r = 20) of different sampling configurations are shown and compared to the probabilistic hypergraph ranking algorithm without random sampling. Here (50, 1000) means that we randomly sample subsets of 50 unlabelled images for 1000 times.

images for 100 times. Using this configuration, we can achieve ranking accuracies close to the algorithm without randomly sampling, but largely decrease the cost of computation time. In the following, we will show both the results using the full Δ matrices and the results by randomly sampling.

Selection of the hyperedge size and the vertex degree in the simple graph. Intuitively, very small-size hyperedges only contain 'micro-local' grouping information which will not help the global clustering over all the images, and very large-size hyperedges may contain images from different classes and suppress diversity information. Similarly, in order to construct a simple graph, usually every vertex in the graph is connected to its K-nearest neighbors. For the fair comparison, in this work we perform a sweep over all the possible K values of the hyperedge size and the vertex degree in the simple graph to optimize the clustering results. For example, as shown in Table 5.1, after the first round of relevance feedback (using the passive learning setting), almost all the methods get optimal values at $K = 40$ if we use full H matrices. So we set both the hyperedge size and the vertex degree in the simple graph as 40 in the experiments on *Corel5K* when full H matrices are used. For experiments using randomly sampling,

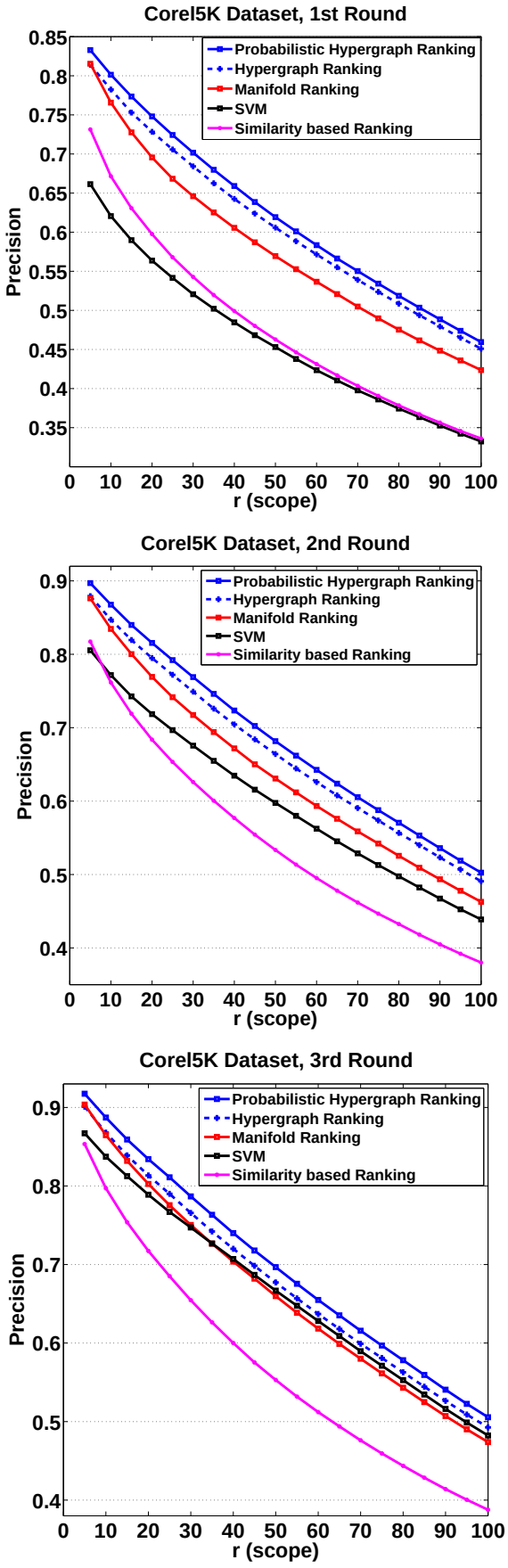

Figure 5.5: Precision vs. scope curves for *Corel5K* (when full Δ matrices images are used), under the passive learning setting. Best viewed in color.

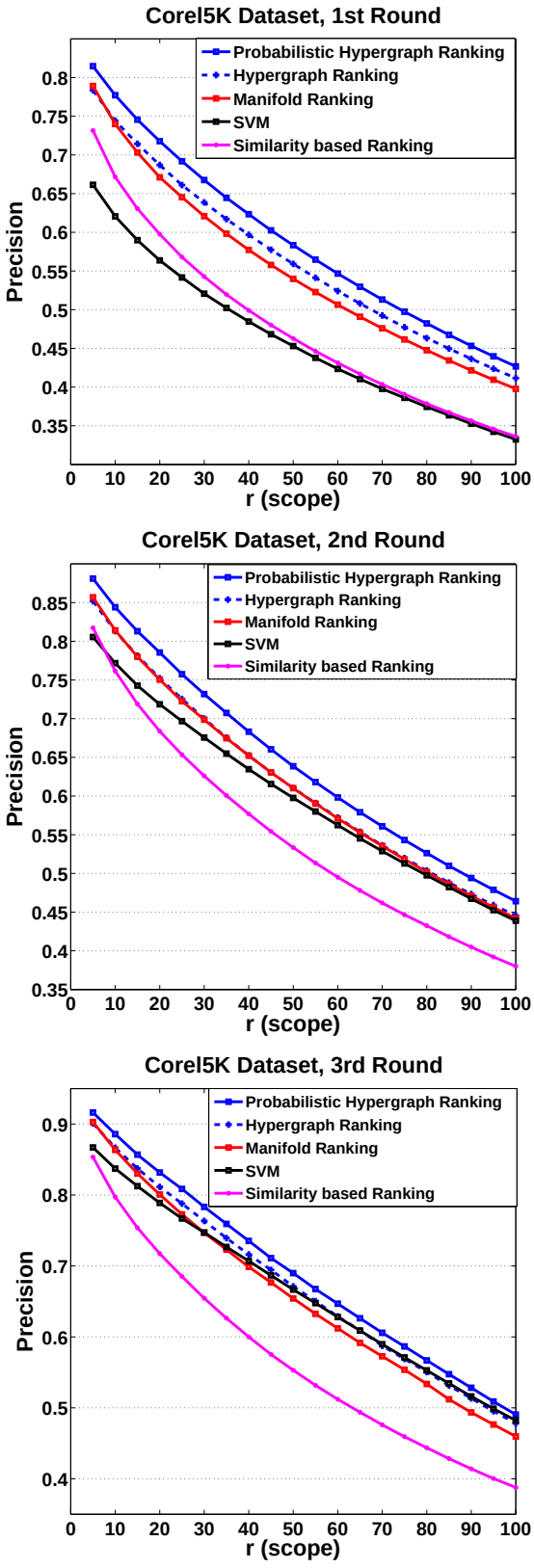

Figure 5.6: Precision vs. scope curves for *Corel5K* (when the (50, 1000) random sampling configuration is used), under the passive learning setting. Best viewed in color.

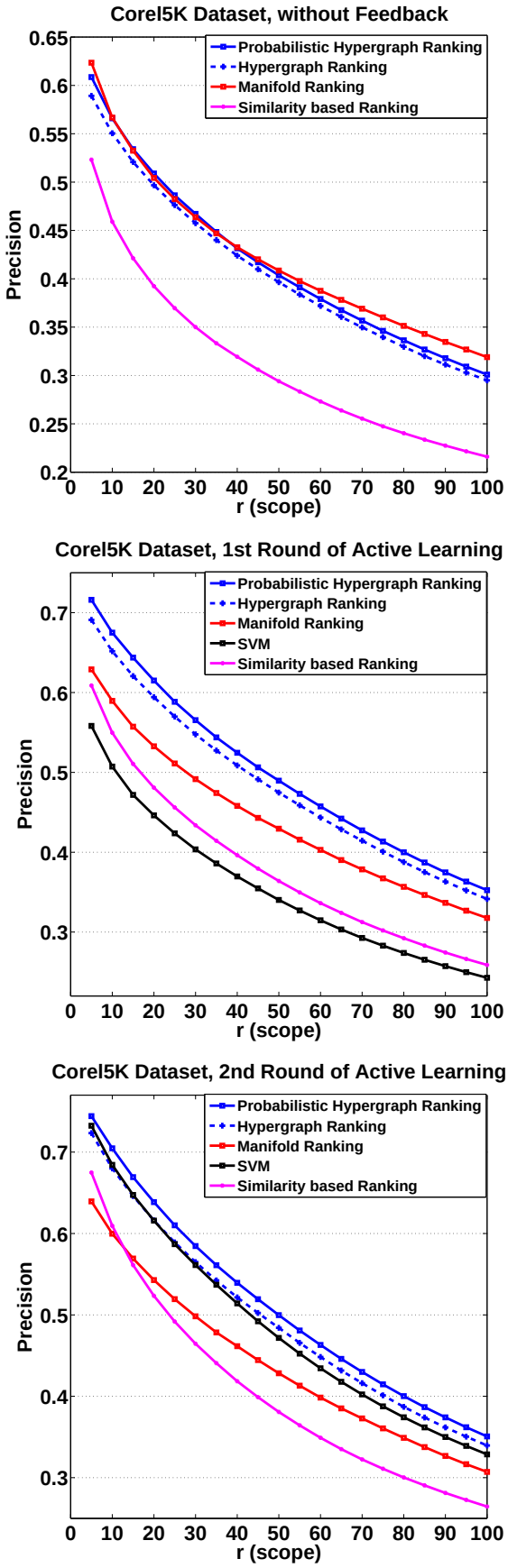

Figure 5.7: Precision vs. scope curves for *Corel5K* (when full Δ matrices images are used), under the active learning setting. Best viewed in color.

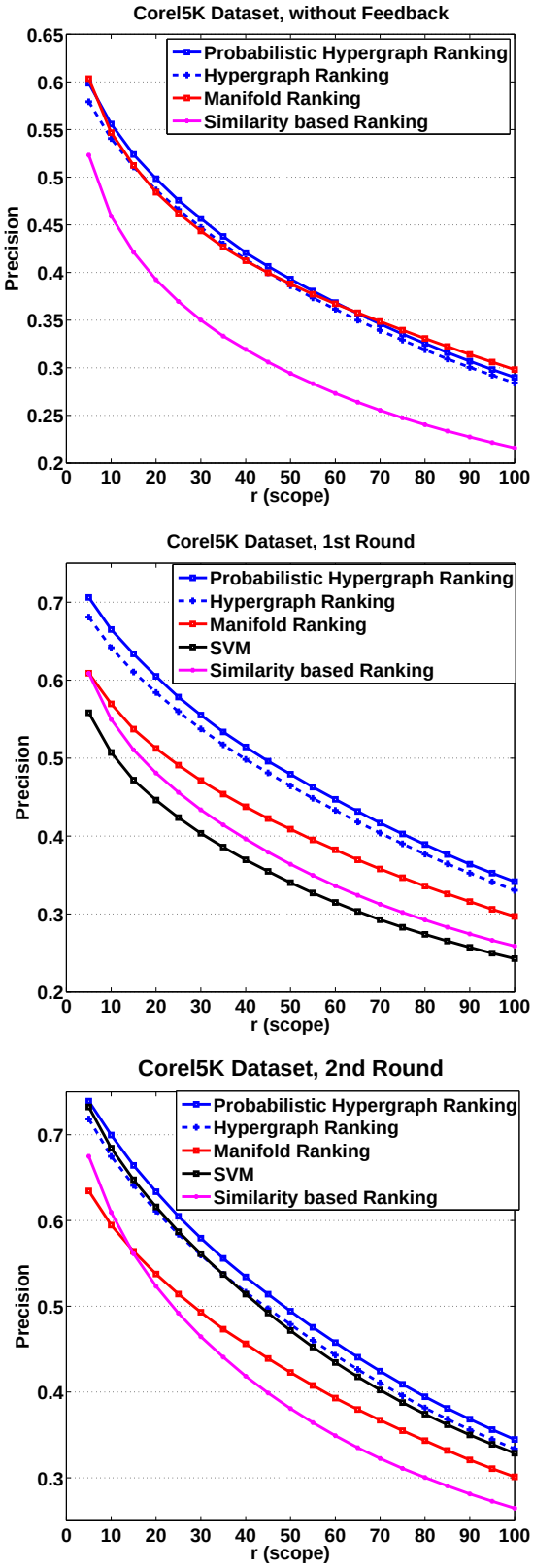

Figure 5.8: Precision vs. scope curves for *Corel5K* (when the (50, 1000) random sampling configuration is used), under the active learning setting. Best viewed in color.

we set $K = 14$.

Comparison under passive learning setting. As shown in Figure 5.5(experiments without random sampling) and Figure 5.6(experiments with random sampling), the probabilistic hypergraph ranking outperforms the manifold ranking by $4\% \sim 5\%$ and the traditional hypergraph ranking by $1\% \sim 3\%$ after each round of relevance feedback. The experiments with random sampling perform slightly worse than the experiments without random sampling.

Comparison under active learning setting. As shown in Figure 5.7(experiments without random sampling) and Figure 5.8(experiments with random sampling), we start the experiment from Round 0, in which only the query image is used for retrieval. Although the probabilistic hypergraph ranking achieved similar precision to the manifold ranking and the hypergraph ranking in the Round 0(without feedback), it progressively spaces out the difference in precision after the first round and the second round, in both two figures. At the end of the second round, it outperforms the manifold ranking by $4\% \sim 10\%$ and the traditional hypergraph ranking by $1\% \sim 2.5\%$ on different retrieval scope. Another observation is that the manifold ranking provides much less increase on precisions at the end of the second round. For example, in Figure 5.7, at $r = 20$ the precision of the manifold ranking increases from 50.4% to 54.3%, while the precision of the probabilistic hypergraph ranking increases from 50.8% to 63.9%.

Our method outperforms the manifold ranking results in [49] and [50] by approximately $8\% \sim 20\%$ under the similar setting.

5.6.3 Results on the Scene Dataset and Caltech-101

The *Scene dataset* [70] consists of 4485 gray-level images which are categorized into 15 groups. It is also important to mention that we only use 3 features for gray-level images (sparse SIFT, dense SIFT and HOG) to compute the similarity matrix in this experiment. For the experiments using full Δ matrices, the optimal hyperedge size is $K = 90$ and the optimal vertex degree of the simple graph is $K = 330$. For the experiments using randomly sampling matrices, the optimal hyperedge size and the optimal vertex degree of the simple graph are $K = 14$. Since every category of the *Scene dataset* contains different number of images, we choose the

precision-recall curves as a more rigorous measurement for the *Scene dataset*. As shown in Figure 5.11(experiments without random sampling) and Figure 5.12(experiments with random sampling), the probabilistic hypergraph ranking outperforms the manifold ranking by $5\% \sim 7\%$ on Precision for $Recall < 0.8$, after each round of feedback using the passive learning setting; the probabilistic hypergraph ranking is slightly better than the hypergraph ranking. In addition, we also show the per-class comparison on precisions (Figure 5.9 and Figure 5.10) at $r = 100$ after the 1st round. Our method exceeds the manifold ranking in 14 classes (out of the total 15 classes).

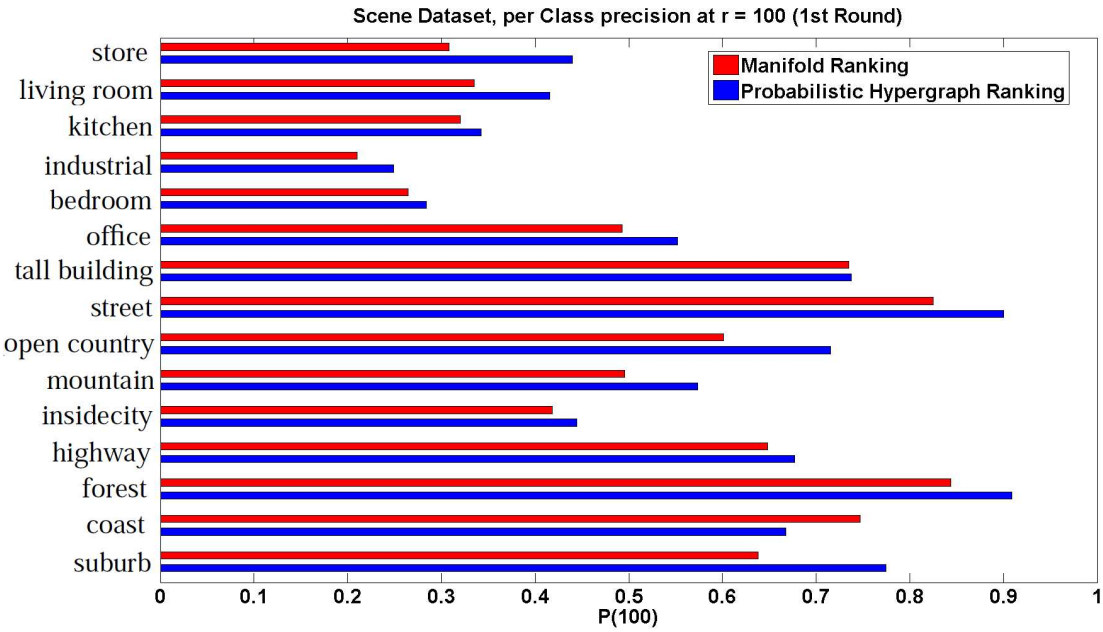

Figure 5.9: Per-class precisions for *Scene dataset* at $r = 100$ after the 1st round (when full Δ matrices images are used). Best viewed in color.

To demonstrate the scalability of our algorithm, we also conduct a comparison on *Caltech-101* [69] which contains 9146 images grouped into 101 distinct object classes and a background class. For *Caltech-101*, both the optimal hyperedge size and the optimal vertex degree of the simple graph are $K = 40$ or $K = 14$ when the experiments using full Δ matrices or random sampling matices. The precision-recall curves are shown in Figure 5.13and Figure 5.14, in which we can observe the advantage of the probabilistic hypergraph ranking on both the hypergraph ranking and the manifold ranking.

Above analysis confirms our proposed method from two aspects: (1) by considering the local

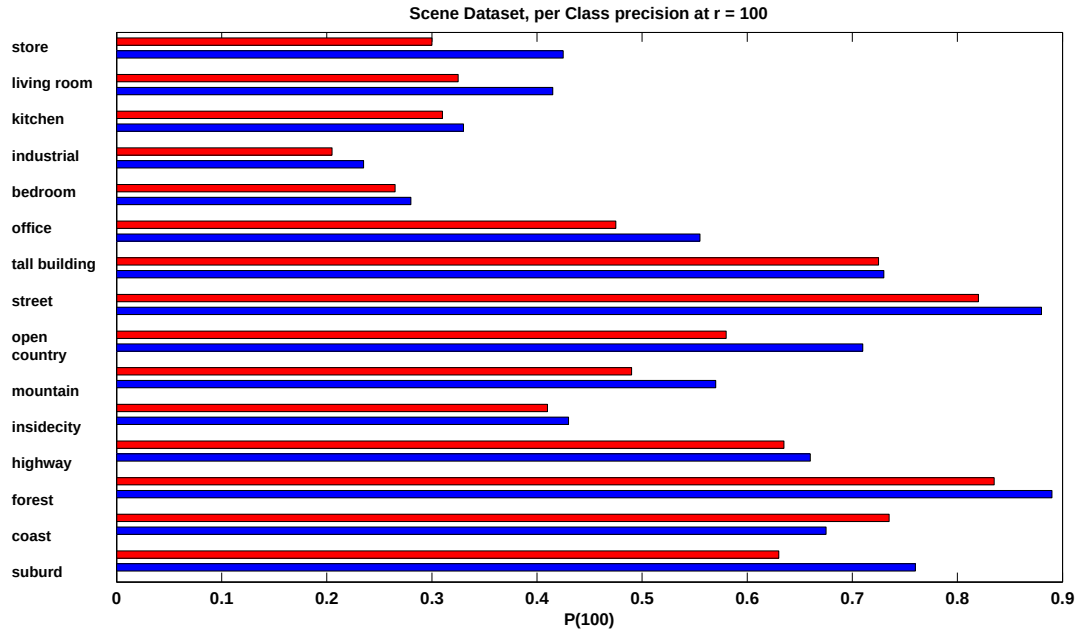

Figure 5.10: Per-class precisions for *Scene dataset* at $r = 100$ after the 1st round (when the (50, 1000) random sampling configuration is used). Best viewed in color.

grouping information, both hypergraph models can better approximate relevance between the labeled data and unlabled images than the simple graph based model; (2) probabilistic incidence matrix H is more suitable for defining the relationship between vertices in a hyperedge.

5.7 Conclusion

We introduced a transductive learning framework for content-based image retrieval, in which a novel graph structure – probabilistic hypergraph is used to represent the relevance relationship among the vertices (images). Based on the similarity matrix computed from complementary image features, we take each image as a 'centroid' vertex and form a hyperedge by a centroid and its k-nearest neighbors. We adopt a probabilistic incidence structure to describe the local grouping information and the probability that a vertex belongs to a hyperedge. In this way, the task of image retrieval with relevance feedback is converted to a transductive learning problem which can be solved by the hypergraph ranking algorithm. The effectiveness of the proposed method is demonstrated by extensive experimentation on three general purpose image databases.

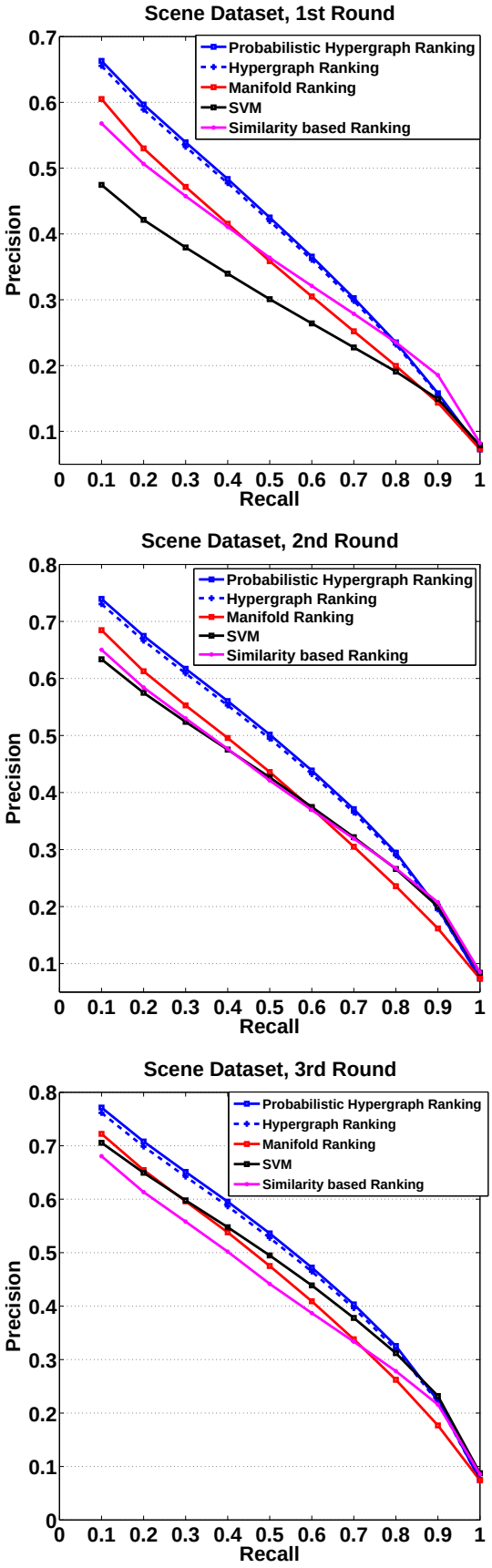

Figure 5.11: The precision-recall curves for *Scene dataset* under the passive learning setting (when full Δ matrices images are used). Best viewed in color.

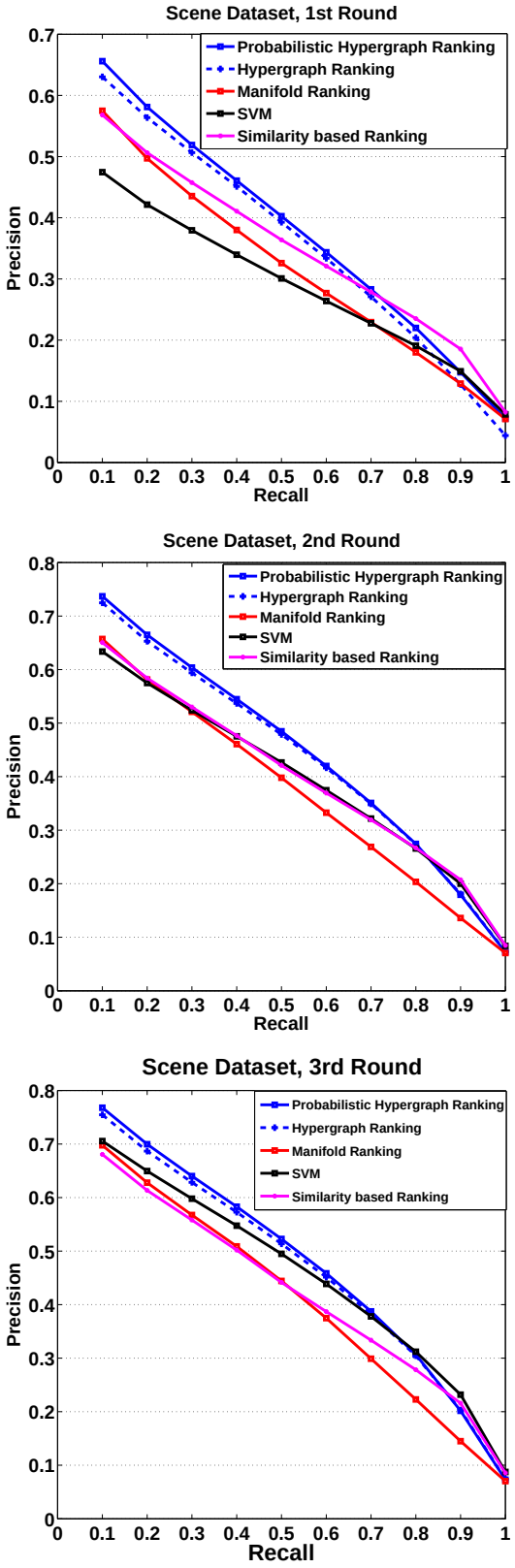

Figure 5.12: The precision-recall curves for *Scene dataset* under the passive learning setting (when the (50, 1000) random sampling configuration is used). Best viewed in color.

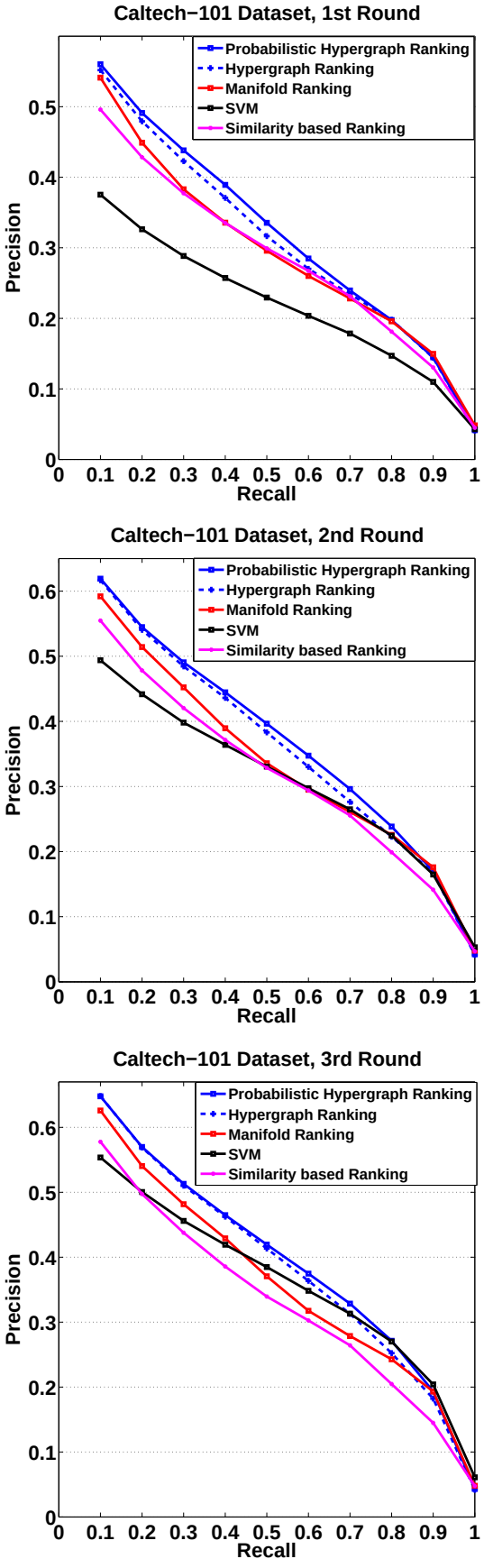

Figure 5.13: The precision-recall curves for *Caltech-101* (when full Δ matrices images are used). Best viewed in color.

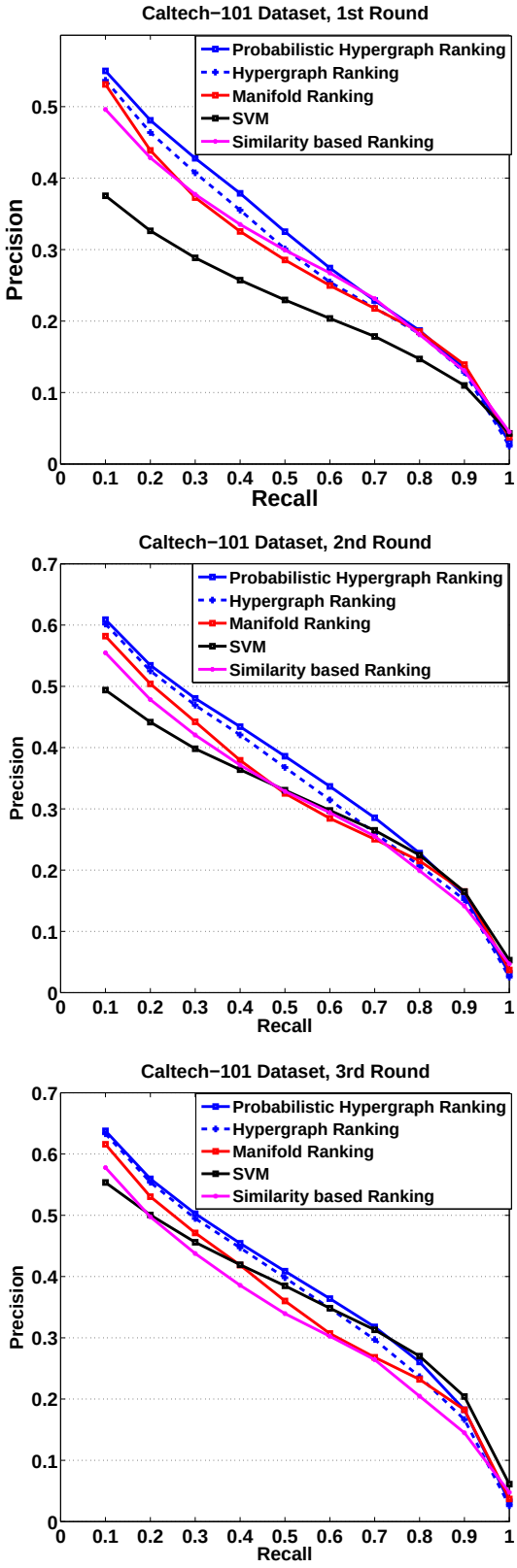

Figure 5.14: *The precision-recall curves for Caltech-101* (when the (50, 1000) random sampling configuration is used). Best viewed in color.

Chapter 6

Conclusion

In this thesis, at first we summarized the basic concept of hypergraphs and relative learning algorithms. Then we construct hypergraph models for three scenarios: (1) video object segmentations, (2) unsupervised image categorization and (3) content based image retrieval. In the first two applications the unsupervised hypergraph cut algorithm are used for clustering, which involves eigen-decomposition of the hypergraph Laplacian matrix. The third application utilized the hypergraph based transductive learning or semi-supervised learning algorithm, which involves the solving of a linear system.

As we indicated in Chapter 4, the advantage of the hypergraph based models lies in the way the neighborhood structures are analyzed. By Cliuqe Expansion [116] a hypergraph can be transferred to a simple graph, in which the pairwise similarity between two vertices is proportional to the sum of their corresponding hyperedge weights. According to the analysis in Agarwal's work [1], it is verified that the eigenvectors of the hypergraph normalized Laplacian are close to the eigenvectors of this pairwise graph. Under specific conditions (i.e. when the hypergraph is uniform), the two sets of eigenvectors are even equivalent to each other. Consider that we transfer hypergraphs constructed in this thesis into simple graphs by Clique Expansion. In the obtained simple graphs, the edge weight between two vertices v_i and v_j is not decided by the pairwise affinity $A_{i,j}$, but the averaged neighboring affinities close to them; this edge weight between v_i and v_j is influenced more by those pairwise affinities whose incident vertices share more hyperedges with v_i and v_j. In this way, the 'correlation information' or 'high order local grouping information' contained in the hyperedge weights is used for the construction of graph neighborhood. We argue that such an 'averaging' effect caused by the hypergraph neighborhood structure is beneficial to the image clustering task, just as local image smoothing may be beneficial to the image segmentation task. We give an example to support our argument in

Chapter 4, Section 4.3.3. Furthermore, we compare our work with simple-graph based methods (and other state-of-the-art work) in all three applications quantitatively and statistically. The effectiveness of the proposed methods is demonstrated by extensive experimentation on various datasets. It is also worth to mention that, besides the enhanced clustering/classification accuracies, another advantage of hypergraph based model is the stability to the parameter selection (the selection of hyperedge size), which is mentioned in Section 4.4.2.

Since hypergraph based algorithm is a open system, in the future work, we may add more feature descriptors (such as texture information) into our frameworks to construct more hyperedges to further improve the expressive power of hypergraph based models. We also plan to introduce prior information into the hypergraph framework for video object segmentation and solve this problem under the semi-supervised setting. Hopefully this will largely enhance the accuracy of segmentation results.

References

[1] S. Agarwal, K. Branson, and S. Belongie. Higher order learning with graphs. In *ICML'06: International Conference on Machine Learning 2005*.

[2] S. Agarwal, J. Lim, L. Zelnik-Manor, P. Perona, D. Kriegman, and S. Belongie. Beyond pairwise clustering. In *Proceedings of the 2005 IEEE Computer Society Conference on Computer Vision and Pattern Recognition (CVPR'05) - Volume 2*, pages 838–845, Washington, DC, USA, 2005.

[3] C. J. Alpert and A. B. Kahng. Recent directions in netlist partitioning: A survey. *Integration: The VLSI Journal*, 19:1–81, 1995.

[4] A. Banerjee, S. Basu, and S. Merugu. Multi-way clustering on relation graphs. In *Proceedings of the SIAM International Conference on Data Mining (SDM-2007)*, 2007.

[5] A. Banerjee, I. Dhillon, J. Ghosh, S. Merugu, and D. S. Modha. A generalized maximum entropy approach to bregman co-clustering and matrix approximation. *Joural Machine Learning Research*, 8:1919–1986, 2007.

[6] H. Bay, T. Tuytelaars, and L. Van Gool. Surf: Speeded up robust features. In *ECCV'06: European Conference on Computer Vision 2006*, 2006.

[7] R. Bekkerman, R. El-Yaniv, and A. McCallum. Multi-way distributional clustering via pairwise interactions. In *ICML '05: Proceedings of the 22nd international conference on Machine learning*, pages 41–48, New York, NY, USA, 2005. ACM.

[8] J. Besag. On the statistical analysis of dirty pictures. *RoyalStat*, B-48(3):259–302, 1986.

[9] C. M. Bishop. Pattern recognition and machine learning. August 2006.

[10] M. Bolla. Spectra, euclidean representations and clustering of hypergraphs. In *Discrete Mathematics*, 1993.

[11] I. Borg and P. Groenen. *Modern Multidimensional Scaling: Theory and Applications*. Springer, 2005.

[12] A. Bosch, A. Zisserman, and X. Munoz. Image classification using random forests and ferns. In *ICCV'07: IEEE International Conference on Computer Vision 2007*.

[13] A. Bosch, A. Zisserman, and X. Munoz. Representing shape with a spatial pyramid kernel. In *CIVR'07: ACM International Conference on Image and Video Retrieval 2007*.

[14] Y. Boykov and V. Kolmogorov. An experimental comparison of min-cut/max-flow algorithms for energy minimization in vision. *IEEE Trans. Pattern Anal. Mach. Intell.*, 26(9):1124–1137, 2004.

[15] D. Cai, X. He, and J. Han. Active subspace learning. In *ICCV'09: IEEE International Conference on Computer Vision 2009*.

[16] D. Cai, X. He, and J. Han. Semi-supervised discriminant analysis. In *ICCV'07: IEEE International Conference on Computer Vision 2007*.

[17] J. Carroll and J. Chang. Analysis of individual differences in multidimensional scaling via an n-way generalization of eckart-young decomposition. *Psychometrika*, pages 283–319, 1970.

[18] P. K. Chan, M. D. F. Schlag, and J. Y. Zien. Spectral k-way ratio-cut partitioning and clustering. In *DAC '93: Proceedings of the 30th international Design Automation Conference*, pages 749–754, New York, NY, USA, 1993. ACM.

[19] J. Chen and Y. Saad. Co-clustering of high order relational data using spectral hypergraph partitioning. *Tech. Report UMSI 2009/xx,University of Minnesota Supercomputing Institute*, 2009.

[20] S. Chen, F. Wang, and C. Zhang. Simultaneous heterogeneous data clustering based on higher order relationships. In *ICDMW '07: Proceedings of the Seventh IEEE International Conference on Data Mining Workshops*, pages 387–392, Washington, DC, USA, 2007. IEEE Computer Society.

[21] H. Cho, I. Dhillon, Y. Guan, and S. Sra. Minimum sum squared residue co-clustering of gene expression data, 2004.

[22] O. Chum and A. Zisserman. An exemplar model for learning object classes. In *Proceedings of the 2007 IEEE Computer Society Conference on Computer Vision and Pattern Recognition (CVPR'07)*.

[23] D. Chung, W. J. MacLean, and S. Dickinson. Integrating region and boundary information for improved spatial coherencein object tracking. In *CVPRW'04: Proceedings of the 2004 Conference on Computer Vision and Pattern Recognition Workshop (CVPRW'04)*, pages 3, Volume 1, 2004.

[24] F. Chung. *Spectral Graph Theory*. American Mathematical Society, 1997.

[25] T. Cour, F. Benezit, and J. Shi. Spectral segmentation with multiscale graph decomposition. In *CVPR '05: Proceedings of the 2005 IEEE Computer Society Conference on Computer Vision and Pattern Recognition (CVPR'05)*, pages II: 1124–1131, 2005.

[26] I. J. Cox, M. L. Miller, T. P. Minka, T. V. Papathomas, and P. N. Yianilos. The Bayesian image retrieval system – Pichunter: Theory, Implementation and Psychophysical Experiments. *IEEE transactions on image processing*, 9:20–37, 2000.

[27] T. Cox, M. Cox, and J. Branco. Multidimensional scaling for n-tuples. *British Journal Mathematical Statistical Psychology*, 44.

[28] N. Dalal and B. Triggs. Histograms of oriented gradients for human detection. In *Proceedings of the 2005 IEEE Computer Society Conference on Computer Vision and Pattern Recognition (CVPR'05)*.

[29] R. Datta, D. Joshi, J. Li, and J. Z. Wang. Image retrieval: Ideas, influences, and trends of the new age. *ACM Comput. Surv.*, 40(2):1–60, April 2008.

[30] D. DeMenthon and R. Megret. Spatio-temporal segmentation of video by hierarchical mean shift analysis. In *CVPR '02: Proceedings of the 2002 IEEE Computer Society Conference on Computer Vision and Pattern Recognition (CVPR'02)*, 2002.

[31] I. S. Dhillon, S. Mallela, and D. S. Modha. Information-theoretic co-clustering. In *KDD '03: Proceedings of the ninth ACM SIGKDD international conference on Knowledge discovery and data mining*, pages 89–98, New York, NY, USA, 2003. ACM.

[32] P. Duygulu, K. Barnard, N. de Freitas, P. Duygulu, K. Barnard, and D. Forsyth. Object recognition as machine translation: Learning a lexicon for a fixed image vocabulary. In *ECCV'02: European Conference on Computer Vision 2002*.

[33] M. Everingham, L. Van Gool, C. K. I. Williams, J. Winn, and A. Zisserman. The PASCAL Visual Object Classes Challenge 2008 (VOC2008) Results.

[34] R. Fergus, L. Fei-Fei, P. Perona, and A. Zisserman. Learning object categories from google's image search. In *ICCV'05: IEEE International Conference on Computer Vision 2005*.

[35] C. M. Fiduccia and R. M. Mattheyses. A linear-time heuristic for improving network partitions. In *DAC '82: Proceedings of the 19th Design Automation Conference*, pages 175–181, Piscataway, NJ, USA, 1982. IEEE Press.

[36] M. Fieldler. Algebraic connectivity of graphs. *Czechoslovak Mathematical Journal*, 23(98):298–305, 1973.

[37] M. A. Fischler and R. C. Bolles. Random sample consensus: a paradigm for model fitting with applications to image analysis and automated cartography. In *Readings in computer vision: issues, problems, principles, and paradigms*, pages 726–740, San Francisco, CA, USA, 1987. Morgan Kaufmann Publishers Inc.

[38] A. Frank and A. Asuncion. UCI machine learning repository, 2010.

[39] B. J. J. Frey and D. Dueck. Clustering by passing messages between data points. *Science*, 315, 2007.

[40] M. Fritz and B. Schiele. Towards unsupervised discovery of visual categories. In *Proceedings of 28th Annual Symposium of the German Association for Pattern Recognition (DAGM'06)*.

[41] M. R. Garey and D. S. Johnson. *Computers and Intractability; A Guide to the Theory of NP-Completeness*. W. H. Freeman & Co., New York, NY, USA, 1990.

[42] D. Gibson, J. Kleinberg, and P. Raghavan. Clustering categorical data: an approach based on dynamical systems. *The VLDB Journal*, 8(3-4):222–236, 2000.

[43] K. Grauman and T. Darrell. The pyramid match kernel: Discriminative classification with sets of image features. In *ICCV'05: IEEE International Conference on Computer Vision 2005*.

[44] K. Grauman and T. Darrell. Unsupervised learning of categories from sets of partially matching image features. In *Proceedings of the 2006 IEEE Computer Society Conference on Computer Vision and Pattern Recognition (CVPR'06)*, pages I: 19–25, 2006.

[45] G. Griffin, A. Holub, and P. Perona. Caltech-256 object category dataset. Technical report, California Institute of Technology, 2007.

[46] G. Griffin and P. Perona. Learning and using taxonomies for fast visual categorization. 2008.

[47] S. W. Hadley. Approximation techniques for hypergraph partitioning problems. *Discrete Appl. Math.*, 59(2):115–127, 1995.

[48] C. Hayashi. Two dimensional quantification based on the measure of dissimilarity among three elements.

[49] J. He, M. Li, H. Zhang, H. Tong, and C. Zhang. Generalized manifold-ranking-based image retrieval. *IEEE transaction on Image Processing*, 15(10):3170–3177, October 2006.

[50] J. He, M. Li, H.-J. Zhang, H. Tong, and C. Zhang. Manifold-ranking based image retrieval. In *ACM MULTIMEDIA '04*.

[51] X. He, W.-Y. Ma, O. King, M. Li, and H. Zhang. Learning and inferring a semantic space from user's relevance feedback for image retrieval. In *ACM MULTIMEDIA '02*.

[52] W. J. Heiser and M. Bennani. Triadic distance models: axiomatization and least squares representation. *J. Math. Psychol.*, 41(2):189–206, 1997.

[53] T. K. Ho. The random subspace method for constructing decision forests. *IEEE Transactions on Pattern Analysis and Machine Intelligence*, 20(8):832–844, 1998.

[54] S. C. H. Hoi and M. R. Lyu. A semi-supervised active learning framework for image retrieval. In *CVPR '05: Proceedings of the 2005 IEEE Computer Society Conference on Computer Vision and Pattern Recognition (CVPR'05)*.

[55] T. Hu and M. K. Multiterimnal flows in hypergraphs. *VLSI Circuit Layout: Theory and Design*, pages 87–93, 1985.

[56] Y. Huang, Q. Liu, and D. Metaxas. Video object segmentation by hypergraph cut. In *CVPR '09: Proceedings of the 2009 IEEE Computer Society Conference on Computer Vision and Pattern Recognition (CVPR'09)*.

[57] E. Ihler, D. Wagner, and F. Wagner. Modeling hypergraphs by graphs with the same mincut properties. *Inf. Process. Lett.*, 45(4):171–175, 1993.

[58] S. Joly and G. Calv. Three-way distances. *Journal of Classification*, 12(2):191–205, 1995.

[59] L. Karlinsky, M. Dinerstein, D. Levi, and S. Ullman. Unsupervised classification and part localization by consistency amplification. In *ECCV'08: European Conference on Computer Vision 2008*.

[60] G. Karypis and V. Kumar. Multilevel k-way hypergraph partitioning. In *DAC '99: Proceedings of the 36th annual ACM/IEEE Design Automation Conference*, pages 343–348, New York, NY, USA, 1999. ACM.

[61] B. W. Kernighan and S. Lin. An efficient heuristic procedure for partitioning graphs. *The Bell system technical journal*, 49(1):291–307, 1970.

[62] G. Kim, C. Faloutsos, and M. Hebert. Unsupervised modeling of object categories using link analysis techniques. In *CVPR '08: Proceedings of the 2008 IEEE Computer Society Conference on Computer Vision and Pattern Recognition (CVPR'08)*.

[63] G. Kim and A. Torralba. Unsupervised detection of regions of interest using iterative link analysis. In Y. Bengio, D. Schuurmans, J. Lafferty, C. K. I. Williams, and A. Culotta, editors, *NIPS*, pages 961–969. 2009.

[64] N. Kumar, L. Zhang, and S. Nayar. What is a good nearest neighbors algorithm for finding similar patches in images? In *ECCV '08: Proceedings of the 10th European Conference on Computer Vision*, pages 364–378.

[65] C. H. Lampert, M. B. Blaschko, and T. Hofmann. Beyond sliding windows: Object localization by efficient subwindow search. In *Proceedings of the 2008 IEEE Computer Society Conference on Computer Vision and Pattern Recognition (CVPR'08)*.

[66] S. Lazebnik and J. Ponce. The local projective shape of smooth surfaces and their outlines. *Int. J. Comput. Vision*, 63(1):65–83, 2005.

[67] S. Lazebnik, C. Schmid, and J. Ponce. Beyond bags of features: Spatial pyramid matching for recognizing natural scene categories. In *Proceedings of the 2006 IEEE Computer Society Conference on Computer Vision and Pattern Recognition (CVPR'06)*.

[68] Y. J. Lee and K. Grauman. Shape discovery from unlabeled image collections. *Computer Vision and Pattern Recognition, IEEE Computer Society Conference on*, 2009.

[69] F. Li, R. Fergus, and P. Perona. Learning generative visual models from few training examples: An incremental Bayesian approach tested on 101 object categories. *Computer Vision and Image Understanding*, 2007.

[70] F.-F. Li and P. Perona. A Bayesian hierarchical model for learning natural scene categories. In *CVPR '05: Proceedings of the 2005 IEEE Computer Society Conference on Computer Vision and Pattern Recognition (CVPR'05)*.

[71] W.-C. W. Li and P. Solé. Spectra of regular graphs and hypergraphs and orthogonal polynomials. *European Journal of Combinatorics*, 17(5):461–477, 1996.

[72] D. Liu and T. Chen. Unsupervised image categorization and object localization using topic models and correspondences between images. In *ICCV'07: IEEE International Conference on Computer Vision 2007*.

[73] B. Long, Z. M. Zhang, X. Wú, and P. S. Yu. Spectral clustering for multi-type relational data. In *ICML '06: Proceedings of the 23rd international conference on Machine learning*, pages 585–592, New York, NY, USA, 2006. ACM.

[74] B. Long, Z. M. Zhang, and P. S. Yu. A probabilistic framework for relational clustering. In *KDD '07: Proceedings of the 13th ACM SIGKDD international conference on Knowledge discovery and data mining*, pages 470–479, New York, NY, USA, 2007. ACM.

[75] D. Lowe. Object recognition from local scale-invariant features. In *ICCV'09: IEEE International Conference on Computer Vision 2009*.

[76] B. D. Lucas and T. Kanade. An iterative image registration technique with an application to stereo vision. In *Proceedings of the 7th International Joint Conference on Artificial Intelligence (IJCAI '81)*, pages 674–679, April 1981.

[77] M. m. Deza and I. Rosenberg. n-Semimetric, 2000.

[78] S. MacArthur, C. Brodley, and C. Shyu. Relevance feedback decision trees in content-based image retrieval. In *CBAIVL '00: Proceedings of the IEEE Workshop on Content-based Access of Image and Video Libraries*, page 68, 2000.

[79] J. B. Macqueen. Some methods of classification and analysis of multivariate observations. In *Proceedings of the Fifth Berkeley Symposium on Mathematical Statistics and Probability*, pages 281–297, 1967.

[80] T. Malisiewicz and A. A. Efros. Beyond categories: The visual memex model for reasoning about object relationships. In *NIPS*, 2009.

[81] A. Ng, M. Jordan, and Y. Weiss. On spectral clustering: Analysis and an algorithm. In *Advances in Neural Information Processing Systems (NIPS)*, 2001.

[82] A. S. Ogale, C. Fermuller, and Y. Aloimonos. Motion segmentation using occlusions. *IEEE Trans. Pattern Anal. Mach. Intell.*, 27(6):988–992, 2005.

[83] J. Pistorius and M. Minoux. An improved direct labeling method for the maxcflow mincut computation in large hypergraphs and applications. *International Transactions in Operational Research*, 10:1–11, 2003.

[84] T. Quack, V. Ferrari, B. Leibe, and L. Van Gool. Efficient mining of frequent and distinctive feature configurations. In *ICCV'07: IEEE International Conference on Computer Vision 2007*.

[85] P. Quelhas, F. Monay, J. Odobez, D. Gatica Perez, T. Tuytelaars, and L. Van Gool. Modeling scenes with local descriptors and latent aspects. In *ICCV'05: IEEE International Conference on Computer Vision 2005*.

[86] J. Rodréquez. On the laplacian spectrum and walk-regular hypergraphs. In *Linear and Multilinear Algebra*, 2003.

[87] Y. Rui, T. S. Huang, and S.-F. Chang. Image retrieval: Current techniques, promising directions, and open issues. *Journal of Visual Communication and Image Representation*, 10(1):39–62, March 1999.

[88] B. C. Russell, A. A. Efros, J. Sivic, W. T. Freeman, and A. Zisserman. Using multiple segmentations to discover objects and their extent in image collections. In *Proceedings of CVPR*, July 2006.

[89] H. Sahbi, J. Audibert, and R. Keriven. Graph-cut transducers for relevance feedback in content based image retrieval. In *ICCV'07: IEEE International Conference on Computer Vision 2007*.

[90] A. Sethi, D. Renaudie, D. Kriegman, and J. Ponce. Curve and surface duals and the recognition of curved 3d objects from their silhouettes. *Int. J. Comput. Vision*, 58(1):73–86, 2004.

[91] J. Shi and J. Malik. Motion segmentation and tracking using normalized cuts. In *IEEE International Conference on Computer Vision (ICCV)*, pages 1154–1160, 1998.

[92] J. Shi and J. Malik. Normalized cuts and image segmentation. *IEEE Transactions on Pattern Analysis and Machine Intelligence*, 22(8):888–905, 2000.

[93] J. Shi and J. Malik. Normalized cuts and image segmentation. *IEEE Trans. Pattern Anal. Mach. Intell.*, 22(8):888–905, vol 8, August 2000.

[94] J. Sivic, B. C. Russell, A. A. Efros, A. Zisserman, and W. T. Freeman. Discovering objects and their location in images. In *IEEE International Conference on Computer Vision*, 2005.

[95] J. Sivic, B. C. Russell, A. Zisserman, I. Ecole, and N. Suprieure. Efros. unsupervised discovery of visual object class hierarchies. In *In Proc. CVPR*, 2008.

[96] P. Smith, T. Drummond, and R. Cipolla. Layered motion segmentation and depth ordering by tracking edges. *IEEE Trans. Pattern Anal. Mach. Intell.*, 26(4):479–494, 2004.

[97] A. Stein, D. Hoiem, and M. Hebert. Learning to find object boundaries using motion cues. In *IEEE International Conference on Computer Vision (ICCV)*, October 2007.

[98] L. Sun, S. Ji, and J. Ye. Hypergraph spectral learning for multi-label classification. In *SIG KDD '08: ACM SIGKDD Conference on Knowledge Discovery and Data Mining (KDD) 2008*.

[99] Z. Tian, T. Hwang, and R. Kuang. A hypergraph-based learning algorithm for classifying gene expression and array cgh data with prior knowledge. *Bioinformatics*, July 2009.

[100] K. Tieu and P. Viola. Boosting image retrieval. In *International Journal of Computer Vision*, pages 228–235, 2000.

[101] S. Todorovic and N. Ahuja. Extracting subimages of an unknown category from a set of images. In *CVPR '06: Proceedings of the 2006 IEEE Computer Society Conference on Computer Vision and Pattern Recognition (CVPR'06)*.

[102] S. Tong and E. Chang. Support vector machine active learning for image retrieval. In *ACM MULTIMEDIA '01*.

[103] T. Tuytelaars, C. H. Lampert, M. B. Blaschko, and W. Buntine. Unsupervised object discovery: A comparison. *IJCV*, 2009.

[104] R. Vaillant and O. Faugeras. Using extremal boundaries for 3-d object modeling. *IEEE Trans. Pattern Anal. Mach. Intell.*, 14(2):157–173, February 1992.

[105] K. E. A. van de Sande, T. Gevers, and C. G. M. Snoek. Evaluating color descriptors for object and scene recognition. *IEEE Transactions on Pattern Analysis and Machine Intelligence*, (in press), 2010.

[106] J. van Gemert, J. Geusebroek, C. Veenman, and A. Smeulders. Kernel codebooks for scene categorization. In *ECCV'08: European Conference on Computer Vision 2008*.

[107] U. von Luxburg. A tutorial on spectral clustering. *Statistics and Computing*, 17(4):395–416, 2007.

[108] X. Wang and X. Tang. Random sampling for subspace face recognition. *Int. J. Comput. Vision*, 70(1):91–104, 2006.

[109] Y. Weiss. Segmentation using eigenvectors: A unifying view. In *IEEE International Conference on Computer Vision (ICCV)*, pages 975–982, 1999.

[110] J. Wills, S. Agarwal, and S. Belongie. What went where. In *CVPR '03: Proceedings of the 2003 IEEE Computer Society Conference on Computer Vision and Pattern Recognition (CVPR'03)*, pages I: 37–44, 2003.

[111] J. Xiao and M. Shah. Accurate motion layer segmentation and matting. In *CVPR '05: Proceedings of the 2005 IEEE Computer Society Conference on Computer Vision and Pattern Recognition (CVPR'05) - Volume 2*, pages 698–703, Washington, DC, USA, 2005. IEEE Computer Society.

[112] D. Zhou, O. Bousquet, T. N. Lal, J. Weston, and B. Schökopf. Learning with local and global consistency. In *NIPS'03: Advances in Neural Information Processing Systems (NIPS) 2003*.

[113] D. Zhou, J. Huang, and B. Schökopf. Learning with hypergraphs: Clustering, classification, and embedding. In *Advances in Neural Information Processing Systems*, 2006.

[114] D. Zhou, J. Huang, and B. Schölkopf. Learning from labeled and unlabeled data on a directed graph. In *ICML'05: International Conference on Machine Learning 2005*.

[115] X. Zhu, Z. Ghahramani, and J. Lafferty. Semi-supervised learning using Gaussian fields and harmonic functions. In *ICML'03: International Conference on Machine Learning 2003*.

[116] J. Y. Zien, M. D. F. Schlag, and P. K. Chan. Multi-level spectral hypergraph partitioning with arbitrary vertex sizes. In *Proc. International Conference on Computer-Aided Design*, pages 201–204. IEEE Press, 1996.

Vita

Yuchi Huang

EDUCATION

October 2010

Ph.D. in Computer Science, Rutgers University, U.S.A.

July 2004

M.E. in Pattern Recognition and Intelligent Systems, Chinese Academy of Sciences, P.R.C.

July 2001

B.S. in Automatic Control, Beijing University of Aeronautics and Astronautics, P.R.C.

EXPERIENCE

Jun. 2005 - Jun.2010

Graduate Assistant, Department of Computer Science, Rutgers University, New Brunswick, NJ, U.S.A.

May 2008 - Aug.2008

Summer Intern, NEC Laboratories America, Inc., Cupertino, CA, U.S.A.

Jul. 2007 - Aug.2007

Summer Intern, Siemens Cooperation Research, Princeton, NJ, USA

Jun. 2004-May 2005

Teaching Assistant, Department of Computer Science, Rutgers University, New Brunswick, NJ, U.S.A.

Jun.2003 - Jul. 2004

Research Assistant, Microsoft Research Asia, Beijing, P.R.C.

Sep.2002-Jun.2003

Research Assistant, Institute of Automation, Chinese Academy of Sciences, Beijing, P.R.C.

PUBLICATION

Unsupervised Image Categorization by Hypergraph Partition, Yuchi Huang, Qingshan Liu, Fengjun Lv, Yihong Gong and Dimitris N. Metaxas, Submitted to *IEEE Transactions on Pattern Analysis and Machine Intelligence (TPAMI)*(The notice of revision was received), 2010.

A Component Based Framework for Generalized Face Alignment, Yuchi Huang, Qingshan Liu, Dimitris N. Metaxas, Accepted by *IEEE Transactions on Systems, Man, and Cybernetics, Part B (TSMC)*, 2010

Image Retrieval via Probabilistic Hypergraph Ranking, Yuchi Huang, Qingshan Liu, Shaoting Zhang, Dimitris N. Metaxas, in Proceedings of *the 23rd International Conferences on Computer Vision and Pattern Recognition (CVPR'10)*, 2010.

Automatic Image Annotation Using Group Sparsity, Shaoting Zhang, Junzhou Huang, Yuchi Huang, Dimitris N. Metaxas, in Proceedings of *the 23rd International Conferences on Computer Vision and Pattern Recognition (CVPR'10)*, 2010.

Random Fuzzy Hypergraph for Image Retrieval, Qingshan Liu, Yuchi Huang, Dimitris N. Metaxas, Submitted to *Journal of Pattern Recognition, Special Issue on Semi-Supervised Learning for Visual Content Analysis and Understanding*(Accepted with minor revision), 2010.

Video Object Segmentation by Hypergraph Cut, Yuchi Huang, Qingshan Liu, Dimitris N. Metaxas, in Proceedings of *the 22nd International Conferences on Computer Vision and Pattern Recognition (CVPR'09)*, 2009.

A Component Based Deformable Model for Generalized Face Alignment, Yuchi Huang, Qingshan Liu and Dimitris N. Metaxas, in Proceedings of *the 11th International Conference on Computer Vision (ICCV'07)*, 2007.

Tracking Facial Features Using Mixture of Point Distribution Models, Atul Kanaujia, Yuchi Huang and Dimitris N. Metaxas, in Proceedings of *Indian Conference on Computer Vision, Graphics and Image Processing (ICVGIP) 2006.*

Emblem Detections by Tracking Facial Features, Atul Kanaujia, Yuchi Huang and Dimitris N. Metaxas, in Proceedings of *International Conference on Computer Vision and Pattern Recognition Workshop on semantic learning*, 2006.

Face Alignment under Variable Illumination, Yuchi Huang, Stephen Lin, Stan Z. Li, Hanqing Lu and Heung-Yeung Shum, in Proceedings of *International Conference on Automatic Face and Gesture Recognition (FGR)*, 2004.

Face Alignment Using Intrinsic Information, Yuchi Huang, Stephen Lin, Hanqing Lu and Heung-Yeung Shum, in Proceedings of *International Conference on Image Processing (ICIP)*, 2004.

A Robust Class-Based Reflectance Rendering for Face Images, Yuchi Huang, Qingshan Liu, Hanqing Lu, in Proceedings of *Asian Conference on Computer Vision (ACCV)*, 2004.